

**DESIGNING BIOENGINEERED SKIN SUBSTITUTES  
CONTAINING MICROFABRICATED BASAL LAMINA  
ANALOGS TO ENHANCE SKIN REGENERATION**

A Dissertation

Submitted to the Faculty of the

WORCESTER POLYTECHNIC INSTITUTE

&

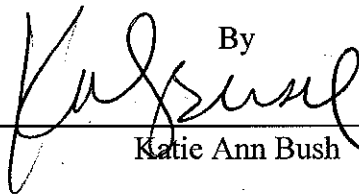
UNIVERSITY OF MASSACHUSETTS GRADUATE SCHOOL OF BIOMEDICAL  
SCIENCES

in partial fulfillment of the requirements for the

Degree of Doctorate of Philosophy in  
Biomedical Engineering & Medical Physics

January 15, 2009

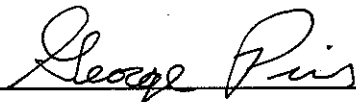
By



---

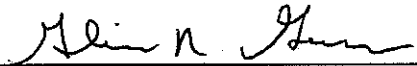
Katie Ann Bush

Approved by:



---

George D. Pins, Ph.D.  
Associate Professor, Advisor  
Biomedical Engineering  
Worcester Polytechnic Institute



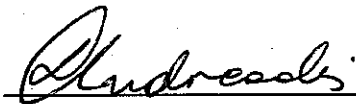
---

Glenn R. Gaudette, Ph.D.  
Assistant Professor, Committee Chair  
Biomedical Engineering  
Worcester Polytechnic Institute




---

Tanja Dominko, DVM, Ph.D.  
Associate Professor  
Biology & Biotechnology  
Worcester Polytechnic Institute



---

Stelios T. Andreadis, Ph.D.  
Professor  
Chemical and Biological Engineering  
SUNY at Buffalo



---

Matthew J. Gounis, Ph.D.  
Assistant Professor  
Radiology  
Biomedical Engineering  
& Medical Physics  
University of Massachusetts

## **ACKNOWLEDGEMENTS**

Over the past years in graduate school I have learned more than I ever thought I would about science and about myself. My deepest thanks go out to my family, friends, colleagues, advisor, mentors, and mentees for your teachings and support. You will all be forever remembered.

## TABLE OF CONTENTS

	<b>Page</b>
<b>Chapter 1: Overview</b>	1
1.1 Introduction	1
1.2 Overall Goal and Hypothesis	3
1.3 Part I: Evaluation of ECM in the Regulation of Keratinocyte Function	3
1.3.1 Objective 1: Establish Relationships Between Keratinocyte Attachment and ECM Proteins on the Surface of Basal Lamina Analogs	3
1.3.2 Objective 2: Evaluate Keratinocyte Responses to Availability of Fibronectin Cellular Binding Domains	4
1.3.3 Objective 3: Investigate Fibronectin Presentation on Basal Lamina Analogs and Evaluate Keratinocyte Morphology, Proliferation, and Differentiation	5
1.4 Part II: Roles of Scaffold Microarchitecture in the Regulation of Keratinocyte Function	6
1.4.1 Objective 4: Incorporate Biochemical and Microtopographic Features Found at the DEJ on the Surface of Bioengineered Skin Substitutes and Evaluate the Effects of the Microenvironment on Epithelialization and Epidermal Stem Cell Localization	6
1.5 References	7
<b>Chapter 2: Background</b>	9
2.1 Introduction	9
2.1.1 The Dermis	9
2.1.2 The Epidermis	10
2.1.3 The Basal Lamina	12
2.2 The Process of Wound Healing	14
2.3 Severe Skin Injuries	16
2.4 Current Therapeutic Strategies	16
2.5 Bioengineered Skin Substitutes	17
2.5.1 Design Considerations	17
2.5.2 Current Bioengineered Skin Substitutes	17
2.5.2.1 Temporary Bioengineered Skin Substitutes-Wound Dressings	18
2.5.2.2 Bioengineered Epidermal Skin Substitutes	19
2.5.2.3 Bioengineered Dermal Skin Substitutes	21
2.5.2.4 Bioengineered Composite Skin Substitutes	22
2.6 Conclusions	23
2.7 References	27

<b>Chapter 3: Fibronectin Enhances Keratinocyte Attachment to Basal Lamina Analogs</b>	32
3.1 Introduction	32
3.2 Materials and Methods	35
3.2.1 High Throughput Screening Device	35
3.2.2 Collagen-GAG Membranes	35
3.2.2.1 Collagen-GAG Dispersion	35
3.2.2.2 Production of Collagen-GAG Membranes	36
3.2.2.3 Dehydrothermal Crosslinking of Collagen-GAG Membranes	36
3.2.2.4 Modification of Crosslinked Collagen-GAG Membranes	36
3.2.2.5 Detection of Protein Modification	37
3.2.3 Keratinocyte Attachment Assay	38
3.2.3.1 Modification of Crosslinked Collagen-GAG Membranes	38
3.2.3.2 Culture of Human Cells	38
3.2.3.3 Quantification of Keratinocyte Attachment	39
3.2.5 Statistical Analyses	40
3.3 Results	41
3.3.1 Protein Adsorption	41
3.3.2 Keratinocyte Attachment to ECM Modified Collagen-GAG Membranes	42
3.4 Discussion	44
3.5 Acknowledgements	48
3.6 References	48
<b>Chapter 4: Fibronectin Cellular Binding Site Availability</b>	51
4.1 Introduction	51
4.2 Materials and Methods	53
4.2.1 Preparation of SAMs	53
4.2.2 Characterization of SAMs	54
4.2.3 Culture of Neonatal Human Keratinocytes	54
4.2.4 FN Adsorption on SAM Surfaces	55
4.2.5 Determining Saturation Density of Adsorbed FN using Ellipsometry	55
4.2.6 SAM Mediated Changes in FN Conformation	56
4.2.7 Cell Spreading	56
4.2.8 Analysis of Keratinocyte Attachment	57
4.2.9 Analysis of Keratinocyte Differentiation	57
4.2.10 Fluorescence Assessment of FA Formation	58
4.2.11 Statistical Analyses	59
4.3 Results	60
4.3.1 Model Surfaces with Precisely Tailored Surface Chemistries	60
4.3.2 Determining Saturation Levels of FN	61
4.3.3 Analysis of SAM Directed Changes in FN Conformation	62
4.3.4 SAM Dependent Changes in FN Treated Surface Direct Keratinocyte Attachment	62

4.3.5 SAM Dependent Changes in FN Treated Surfaces Direct Keratinocyte Morphology	63
4.3.6 SAM Dependent Changes in FN Treated Surface Direct Keratinocyte Differentiation	64
4.3.7 Quantification of FAs on FN Treated SAM Surfaces	65
4.4 Discussion	66
4.5 Acknowledgements	70
4.6 References	71
<b>Chapter 5: Carbodiimide Conjugation of Fibronectin on Collagen Binding Domains and Epithelialization</b>	<b>74</b>
5.1 Introduction	74
5.2 Materials and Methods	77
5.2.1 Air Liquid Interface Culture Devices	77
5.2.2 Basal Lamina Analog Production	77
5.2.2.1 Collagen-GAG Membranes	77
5.2.2.2 Self-Assembled Type I Collagen Membranes	78
5.2.3. FN Surface Modification of Collagen Membranes	79
5.2.3.1 Passive Adsorption of FN to Collagen Membranes	79
5.2.3.2 EDC Conjugation of Fibronectin to Collagen Membranes	79
5.2.4 Culture of Neonatal Human Keratinocytes	80
5.2.5 <i>In vitro</i> Culture of Keratinocytes on Basal Lamina Analogs	80
5.2.6 Evaluation of Epithelialization	81
5.2.7 FN Cellular Binding Site Detection	83
5.2.8 Statistical Analyses	83
5.3 Results	84
5.3.1 FN Enhances Epithelialization of Keratinocytes on Basal Lamina Analogs	84
5.3.1.1 Graft Morphology and Epidermal Layer Thickness on Collagen-GAG Basal Lamina Analogs	84
5.3.1.2 Keratinocyte Proliferation on Collagen-GAG Basal Lamina Analogs	85
5.3.2 Availability of Cellular Binding Domain of FN Corresponds to Keratinocyte Attachment on Collagen-GAG Basal Lamina Analogs	87
5.3.3 EDC Conjugation of FN on Self-Assembled CI Basal Lamina Analogs Promotes Increased Cellular Binding Site Availability	88
5.3.4 EDC Conjugation of FN on Self-Assembled CI Basal Lamina Analogs Enhances Epidermal Layer Thickness	90
5.4 Discussion	91
5.5 Acknowledgments	95
5.6 References	95

<b>Chapter 6: Microenvironments of Basal Lamina Analogs Influence Epithelialization and Epidermal Stem Cell Localization on Bioengineered Skin Substitutes</b>	99
6.1 Introduction	99
6.2 Materials and Methods	103
6.2.1 Production of Dermal Scaffold Containing a Microfabricated Basal Lamina Analog	103
6.2.1.1 Photolithography of a Master Pattern and Negative Replicates	103
6.2.1.2 Purification of CI	104
6.2.1.3 Dermal Scaffold Production	104
6.2.1.4 Production of Dermal Scaffolds with Microfabricated Basal Lamina Analogs	105
6.2.1.5 FN Conjugation to Microfabricated Basal Lamina Analogs Laminated to Dermal Scaffolds	105
6.2.2 Preparation of De-Epithelialized Acellular Dermis	106
6.2.3 <i>In vitro</i> Culture of Dermal Scaffolds Containing Microfabricated Basal Lamina Analogs	107
6.2.3.1 Sterilization of Dermal Scaffolds Containing Microfabricated Basal Lamina Analogs	107
6.2.3.2 Culture of Neonatal Human Keratinocytes	107
6.2.3.3 Culture of Dermal Scaffolds Containing Microfabricated Basal Lamina Analogs	108
6.3.3 Quantitative Morphometric Analysis of Microfabricated Features of Basal Lamina Analogs	109
6.3.4 Analyses of Epithelialization and Regenerative Capacity of Bioengineered Skin Substitutes Containing Microfabricated Basal Lamina Analogs	110
6.3.4.1 Epidermal Thickness and Graft Morphology	110
6.3.4.2 Keratinocyte Proliferation	111
6.3.4.3 <i>Beta-1</i> Analysis of Keratinocyte Colonies	112
6.3.4.4 <i>Beta-1</i> Expression in Bioengineered Skin Substitutes, Epithelialized DEDs, and Human Tissue	113
6.3.5 Statistical Analyses	114
6.4 Results	115
6.4.1 Development of Bioengineered Skin Substitutes Containing Microfabricated Basal Lamina Analogs	115
6.4.2 Microenvironments Provided By a Microfabricated Basal Lamina Analog Influence Epidermal Thickness and Morphology of the Epidermal Layer of Bioengineered Skin Substitutes	117
6.4.3 Proliferation Capacity of Bioengineered Skin Substitutes is Affected by the Microenvironment Provided by a Microfabricated Basal Lamina Analog	121
6.4.4 <i>Beta-1</i> Expression in Keratinocyte Colonies Detected in Edge Keratinocytes	123

6.4.5 Microenvironments Control Spatial Localization of $\beta_1$ -Bright Basal Keratinocytes	124
6.5 Discussion	126
6.6 Acknowledgements	134
6.6 References	134
<b>Chapter 7: Conclusions and Future Work</b>	138
7.1 Overview	138
7.2 Results and Conclusions	138
7.2.1 Part I: Evaluation of ECM in the Regulation of Keratinocyte Function	138
7.2.2 Part II: Role of Scaffold Microarchitecture in the Regulation of Keratinocyte Function	142
7.3 Future Work	146
7.3.1 The Next Generation of Bioengineered Skin Substitutes	143
7.3.2 Model System	149
7.4 Final Conclusions	149
7.5 References	150

## TABLE OF FIGURES

	Page
Figure 2.1 Anatomy of Human Skin	9
Figure 2.2 Hematoxylin and Eosin Stained Histological Representation of the Dermis	10
Figure 2.3 Hemotoxylin and Eosin Stained Histological Representation of the Epidermis	11
Figure 2.4 The Topography Found at the Dermal-Epidermal Junction	12
Figure 2.5 A Model of the Molecular Structure of the Basal Lamina	13
Figure 2.6 [ $^3\text{H}$ ]thymidine Incorporation in Basal Keratinocytes in Bottom of Deep Rete Ridges	13
Figure 2.7 Phases of Repair in Normal Cutaneous Wound Healing	14
Figure 3.1 High Throughput Screening Device	35
Figure 3.2 Analysis of ECM Protein Conjugation to Collagen-GAG Membranes	37
Figure 3.3 ECM Protein Conjugation to Collagen-GAG Membrane	41
Figure 3.4 Percent Keratinocyte Attachment on Biochemically Modified Collagen-GAG Membranes	43
Figure 3.5 Effects of Protein Concentration on Percent Keratinocyte Attachment	44
Figure 3.6 Reepithelialization of Wound in Native Skin	46
Figure 4.1 Structure of FN Monomer	51
Figure 4.2 FA Validation on Tissue Culture Plastic	58
Figure 4.3 SAMs on Gold Surface	60

Figure 4.4 Relationship Between FN Concentration and Thickness on SAM Surfaces	61
Figure 4.5 Analysis of Changes in FN Conformation on SAM Surfaces	62
Figure 4.6 Keratinocyte Attachment on FN Treated SAM Surfaces	63
Figure 4.7 Keratinocyte Spreading on FN Treated SAM Surfaces	64
Figure 4.8 The Effect of SAM Dependent Changes in FN on Keratinocyte Differentiation	64
Figure 4.9 FA Analysis on SAM Surfaces	65
Figure 4.10 Focal Adhesion Area Density Measurements	66
Figure 5.1 Custom Build A/L Interface Culture Devices	77
Figure 5.2 Histological Representations of the Thicknesses of Epidermal Layers on Collagen-GAG Membranes	85
Figure 5.3 Quantitative Evaluation of Epidermal Thickness on Collagen-GAG Membranes	85
Figure 5.4. Histological Representations of Ki67 Positive Keratinocytes on Collagen-GAG Membranes	86
Figure 5.5 Quantitative Analyses of Ki67 Positive Basal Keratinocytes on Collagen-GAG Membranes	86
Figure 5.6. Availability of Cellular Binding Domains for FN Passively Adsorbed on Collagen-GAG Basal Lamina Analogs	87
Figure 5.7 Schematic Representation of EDC-Mediated Conjugation of FN to Collagen	88
Figure 5.8 Availability of Cellular Binding Domain of FN on Collagen-GAG and Self-Assembled CI Basal Lamina Analogs	89
Figure 5.9 Low and High Magnification of Histological Images of Self-Assembled CI Basal Lamina Analogs Treated with FN	90
Figure 5.10 EDC Conjugation of Fibronectin on Self-Assembled Type I Collagen Basal Lamina Analogs Enhances Epithelial Thickness	91
Figure 6.1 Production of a Bioengineered Skin Substitutes Containing Microfabricated Basal Lamina Analogs	115
Figure 6.2 Topographical Measurements of the Surfaces of Bioengineered Basal Lamina Analogs	116
Figure 6.3 Histological Representation of Hematoxylin and Eosin Stained Bioengineered Skin Substitutes	117
Figure 6.4 Epidermal Thickness of Bioengineered Skin Substitutes	118
Figure 6.5 Epidermal Thickness at Papillary Plateau	119
Figure 6.6 Histological Representation of Ki67 Expression of Basal Keratinocytes Present in Bioengineered Skin Substitutes	120
Figure 6.7 Percentage of Ki67 Positive Basal Keratinocytes in Bioengineered Skin Substitutes	121
Figure 6.8 Keratinocyte Colonies with $\beta_1$ and Nuclear Expression	122
Figure 6.9 <i>Beta-1</i> Expression of Basal Keratinocytes in Bioengineered Skin Substitutes	125



## TABLE OF TABLES

	<b>Page</b>
Table 2.1 Summary of Commercially Available Bioengineered Skin Substitutes	24
Table 3.1 Effects of ECM on Keratinocyte Functions	33
Table 4.1 Contact Angle and Characteristic Properties of SAMs	61
Table 6.1 Specified and Measured Topographical Features of Basal Lamina Analogs	116

## ABBREVIATIONS

ANOVA: Analysis of variance  
A/L: Air liquid interface  
CI: Type I collagen  
CIV: Type IV collagen  
CEA: Cultured epithelial autografts  
CFE: Colony forming efficiency  
DED: De-epithelialized acellular dermis  
DEJ: Dermal-epidermal junction  
DHT: Dehydrothermal  
DMEM: Dulbecco's Modified Eagle's Medium  
DPBS: Dulbecco's phosphate buffered saline  
ECM: Extracellular matrix  
EDC: Carbodiimide 1-ethyl-3-(3-dimethylaminopropyl)carbodiimide hydrochloride  
ESC: Epidermal stem cell  
FA: Focal adhesions  
FN: Fibronectin  
FACs: Fluorescence activated cell sorting  
GAG: Glycosaminoglycan  
HFN 7.1 Antibody against central cellular binding domain of fibronectin  
HTS: High throughput screening  
KCM: Keratinocyte medium  
KCM (-S-GF): Serum free growth factor free keratinocyte media  
Ki67: Cell cycle associated antigen  
LN: Laminin  
LRCs: Label retaining cells  
MMPs: Matrix metalloproteinases

MTT: Thiazoyl blue tetrazolium bromide  
NHK: Neonatal human keratinocytes  
SAM: Self-assembled monolayer  
PBSABC: Phosphate buffered saline with calcium and magnesium salts  
PDMS: Polydimethylsiloxane  
PEG: Polyethylene glycol  
PHSRN: Proline, histidine, serine, arginine, asparagine  
PLGA: Poly(lactic-co-glycolic acid)  
RGD: Arginine-glycine-aspartic acid  
ROI: Region of interest  
RTT: Rat tail tendon  
TA: Transit amplifying cells

## ABSTRACT

Bioengineered skin substitutes have been developed to treat burn and non-healing wounds; however limitations still hinder their clinical success rates. Optimizing these current design strategies requires an understanding of how biochemical and topographical features of the native tissue modulate keratinocyte processes involved in tissue functionality. In this thesis, a novel bioengineered skin substitute was developed that contains a microfabricated basal lamina analog that recapitulates the native microenvironment found at the dermal-epidermal junction (DEJ). In native skin, this microenvironment consists of both biochemical and topographical cues which play critical roles in maintaining tissue architecture and overall homeostasis with the external environment.

*Therefore, we hypothesize that microfabricated basal lamina analogs with extracellular matrix cues and three-dimensional features that mimics the cellular microenvironment of the DEJ will promote enhanced epithelialization and increase epidermal stem cell clustering on the surface of bioengineered skin substitutes.*

We determined that the extracellular matrix protein fibronectin (FN) found in the cellular microenvironment of the DEJ enhanced keratinocyte attachment, proliferation, and epithelialization of a collagen based basal lamina analog. It was also found that the collagen material used to create the basal lamina analog as well as the FN conjugation strategy to this material significantly influenced the bioactivity of FN and its ability to modulate keratinocyte functions through integrin based mechanism. To investigate spatial tissue organization and the role it plays in the cellular microenvironment of the DEJ on epithelialization and epidermal stem cell localization, we used photolithography coupled with materials processing techniques to create microfabricated basal lamina analogs. It was determined that epidermal thicknesses found in narrow channels of microfabricated basal lamina analogs (50  $\mu\text{m}$  and 100  $\mu\text{m}$  widths with 200  $\mu\text{m}$  depths) were similar to cultures on de-epithelialized acellular dermis and native foreskin tissues after 7 days of *in vitro* culture. We also determined that the microfabricated basal lamina analogs created an epidermal stem cell niche that promoted epidermal stem cell clustering in the channels which is critical for longevity of the tissue.

Overall, we developed a platform technology that was specifically used to produce a highly functional bioengineered skin substitute with regenerative capacity that mimics native skin. We anticipate through the use of this technology, we can further improve bioengineered skin substitutes by incorporating epidermal structures of native skin including hair follicles and sweat glands as well as improve overall cosmetic appearance. Additionally, this novel bioengineered skin substitute can serve as a model system to further our understanding of pathological conditions and diseases of the skin as well as facilitate robust preclinical screenings of epidermal responses to new therapeutic agents as well as to cosmetic and chemical products.

---

---

# Chapter 1: Overview

---

## 1.1 INTRODUCTION

Every year in the United States 2.4 million burn injuries are reported and approximately 12,000 people are burned severely enough to require skin grafting.<sup>1</sup> Diabetic and venous ulcers, as well as pressure sores, affect an additional 3 to 4 million people and it is anticipated these figures will continue to increase with the rises in the average age of the population as well as the incidences of diabetes.<sup>2,3</sup> A critical component in preventing infection, water loss, scarring, amputation, and death from severe skin wounds is the prompt restoration of skin integrity. While autografts are considered the “gold standard” to treat localized skin injuries, a lack of available donor sites as well as donor site morbidity routinely hinders the recovery of patients with large burns or skin traumas.<sup>4-6</sup> As such, the successful development of bioengineered skin substitutes that provide permanent coverage to the wound site and restore the anatomy and physiology of uninjured skin will have significant impact on the treatment of patients with serious skin injuries.<sup>5-7</sup>

Over the past three decades, composites of cultured cells and biomaterials have been investigated for potential use as bioengineered skin substitutes.<sup>5,8-11</sup> Regeneration of skin tissues, including neodermal formation and vascularization as well as reepithelialization of barrier layers, has been examined in a variety of engineered tissue analogs consisting of collagen-glycosaminoglycan (GAG) sponges,<sup>12-19</sup> collagen gels,<sup>20-23</sup> hyaluronic acid derivatives,<sup>24</sup> and synthetic polymers.<sup>25</sup> While bioengineered skin substitutes have achieved some clinical success restoring damaged skin, prolonged healing times, scarring, and mechanically induced graft failure remain persistent problems.<sup>5,23,26</sup> In order to address these

limitations and improve the performance of bioengineered skin substitutes, it is critical to investigate how tissue scaffolds can be precisely tailored to present critical environmental cues that direct keratinocyte adhesion, proliferation and differentiation, and overall rapid epidermal formation.<sup>5,7-11</sup>

A common design feature of current skin substitutes, composed of cultured cells and biomaterials, is a flat interface between the dermal and epidermal dermal components. In native skin, the basal lamina is located at the dermal-epidermal junction (DEJ) and is not flat, but rather conforms to a series of three-dimensional ridges and invaginations formed by papillae located in the papillary region of the dermis. Several studies have examined the role of native basal lamina topography on providing a microenvironment that has the capability of modulating keratinocyte functions. Keratinocyte proliferation has been found to be affected with a higher percentage of proliferating basal and suprabasal cells found in deep rete ridges.<sup>27,28</sup> It has also been shown that the expression of  $\alpha_2\beta_1$  integrin, a suggested marker for epidermal stem cells, can be found localized on the tips of the dermal papillae or at the bottom of the deep rete ridges.<sup>29-31</sup> The complex microtopography of the basal lamina has been found to provide structural stability to the epidermis. Analyses of areas of skin exposed to excessive friction such as the plantar and the palmar surfaces, indicate that dermal papillae and epidermal ridges are longer and more numerous in those locations.<sup>32</sup>

The basal lamina is not only responsible for creating an interface between keratinocytes and the connective tissue of the dermal layer but it also provides instructive cues through extracellular matrix (ECM) proteins which direct keratinocyte polarity, proliferation, and differentiation, as well as preserving tissue architecture and organization. The ECM of the basal lamina is composed of collagenous and non-collagenous molecules including type IV collagen, laminin, fibronectin, and heparin sulfate proteoglycans.<sup>32-34</sup>

## **1.2 OVERALL GOAL AND HYPOTHESIS**

The overall goal of this project is to enhance the performance of bioengineered skin substitutes by analyzing the effects of biochemical and microstructural cues on keratinocyte function, stem cell enrichment and localization, and the rapid epithelialization on the surfaces of tailored bioengineered skin substitutes containing microfabricated basal lamina analogs at the DEJ.

*We hypothesize that microfabricated basal lamina analogs with extracellular matrix cues and three-dimensional features that mimic the cellular microenvironments of the dermal-epidermal junction will promote enhanced epithelialization and increase epidermal stem cell clustering on the surface of bioengineered skin substitutes.*

In this study, epithelialization is defined as keratinocyte attachment, proliferation, and differentiation, as well as cellular and graft morphology and graft thickness. The expected outcome of this project is the identification of a series of parameters critical for improving the design of bioengineered skin substitutes, as well as for promoting the rapid regeneration of highly functional skin tissue with increased structural stability.

To systematically test this hypothesis, this thesis was separated into two parts with a total of four objectives.

## **1.3 PART I: EVALUATION OF ECM IN THE REGULATION OF KERATINOCYTE FUNCTION**

### **1.3.1 Objective 1: Establish Relationships Between Keratinocyte Attachment and ECM Proteins on the Surface of Basal Lamina Analogs**

The DEJ of skin contains ECM proteins that are involved in initiating and controlling keratinocyte signaling events such as attachment, proliferation, and terminal differentiation. To characterize the relationship between ECM proteins and keratinocyte attachment, Chapter

3 discusses a biomimetic design approach that was used to tailor the surface of basal lamina analogs with biochemistries that emulate the biochemical composition found at the DEJ. A high-throughput screening device was developed by our laboratory that allows for the simultaneous investigation of the effect of ECM proteins, (types I and IV collagen (CI and CIV), laminin (LN), or fibronectin (FN)) passively adsorbed on the surface of an implantable collagen membrane, on keratinocyte attachment. Fluorescence microscopy coupled with quantitative digital image analyses indicated that the ECM proteins adsorbed to the collagen-GAG membranes in a dose-dependent manner and saturation was achieved. To determine the relationship between ECM protein signaling cues and keratinocyte attachment, cells were seeded on collagen-GAG membranes treated with the ECM proteins and a tetrazolium-based colorimetric assay was used to quantify viable keratinocyte attachment. Our results indicate that keratinocyte attachment was significantly enhanced on the surfaces of collagen-GAG membranes that were treated with FN. These findings define a set of design parameters that will enhance keratinocyte binding efficiency on the surface of collagen membranes and ultimately improve the rate of epithelialization for dermal equivalents. *Bush KA, Downing BR, Walsh SE, Pins GD. Conjugation of extracellular matrix proteins to basal lamina analogs enhances keratinocyte attachment. J Biomed Mater Res A 2007;80(2):444-52.*

### **1.3.2 Objective 2: Evaluate Keratinocyte Responses to Availability of FN Cellular Binding Domains**

Precisely engineering the surface chemistry of biomaterials to modulate the adsorption and functionality of biochemical signaling molecules that direct cellular functions is critical in the development of bioengineered scaffolds. In chapter 4 of this thesis, we describe the use of functionalized self-assembled monolayers (SAMs) as a model system to assess the effects of biomaterial surface properties on controlling FN conformation and concentrations as well as keratinocyte function. By systematically analyzing FN adsorption at low and saturated surface densities, we distinguished between SAM dependent effects of FN concentration and conformation on presenting cellular binding domains that direct cellular functions.

Quantitative image analyses of immunostained samples showed that modulating the availability of the FN synergy site corresponded with changes in keratinocyte attachment, spreading, and differentiation, through integrin mediated signaling mechanisms. The results of this study will be used to elucidate design features that can be incorporated onto dermal equivalents and percutaneous implants to enhance the rate of epithelialization and tissue regeneration. Furthermore, these findings indicate that SAM based model systems are a valuable tool for designing and investigating the development of scaffolds that regulate the conformation of ECM cues and cellular functions that accelerate the rate of tissue regeneration. *Bush, K.A., Driscoll, P.F., Soto, E.R., Lambert, C.R., McGimpsey, W.G., and Pins, G.D. "Designing Tailored Biomaterial Surfaces to Direct Keratinocyte Morphology, Attachment, and Differentiation." JBMR Part A, 2008. July 24 [Epub].*

### **1.3.3 Objective 3: Investigate FN Presentation on Basal Lamina Analogs and Evaluate Keratinocyte Morphology, Proliferation, and Differentiation.**

In order to improve the regenerative potential of biomaterials used as bioengineered scaffolds, it is necessary to incorporate biologically active molecules that promote *in vivo* cellular processes that lead to a fully functional tissue. Research has shown that the surface characteristics of a biomaterial greatly influence the conformation of the biomolecules which directly influences its bioactivity. In chapter 5 of this thesis, we evaluated the effects of strategically binding FN to collagen scaffolds to enhance keratinocyte function and epithelialization on basal lamina analogs for skin regeneration. We found that FN enhanced epithelial thickness and keratinocyte proliferation when compared to non-treated basal lamina analogs at 3 days of air/liquid (A/L) interface culture. Additionally we evaluated the availability of FN cellular binding site domains when FN was either passively adsorbed or conjugated to collagen scaffolds fabricated from collagen-GAG coprecipitate or self-assembled type I collagen sources using 1-ethyl-3-(3-dimethylaminopropyl)carbodiimide hydrochloride (EDC). It was found that EDC conjugation significantly enhanced FN binding site presentation as well as epithelial thickness. Overall the results gained from this study



can be used to improve the regenerative capacity of basal lamina analogs as well as the development of other bioengineered scaffolds. *Bush KA, Pins GD. Carbodiimide Conjugation of Fibronectin on Collagen Basal Lamina Analogs Enhances Cellular Binding Domains and Epithelialization. In preparation 2009.*

## **1.4 PART II: ROLE OF SCAFFOLD MICROARCHITECTURE IN THE REGULATION OF KERATINOCYTE FUNCTION**

### **1.4.1 Objective 4: Incorporate Biochemical and Microtopographic Features Found at the DEJ onto the Surface of Bioengineered Skin Substitutes and Evaluate the Effects of the Microenvironment on Epithelialization and Epidermal Stem Cell Localization.**

In native tissues, the basal lamina provides cues to modulate skin architecture, cellular organization, and the regeneration of the epithelial layer. In chapter 6 of this thesis, we developed a novel dermal scaffold that recapitulates biochemical and microtopographic features provided by the basal lamina to enhance epithelialization and epidermal stem cell (ESC) localization. To create the complete microenvironment, we combined photolithography, collagen processing, and biochemical conjugation techniques. After 3 days of A/L interface culture we evaluated the epidermal layer of bioengineered skin substitutes and found that keratinocytes cultured in 50  $\mu\text{m}$  width channels with 200  $\mu\text{m}$  depths had statistically similar epidermal thickness values as keratinocyte cultured on de-epithelialized acellular dermis (DED). At 7 days of A/L interface culture the 50  $\mu\text{m}$  width and 100  $\mu\text{m}$  width channels with 200  $\mu\text{m}$  depths exhibited the same epidermal thicknesses as keratinocyte cultured on DED and native skin samples. Furthermore, these conditions were statistically different from cultures in 200  $\mu\text{m}$  width and 400  $\mu\text{m}$  width channels with 200  $\mu\text{m}$  depths. It was also found that the percentage of Ki67 positive basal keratinocytes, a marker for proliferative cells, was statistically similar for the bioengineered skin substitutes, DED cultures, and in native tissues at 7 days of A/L interface culture. In addition to epidermal thickness and proliferation, we evaluated ESC localization by evaluating integrin expression, specifically  $\beta_1$ . We determined that integrin-bright regions of cultured keratinocytes were found in the channels (rete ridges) in our bioengineered skin substitutes, whereas in native

foreskin tissue, these cells were identified at the tips of the papillary projections. Based on the results of our epidermal thickness measurements, as well as keratinocytes proliferation and ESC studies, we have defined a set of criteria for the design of the next generation of bioengineered skin substitutes to enhance epithelialization rates and control stem cell localization, as well as the potential for increasing mechanical stability, based on the increase in cellular interaction surface area. Additionally, our bioengineered skin substitutes are an excellent model system to evaluate the microenvironmental cues that provide an ESC niche on a bioengineered skin substitute and will ultimately lead to the enhanced regenerative capacity and overall performance of our scaffolds. *Bush KA, Toner, M., Pins GD. Microenvironments of the Basal Lamina Influence Epithelialization and Stem Cell Localization on Bioengineered Skin Substitutes. In preparation 2009.*

## 1.5 REFERENCES

1. Burn incidence and treatment in the United States: 1999 Fact Sheet. Philadelphia, PA: The Burn Foundation; 1999.
2. Clark RA, Singer AJ. Wound Repair: Basic Biology to Tissue Engineering. In: Lanza RP, Langer R, Vacanti J, editors. Principles of Tissue Engineering, Second Edition. Boston: Academic Press; 2000. p 857-878.
3. Morgan JR, Sheridan RL, Tompkins RG, Yarmush ML, Burke JF. Burn Dressings and Skin Substitutes. In: Ratner BD, Hoffman AS, Schoen FJ, Lemons JE, editors. Biomaterials Science: An Introduction to Materials in Medicine. San Diego: Academic Press; 2004. p 360-370.
4. Jones I, Currie L, Martin R. A guide to biological skin substitutes. *Br J Plast Surg* 2002;55(3):185-93.
5. Sheridan RL, Tompkins RG. Skin substitutes in burns. *Burns* 1999;25(2):97-103.
6. Supp DM, Boyce ST. Engineered skin substitutes: practices and potentials. *Clin Dermatol* 2005;23(4):403-12.
7. Boyce ST. Design principles for composition and performance of cultured skin substitutes. *Burns* 2001;27(5):523-33.
8. Boyce ST. Cultures Skin Substitutes: A Review. *Tissue Eng* 1996;2:255-266.
9. Clark RA, Ghosh K, Tonnesen MG. Tissue engineering for cutaneous wounds. *J Invest Dermatol* 2007;127(5):1018-29.
10. Ehrenreich M, Ruszczak Z. Update on tissue-engineered biological dressings. *Tissue Eng* 2006;12(9):2407-24.
11. Phillips T. New Skin for Old: Developments in Biological Skin Substitutes. *Arch. Dermatol.* 1998;134:344-349.
12. Yannas IV, Burke JF, Gordon PL, Huang C, Rubenstein RH. Design of an artificial skin. II. Control of chemical composition. *J Biomed Mater Res* 1980;14(2):107-32.
13. Yannas IV, Burke JF, Orgill DP, Skrabut EM. Wound tissue can utilize a polymeric template to synthesize a functional extension of skin. *Science* 1982;215(4529):174-6.

14. Heimbach D, Luterman A, Burke J, Cram A, Herndon D, Hunt J, Jordan M, McManus W, Solem L, Warden G and others. Artificial dermis for major burns. A multi-center randomized clinical trial. *Ann Surg* 1988;208(3):313-20.
15. Boyce ST, Christianson DJ, Hansbrough JF. Structure of a collagen-GAG dermal skin substitute optimized for cultured human epidermal keratinocytes. *J Biomed Mater Res* 1988;22(10):939-57.
16. Boyce ST, Hansbrough JF. Biologic attachment, growth, and differentiation of cultured human epidermal keratinocytes on a graftable collagen and chondroitin-6-sulfate substrate. *Surgery* 1988;103(4):421-31.
17. Black AF, Berthod F, L'Heureux N, Germain L, Auger FA. In vitro reconstruction of a human capillary-like network in a tissue-engineered skin equivalent. *Faseb J* 1998;12(13):1331-40.
18. Hudon V, Berthod F, Black AF, Damour O, Germain L, Auger FA. A tissue-engineered endothelialized dermis to study the modulation of angiogenic and angiostatic molecules on capillary-like tube formation in vitro. *Br J Dermatol* 2003;148(6):1094-104.
19. Burke JF, Yannas IV, Quinby WC, Jr., Bondoc CC, Jung WK. Successful use of a physiologically acceptable artificial skin in the treatment of extensive burn injury. *Ann Surg* 1981;194(4):413-28.
20. Bell E, Sher S, Hull B, Merrill C, Rosen S, Chamson A, Asselineau D, Dubertret L, Coulomb B, Lapiere C and others. The reconstitution of living skin. *J Invest Dermatol* 1983;81:2s-10s.
21. Bell E, Ehrlich HP, Buttle DJ, Nakatsuji T. Living tissue formed in vitro and accepted as skin-equivalent tissue of full thickness. *Science* 1981;211(4486):1052-4.
22. Wilkins LM, Watson SR, Prosky SJ, Meunier SF, Parenteau NL. Development of a Bilayered Living Skin Construct for Clinical Applications. *Biotech. Bioeng.* 1994;43:747-756.
23. Parenteau N, Sabolinski M, Prosky S, Nolte C, Oleson M, Kriwet K, Bilbo P. Biological and physical factors influencing the successful engraftment of a cultured skin substitute. *Biotech. Bioeng.* 1996;52:3-14.
24. Zacchi V, Soranzo C, Cortivo R, Radice M, Brun P, Abatangelo G. In vitro engineering of human skin-like tissue. *J Biomed Mater Res* 1998;40(2):187-94.
25. El-Ghalbzouri A, Lamme EN, van Blitterswijk C, Koopman J, Ponc M. The use of PEGT/PBT as a dermal scaffold for skin tissue engineering. *Biomaterials* 2004;25(15):2987-96.
26. Boyce ST, Goretsky MJ, Greenhalgh DG, Kagan RJ, Rieman MT, Warden GD. Comparative assessment of cultured skin substitutes and native skin autograft for treatment of full-thickness burns. *Ann Surg* 1995;222(6):743-52.
27. Lavker RM, Sun TT. Heterogeneity in epidermal basal keratinocytes: morphological and functional correlations. *Science* 1982;215(4537):1239-41.
28. Lavker RM, Sun TT. Epidermal stem cells. *J Invest Dermatol* 1983;81(1 Suppl):121s-7s.
29. Carter WG, Symington BE, Kaur P. Cell adhesion and the basement membrane in early epidermal morphogenesis. In: Fleming TP, editor. *Epithelial Organization and Development*. London: Chapman and Hall; 1992. p 299-327.
30. Jensen UB, Lowell S, Watt FM. The spatial relationship between stem cells and their progeny in the basal layer of human epidermis: a new view based on whole-mount labelling and lineage analysis. *Development* 1999;126(11):2409-18.
31. Jones PH, Harper S, Watt FM. Stem cell patterning and fate in human epidermis. *Cell* 1995;80(1):83-93.
32. Odland GF. The morphology of the attachment between the dermis and the epidermis. *Anat Rec* 1950;108(3):399-413.
33. Burgeson RE. Basement Membranes. *Dermatology in General Medicine*. New York, NY: McGraw-Hill; 1987. p 288-303.
34. Vracko R. Basal lamina scaffold-anatomy and significance for maintenance of orderly tissue structure. *Am J Pathol* 1974;77(2):314-46.

---

---

## Chapter 2: Background

---

### 2.1 SKIN STRUCTURE AND FUNCTION

Skin is the largest organ in vertebrate organisms and is responsible for many complex physiological functions that maintain homeostasis of the body with its surrounding environment. This includes protection against pathogens, acting as a physical barrier, absorption of harmful UV rays, sensory detection, and providing thermal and hydration regulation. These functions are carried out through integration of specialized cells and structures

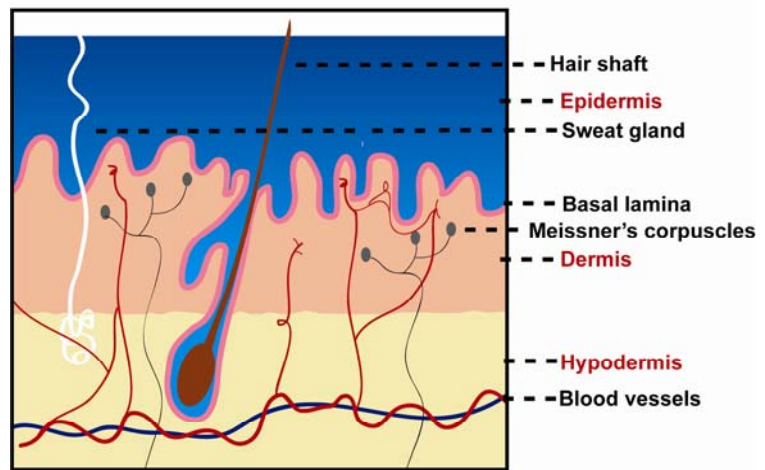


**Figure 2.1 Anatomy of Human Skin.** Skin is composed of two main layers, the epidermis and dermis. The epidermis is responsible for providing a physical barrier, whereas the dermis is responsible for maintaining physical strength of skin. Below the dermis is the hypodermis, which contains the source of blood vessels and is composed of adipose tissue.<sup>3</sup>

found in the dermal and epidermal layers of the skin.<sup>1,2</sup> Figure 2.1 displays a cartoon of the anatomy of human skin.<sup>3</sup>

#### 2.1.1 The Dermis

The innermost layer of skin, the dermis, is predominantly composed of interwoven connective tissue containing collagen fibrils with elastic and reticular fibers interspersed to provide physical strength, elasticity, and scaffolding for accessory features. The dermis has a three-dimensional organization with an upper papillary region and a lower reticular region.

The upper region, the papillary dermis (PD: Figure 2.2<sup>1</sup>), is composed of loose, small diameter collagen and immature elastic fibers. Exclusive to this layer are fingerlike projections called papillae, which extend toward the epidermis, and contain either capillaries that nourish the epidermis, or Meissner's corpuscles which are sensory touch receptors. Fibroblasts, the major cell type of the dermis, are most abundant in this region, as well as having a higher rate of metabolic activity, an enhanced capacity for proliferation, and a longer replication life span in comparison to fibroblasts found in the lower dermis.<sup>4,5</sup>



**Figure 2.2 Hematoxylin and Eosin Stained Histological Representation of the Dermis.** The upper region of the dermis, the papillary dermis (PD), contains small diameter collagen and immature elastic fibers. The lower region of the dermis, the reticular dermis (RD), is responsible for providing mechanical stability.<sup>1</sup>

The lower region of the dermis, the reticular layer (RD: Figure 2.2<sup>1</sup>), contains a much denser concentration of thick collagen fibers and mature elastic fibers that form a basket weave pattern than found in the upper region of the dermis. This

layer is responsible for providing the mechanical stability of the dermis as well as containing specialized cells and receptors including, sebaceous glands, apocrine glands, blood vessels, nerve endings, lymph vessels, arrector pili muscles, hair follicles, and Pacinian corpuscles.<sup>4,5</sup>

### 2.1.2 The Epidermis

The epidermis is the outer most layer of skin. This layer is responsible for providing the protective barrier against the surrounding environment and is in constant regeneration with a turnover of approximately 4 weeks. The predominant cell type responsible for providing the barrier properties of the epidermis and in its repair and regeneration is the keratinocyte, representing approximately 80% of the total population of cells. The other 20% of cells are a combination of cells that provide immunologic protection (Langerhans cells), absorption of

ultraviolet light (melanocytes), and sense mechanical events within the epidermis and at the surface of skin (Merkel cells).<sup>6</sup>

Within the epidermis, there are four distinct layers, with each layer being defined by position, morphology, and state of differentiation of the keratinocytes.<sup>6</sup> The bottom layer, the stratum basal (also referred to as the stratum germinativum) (Figure 2.3<sup>1</sup> SG), contains a single row of columnar undifferentiated basal keratinocytes, consisting of epidermal stem cells (ESCs) and transit amplifying (TA) keratinocytes that are attached to the underlying basement membrane.<sup>7,8</sup> Epidermal stem cells are responsible for maintaining the entire population of keratinocytes by i) giving rise to additional ESCs by tissue demand or specific stimuli or by ii) giving rise to daughter TAs that amplify the number of cells derived from each ESC mitosis by undergoing 3-5 rounds of division.<sup>9-11</sup> Cells resulting from TAs do not proliferate and terminally differentiate as they move through the upper three layers of skin, the spinosum (SS: Figure 2.3<sup>1</sup>), granulosum (SGR: Figure 2.3<sup>1</sup>), and corneum (SC: Figure 2.3<sup>1</sup>), through a process that involves down regulation of integrin expression and function.<sup>12,13</sup>

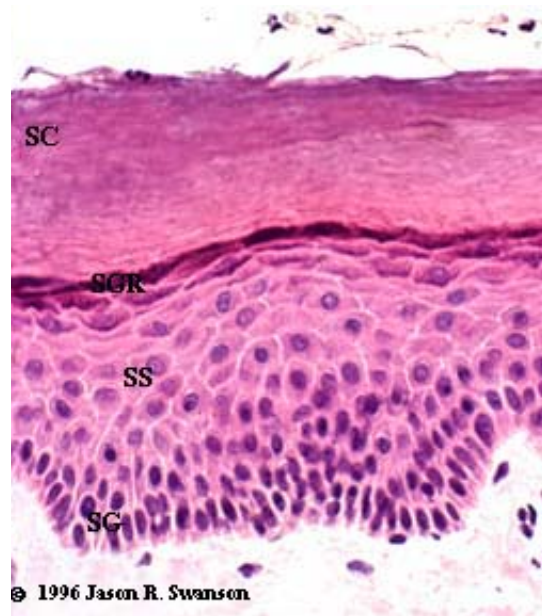


**Figure 2.3 Hematoxylin and Eosin Stained Histological Representation of the Epidermis.** The epidermis is responsible for providing a protective barrier against the surrounding environment. This layer of skin contains four layers, the stratum germinativum (SG), the stratum spinosum (SS), the stratum granulosum (SGR), and the stratum corneum.<sup>1</sup>

As the cells progress through the upper layers of the epidermis, they begin to produce and organize specific keratin filaments responsible for structural integrity of the cytoskeleton as well as water proofing lipids responsible for the permeability barrier. Although these peptides do not play any role in directing epithelial differentiation, their expression is specific

to keratinocyte layer location as well as function of the keratinocyte.<sup>14</sup> Keratinocytes found in the second layer, the stratum spinosum contain 50% more keratin than cells in the basal layer. This additional keratin is responsible for increasing the ability of the cell to sustain mechanical stress.<sup>15</sup> In the uppermost spinous cells and in the third layer of the epidermis, the granulosum, new organelles, lamellar granules, are present which contain a variety of lipids, carbohydrates complexes with protein and lipid, and hydrolytic enzymes. Lamellar granules are exocytosed and generate a waterproof barrier.<sup>16</sup> The stratum granulosum typically contains 1 to 3 rows of squamous cells with these granules and is the highest layer in the epidermis where living cells are found. Above the stratum granulosum is the stratum corneum which is a multilayered zone of terminally differentiated keratinocytes suspended in an extracellular lipid matrix.<sup>17</sup> The number of cell layers found in the stratum corneum varies on location of the body, with thicker skin regions of skin such as the soles and palms containing many more layers than skin regions such as the eyelids that are very thin. Additionally, cornified keratinocytes are much different in morphology and larger in dimension than basal, spinosum, and granulosum cells. A cornified keratinocyte has a more flattened morphology and is 30-40  $\mu\text{m}$  in diameter, whereas a basal keratinocyte has a more square-like morphology and is only 6-8  $\mu\text{m}$  in diameter.<sup>18,19</sup>

### 2.1.3 The Basal Lamina

Located at the dermal-epidermal junction (DEJ) is the basal lamina which conforms to a series of three-dimensional ridges and invaginations formed by papillae located in the papillary region of the dermis (Figure 2.4<sup>20</sup>).<sup>21</sup> The basal lamina is approximately 40-360 nm thick<sup>22</sup> and is composed of collagenous and non-collagenous extracellular matrix (ECM) molecules including type IV collagen, laminin, fibronectin, and heparin sulfate proteoglycans (Figure 2.5<sup>23</sup>). This specialized layer is

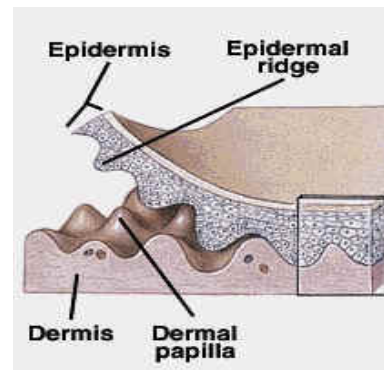


**Figure 2.4 The Topography Found at the Dermal-Epidermal Junction.** At the dermal-epidermal junction there is a series of three-dimensional ridges and invaginations formed by the papillae located in the papillary region of the dermis.<sup>20</sup>

responsible for creating an interface between keratinocytes and the connective tissue of the dermal layer, providing instructive cues to direct keratinocyte polarity, proliferation, and differentiation, as well as preserving tissue architecture and organization. Additionally, the basal lamina acts as a barrier that prevents fibroblasts in the dermal layer from directly contacting epidermal keratinocytes, however, it does not prevent diffusion of macromolecules into or out of the epidermis, nor does it prevent the innervation of the epidermis.<sup>24</sup>

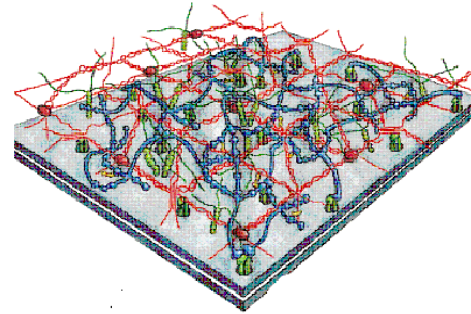


**Figure 2.5 A Model of the Molecular Structure of the Basal Lamina.** Model of interactions between the proteins CIV (red), laminin (blue), nidogen (yellow), and proteoglycans perlecan (green) found to make up the basal lamina.<sup>23</sup>

Several studies have examined the role of basal lamina topography on regulating keratinocyte function. In human palmar epidermis, the highest percentage of proliferating basal and suprabasal cells is in the deeper rete ridges (Figure 2.6<sup>25</sup>).<sup>25,26</sup> It also has been shown that the expression of  $\alpha_2\beta_1$  integrin, a suggested marker of epidermal stem cells, varies with topography. High expression found in patches of basal keratinocytes located on the tips of the dermal papillae or at the bottom of the deep rete ridges suggest that cells in these microenvironments have high proliferation potentials.<sup>11,27,28</sup> The complex topography of the DEJ also provides structural stability to the epidermis. In areas of the skin exposed to excessive friction, the dermal papillae and epidermal ridges are longer and more numerous, suggesting that increased interfacial area between the epidermis and dermis helps provide additional mechanical stability.<sup>29</sup>

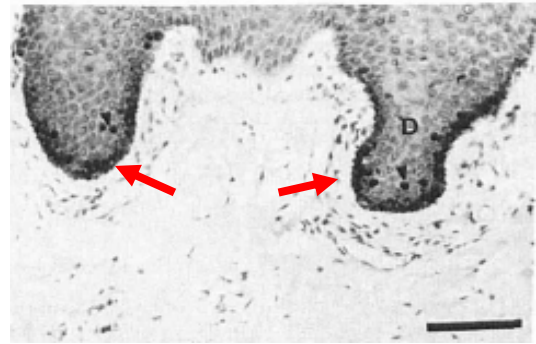


**Figure 2.6 [3H]thymidine Incorporation in Basal Keratinocytes in Bottom of Deep Rete Ridges.** [3H]thymidine was used to evaluate the location of highly proliferative basal keratinocytes. Scale bar represents 50  $\mu\text{m}$  and arrows indicate [3H]thymidine incorporation.<sup>25</sup>



## 2.2 THE PROCESS OF WOUND HEALING

When skin is injured, the body has the ability to regenerate dermal and epidermal tissues. This process is not linear, but is an integration of many complex events involving biochemical factors and multiple cell types. These events overlap and follow a specific time sequence that can be temporally categorized into three separate steps: inflammation, cell proliferation and matrix deposition, and matrix remodeling (Figure 2.7<sup>30</sup>). During inflammation, blood coagulation and platelet aggregation generate a clot that plugs severed vessels and provides a temporary repair of the injured skin. The fibrin rich clot also provides a provisional matrix for neutrophils which are important for the removal of bacteria and debris from the wounded site.<sup>31,32</sup>

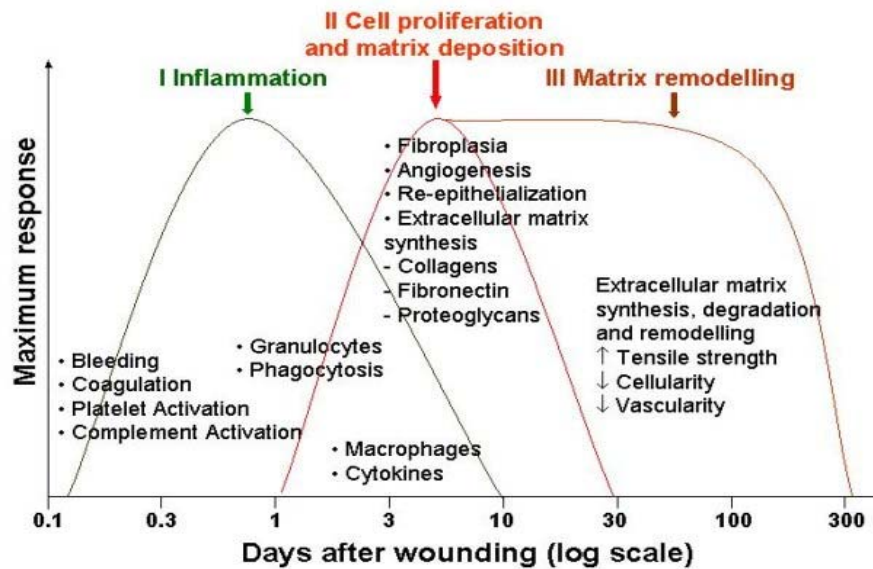


**Figure 2.7 Phases of Repair in Normal Cutaneous Wound Healing.** The process of wound healing is not linear, but is an integration of many complex events that can be temporally categorized into three separate steps: inflammation, cell proliferation and matrix deposition, and matrix remodeling.<sup>30</sup>

Cytokines released by platelets found in the clot as well as the provisional matrix provided by the clot are important mediators involved in the tissue formation phase. Within hours of injury, keratinocytes respond to chemotactic and mitogenic factors as well as the loss of contact with neighboring cells and begin to migrate laterally through the wound to reestablish

a cutaneous cover.<sup>33,34</sup> As reepithelialization of the wound ensues, keratinocytes located behind the actively migrating keratinocytes begin to proliferate (1-2 days post injury)<sup>35</sup> and basement membrane proteins begin to reappear from the margin of the wound inward.<sup>33,34</sup>

Three to 4 days post injury, granulation tissue begins to form. The fibrin clot provides a scaffold to promote contact guidance and acts as a reservoir for cytokines to promote the migration of fibroblasts, macrophages, and blood vessels into the wound site.<sup>36</sup> Macrophages are responsible for providing a continuing source of growth factors necessary to stimulate fibroplasias and angiogenesis,<sup>37</sup> fibroblasts dynamically interact with the extracellular matrix to synthesize, deposit, and remodel the provisional matrix,<sup>38,39</sup> and blood vessels carry oxygen and nutrients to allow for new tissue formation.<sup>34</sup>

Approximately 2 to 3 weeks post wounding, granulation tissue is well established. In this tissue, TGF- $\beta$ 1 and other growth factors activate fibroblasts to transform into myofibroblasts which can be characterized by large bundles of actin containing microfilaments and the capacity to generate contractile forces.<sup>37</sup> The appearance of myofibroblasts corresponds with connective tissue compaction and contraction of the wound.<sup>34</sup> The remodeling of collagen during the transition from granulation tissue to scar is dependent on collagen degradation and synthesis as well as the interaction of the matrix with myofibroblasts. Newly formed collagen fibrils have the ability to make covalent crosslinks with themselves as well as with the collagen bundles of the adjacent dermis.<sup>40,41</sup> Myofibroblasts interact with these fibrils, as well as with themselves and a combination of the collagen-collagen, collagen-cell, and cell-cell interactions provides the network which causes contraction across the wound and results in scarring of the tissue.<sup>42</sup> By the third week after the initial injury, wounds only have 20% of their final strength and thereafter the rate at which the wound gains tensile strength is slow and correlates with the rate of collagen accumulation. The maximum final strength of a scar never reaches maximum strength of uninjured skin, and at best is 70% as strong.<sup>43</sup>

### **2.3 SEVERE SKIN INJURIES**

Although the epidermis and dermis have the ability to heal on their own when injured, there are situations when the damage exceeds the capacity for normal regeneration, and if not treated may result in infection, scarring, amputation, or even death of the individual. The most common cause of significant skin loss occurs from thermal injury. In the United States, more than 2.5 million burn injuries are reported annually.<sup>44</sup> Severe burns result in 60,000-80,000 hospitalizations and costs for recovery from acute injuries range from \$36,000-1117,000 per patient.<sup>45,46</sup> It is reported that 4,500 deaths occur annually,<sup>45</sup> however, advances in the initial resuscitation phase of wound care have led to a decline in mortality.<sup>47</sup> Currently, most patients survive burns that cover 50% of their total body surface area and half of children who receive burns that cover 98% of their total body surface area survive.<sup>48</sup> Other causes of skin loss include diabetic and venous as well as pressure sores which affect an additional 3 to 4 million people in the United States annually. Sadly enough, the statistics for diabetic ulcers as well as venous and pressure sores are only expected to increase with the increase incidences of diabetes as well as the increase age of the average population. This predicted rise in statistics along with the increase in survival rate of increased total body surface burns, and a nearly epidemic increase in burn incidents has led to an increase need for wound management products. It is expected that the burn treatment market will grow in revenues reaching \$2.6 billion by 2011, with a compound annual growth rate of 6.9% during that timeframe.<sup>49</sup>

### **2.4 CURRENT THERAPEUTIC STRATEGIES**

Autografting, which has been considered the preferred treatment for coverage of excised wounds, consists of removing healthy skin from the patient's body using a dermatome and placing in onto the wound bed. At present, most full thickness wounds are best closed with a split thickness autograft that contains the dermis and portion of the epidermis. While this option is considered the "gold standard" it is often limited for patients with large burns or skin traumas due to the lack of available donor sites as well as patients suffering from diabetes due to their already compromised wound healing ability. Additionally, split

thickness autografts are also associated with donor site morbidity.<sup>50</sup> The successful development of a tissue engineered skin substitute that provides permanent coverage to the wound site and restores the anatomy and physiology of uninjured skin will have an enormous impact on the care of patients with serious burns, chronic ulcers, and pressure sores.

## **2.5 BIOENGINEERED SKIN SUBSTITUTES**

To address the limitations of autografts for serious skin injuries, tissue engineers have devised methods that combine cultured cells, biomaterials, or composites of these to provide a new alternative therapeutic approach to treating severe skin injuries. The ultimate objective for these bioengineered skin substitutes is to reestablish the anatomy and physiology of native skin after placement in the wound bed.<sup>51</sup>

### **2.5.1 Design Considerations**

In order to develop the ideal bioengineered skin substitute there are several clinical and engineering design criteria that must be met. These bioengineered skin substitutes should be readily available off-the-shelf, inexpensive, possess physical and mechanical properties that facilitate easy handling, suturing, and adhesion to the wound bed, prevent water loss, and act as a microbial barrier. To minimize scarring and to actively promote regeneration of native skin functionality, engineered skin substitutes should also integrate with native host tissue, delivering growth factors, cytokines and ECM components that direct host cells to facilitate angiogenesis, neodermal, and neoepidermal regeneration. Specifically, the design of future skin substitutes must direct cellular migration, proliferation, and differentiation as well as cellular processes that mediate the morphogenesis of cells into analogs of functional skin that promote rapid barrier formation, reduce healing times, and restore the native tissue physiology.<sup>50,52</sup>

### **2.5.2 Current Bioengineered Skin Substitutes**

To date no bioengineered skin substitute has been developed that replaces skin in its entirety. Conceptually, bioengineered skin substitutes offer either temporary, semi-permanent, or

permanent coverage, composed of epidermal, dermal, or a composite of the two, and are either made from biological or synthetic materials.<sup>50</sup> Table 2.1 provides a summary of commercially available bioengineered skin substitutes including a cartoon schematic of the layers, the preservation technique used, and the development status of the product.

### **2.5.2.1 Temporary Bioengineered Skin Substitutes-Wound Dressings**

Temporary bioengineered skin substitutes are designed to provide physiologic wound closure, protection from mechanical trauma and bacteria, and allow vapor transmission to occur between the wound bed and the environment. Common uses of temporary bioengineered skin substitutes fall into the following categories: (i) a dressing for a donor site or for superficial wounds, (ii) to provide temporary wound closure while waiting for an autograft, and (iii) to test if an autograft would succeed in a questionable wound bed. Currently, there are three main types of temporary bioengineered skin substitutes available consisting of xenografts, synthetic membranes, and allogenic substitutes.<sup>50</sup>

Skin xenografts are skin from one species grafted onto another species and have been used since 1500 BC to provide temporary cover of wounds. The most commonly used species for xenografts for humans are domestic swine, however skin from frog, lizard, and dog have also been used. Although there have been many favorable reports using xenografts for wound closure, these tissues have many problems including availability, storage, rejection, and the short life of a living tissue.<sup>50</sup>

Synthetic membranes for use as temporary bioengineered skin substitutes are designed to be semipermeable to provide protection against bacteria, while allowing for proper vapor exchange between the wound and the environment. Additionally, synthetic membranes also help to control pain while the underlying superficial wound or donor site re-epithelializes. Biobrane® (Dow-Hickham, Sugarland, TX) is a commercially available temporary bioengineered skin substitute which was first developed in 1979. This product consists of both a dermal and an epidermal analog. The dermal analog is composed of a complex three-

dimensional structure of trifilament thread to which bovine collagen has been chemically bound and allows for fibrovascular ingrowth. The epidermal portion is composed of silastic that serves as a vapor and bacterial barrier.<sup>53</sup> Biobrane® meets many of the important properties and is the most commonly used bioengineered skin substitute for partial thickness burns or excised wounds. Although this product helps restore normal tissue architecture as well as preventing scar contracture, it is not a permanent solution, and autologous keratinocytes are required to provide an epithelial barrier.<sup>54</sup>

Allogenic substitutes are another form of temporary bioengineered skin substitutes. These bioengineered skin substitutes consist of split thickness human cadaver grafts that contain both dermal and epithelial cell layers. Allogenic skin substitutes do not provide permanent coverage because of host rejection and are limited in use based on disease transmission and need for donated cadaver tissue.<sup>55-57</sup>

#### **2.5.2.2 Bioengineered Epidermal Skin Substitutes**

Restoring an epidermal layer that provides a barrier against fluid loss and infection is critical to wound healing and skin regeneration. In the mid 1970s, Rheinwald and his colleagues developed *in vitro* techniques to subculture keratinocytes into large confluent sheets of epithelial tissues.<sup>58,59</sup> These cultured epithelial autografts (CEAs) are enzymatically removed from the culture substrate and placed onto the wound of the patient. This technique provides clinicians with large areas of epithelial wound dressing from small pieces of biopsy tissue.

Clinical trials demonstrated that CEAs were a major surgical innovation, providing permanent coverage to large surface area burns as well as to acute and chronic wounds. Genzyme Tissue Repair is a commercially available CEA product that provides permanent wound coverage.<sup>60</sup> While this product and other CEAs provide acceptable cosmetic results and eventually regenerate dermal tissue, there are several limitations. Cultured epithelial autografts require biopsies from the patients and a 2-3 week interval to produce sufficient quantities of graft material. Additionally, CEAs are thin and fragile, very expensive, and they

require custom preparation. They also fail to provide adequate epithelial coverage, blistering often occurs, and engraftment rates are suboptimal.<sup>50,61-63</sup> One of the primary reasons for suboptimal graft integration is the enzymatic treatment required to remove the cultured CEA from the culture plate. This treatment disrupts keratinocyte interactions with the underlying ECM proteins that are deposited on the substrate and causes contraction of the CEA. Furthermore, this process decreases mechanical stability of the grafts and hinders their attachment to wound beds.<sup>61,64</sup>

To improve the durability and the engraftment rate of CEAs, several investigators have attempted to create carrier devices that support keratinocyte culture which can be transferred to the wound bed, eliminating the need for enzymatic treatment prior to implantation. Microfabrication techniques have been used to create support scaffolds with microenvironments that emulate native tissue properties and promote keratinocyte attachment as well as the deposition of cell-mediated ECM proteins. Fidia Advanced Biopolymers, Inc., developed a 100% benzyl esterified hyaluronic acid derivative (HYAFF-11<sup>®</sup>) that can be manufactured into thin transparent membranes with thicknesses of 20 or 200  $\mu\text{m}$  (Laserskin<sup>™</sup>).<sup>65</sup> This product allows keratinocytes to grow to confluence and findings have demonstrated that CEAs cultured on Laserskin<sup>™</sup> can be transferred to wound beds in a shorter time period, then culturing alone, substantially reducing the time required to wait for cultured autologous epithelial cells.<sup>66,67</sup> Additionally keratinocytes have also been delivered to the wound intermixed with fibrin sealant as a spray<sup>68</sup> or grown on fibrin glue and placed in the wound bed.<sup>69,70</sup>

The results of studies using CEAs to transplant epithelial layers indicate that the presence of a dermal substitute pregrafted in the wound site enhances the function and the quality of the regenerating tissue. When full thickness wounds were treated with CEAs alone, or with CEAs on carrier devices, engraftment rates were less effective than when CEAs were applied to a dermal wound bed that was prepared with an allograft, autologous dermal tissue, or an engineered dermal substitute.<sup>50,65,66,71-75</sup> A functioning dermal layer allows for increased

vascularization and improves initial engraftment rates and as well as long term durability. Additionally, a dermal component that contains fibroblasts provides a regulatory environment that contains both biochemical and structural cues to direct the growth and differentiation of keratinocytes in CEAs.<sup>76,77</sup> These findings suggest that future research efforts should focus on the development of cell seeded dermal substitutes to augment the regenerative properties of epidermal scaffolds.

### **2.5.2.3 Bioengineered Dermal Skin Substitutes**

To promote dermal regeneration, Yannas and his colleagues pioneered the use of a collagen-glycosaminoglycan (GAG) sponge coupled with a silicone membrane barrier that acts as a temporary wound covering.<sup>78,79</sup> The collagen-GAG sponge promotes vascularized neodermal formation and the silicone layer is eventually replaced with a thin epidermal autograft.<sup>80</sup> This dermal material has been successful in treating burns and has received FDA approval for this indication (Integra, LifeSciences Corporation, Plainsboro, NJ).<sup>60,80</sup> Although Integra has achieved some clinical success, a second surgical procedure is necessary to reepithelialize the surface, and the cosmetic appearance of the regenerated skin is often flat and featureless.

Additional acellular products that are on the market that serve as dermal substitutes are Alloderm® (LifeCell Corporation, Woodlands, TX) which is cadaver skin that has been chemically treated to decellularize and remove immunogenic cellular elements. This product has been effectively used alone or in combination with cultured autologous keratinocytes for closure of burns and chronic wounds. Decellularized allografts are advantageous because the dermal component retains the biochemical components of the basement membrane, the microtopology, and the porosity of native dermis,<sup>81,82</sup> Although these analogs have proven successful in increasing the regenerative healing process, their limitations include the potential of disease transmission, high cost, second donor site, and the need for donated cadaver tissue.<sup>64,83-86</sup>



Hyalomatrix® (Fidia Advanced Biopolymers, srl) is another type of acellular dermal replacement that consists of an acellular hyaluronic acid matrix with esterification. Fidia Advanced Biopolymers, srl as well as Advanced BioHealing have developed cellular dermal replacement products that contain fibroblasts. Hyalograft-3D® (Fidia Advanced Biopolymers) incorporates autologous fibroblasts into their esterified hyaluronic acid matrix, whereas Dermagraft (Advanced BioHealing) incorporates human foreskin fibroblasts into a biodegradable polyglactin mesh. Currently, Dermagraft is off of the market and further production is ongoing to improve the product.

While each of these design strategies has produced bioengineered skin substitutes that have achieved some clinical success in restoring damaged skin, the need for a second surgery, prolonged healing times, scarring and limited tissue functionality remain persistent problems. As such, future tissue analogs must incorporate both epidermal and dermal components in order to restore a fully functional tissue that is both anatomically and physiologically comparable to native skin.

#### **2.5.2.4 Bioengineered Composite Skin Substitutes**

Research has shown that when a CEA is engrafted onto a wound bed pretreated with a dermal substitute, the number of successful engraftments are increased, thus effort has been focused on developing a composite skin graft that consists of both dermal and epidermal layers.<sup>50,65,66,71-75</sup> One of the first attempts to create a composite skin graft was by Bell et al.<sup>87</sup> who combined a gel of type I bovine collagen with living allogenic neonatal fibroblasts. On the surface of the collagen gel, allogenic neonatal keratinocytes were cultured and over time created a stratified cornified barrier layer. Apligraf (Organogenesis Inc, Canton, MA and Novartis Pharmaceuticals Corporation, NJ) is a commercially available composite bioengineered skin substitute that utilizes this technology. Its primary role is as a treatment for chronic ulcers. The efficacy of the product in healing venous ulcers was evaluated and it was found that the product was three times more effective than compression therapy alone in achieving complete wound closure at 8 weeks.<sup>88-91</sup>




OrCel is another composite skin graft. This product was developed for the treatment of dystrophic epidermal biolysis, and then further developed by Ortec International (New York, NY) and is now FDA approved for the treatment of burns. This product, like Apligraf, consists of type I bovine collagen that contains fibroblasts and an epithelial layer on the surface. The major difference between the two products is that the fibroblasts in OrCel are seeded into a preformed collagen sponge whereas Apligraf the fibroblasts are seeded within a collagen gel that then polymerizes.

An additional composite system was developed by Boyce and his colleagues, who have modified the first approach taken by Yannas et al.<sup>78,79</sup> Their modified approach to create a composite skin substitute consists of a porous collagen-GAG sponge with fibroblasts and then culturing a flat epidermal layer on the laminated surface of the sponge.<sup>92,93</sup> In clinical studies, these composite skin substitutes showed some success for the treatment of full-thickness burns, although engraftment rates were suboptimal.<sup>94,95</sup>





## **2.6 CONCLUSIONS**

Overall, composite skin grafts offer an approach for an artificial full thickness skin graft that can be applied in one surgery for the treatment of chronic ulcers and burns. The duration of these products however, is limited and they only persist for approximately 4 weeks. Additionally, prolonged healing times and mechanically induced graft failure remain persistent problems. A design feature common to each of these skin substitutes is a flat interface between the epidermal and dermal components. In native skin, this interface both topographically and biochemically, provided by the dermal papillae and basal lamina, respectively, is an important feature for maintaining homeostasis of skin. The design of future skin substitutes must examine the mechanisms by which the three-dimensional architecture and biochemical composition of tissue scaffolds modulate cellular adhesion, proliferation and differentiation, as well as regeneration of dermal and epidermal tissues.



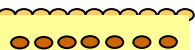

**Table 2.1 Summary of Commercially Available Bioengineered Skin Substitutes**

Application	Composition	Product	Schematic Representation	Layers		Preservation Technique	Development Status
				Epidermal	Dermal		
<b>Temporary Wound Coverage</b>	Acellular	Biobrane® (Dow Hickman Pharmaceuticals, Inc., Sugarland, TX)		Silastic layer. Need for autograft.	Trifilament nylon fabric with bovine collagen chemically bound.	Stored at 25°C	FDA approval for ulcers, lacerations, and full-thickness burns.
		TransCyte® (Advanced BioHealing, Inc., La Jolla, CA)		Silicon covering. Need for autograft.	Nylon mesh with human foreskin fibroblasts that undergo freeze thaw after ECM and growth factor production.	Cryopreserved	FDA approval for temporary wound coverage for burns and diabetic foot ulcers, however not on market and further development is ongoing.
	Cellular	Cadaveric allografts (from nonprofit skin banks)		Epidermal layer of human skin.	Dermal layer of human skin.	Glycerolized	FDA approval for burns and scar revision.

**Table 2.1 Summary of Commercially Available Bioengineered Skin Substitutes - continued**

Application	Composition	Product	Schematic Representation	Layers		Preservation Technique	Development Status
				Epidermal	Dermal		
<b>Epidermal Replacement</b>	Cellular	Epicel™ (Genzyme Tissue Repair, Cambridge, MA)		Cultured epithelial autograft.	None. Placed onto wound bed.	Stored at 37°C	FDA approved for treatment of burns, chronic ulcers, diabetic leg ulcers, donor sites, and scar revision.
		Laserskin™ (Fidia Advanced Biopolymers srl, Abano Terme, Italy)		Cultured epithelial autograft on hyaluronic acid with laser perforations.	None. Place onto wound bed.	Stored in cool dry place	FDA approval for biodegradable keratinocyte delivery system.
<b>Dermal Replacement</b>	Acellular	Integra™ (Life Sciences Corporation, Plainsboro, NJ)		Silicone covering. Need for autograft.	Bovine collagen I and chondroitin-6-sulfate from shark cartilage.	Isopropyl alcohol at 2-8°C	FDA Approval for treatment of burns and scar revision.
		Alloderm® (LifeCell Corporation, Woodlands, TX)		None. Need for autograft,	Acellular deepithelialized cadaver dermis.	Lyophilized	FDA Approval for burns and scar revision.

**Table 2.1 Summary of Commercially Available Bioengineered Skin Substitutes - continued**

Application	Composition	Product	Schematic Representation	Layers		Preservation Technique	Development Status
				Epidermal	Dermal		
<b>Dermal Replacement</b>	Cellular	Dermagraft® (Advanced BioHealing, La Jolla, CA)		None. Need for autograft.	Human foreskin fibroblasts cultured in biodegradable polyglactin mesh.	Cryopreserved	FDA Approval for burns and diabetic Foot Ulcers, however off the market and further production and marketing is ongoing.
		Hyalograft-3D® (Fidia Advanced Biopolymers srl, Abano Terme, Italy)		Silicone covering. Need for autograft.	Esterified hyaluronic acid matrix with autologous fibroblasts.	Store in cool, dry place	FDA Approval for burns and diabetic foot ulcers.
<b>Composite Replacement</b>	Cellular	Apligraf® (Organogenesis, Canton, MA and Novartis Pharmaceuticals, East Hanover, NJ)		Neonatal foreskin keratinocytes.	Bovine collagen I with neonatal foreskin fibroblasts.	Stored at 37°C	FDA approval for burns, and venous and diabetic ulcers.
		OrCel™ (Ortec International Inc., New York, NY)		Allogenic keratinocytes cultured on bilayered collagen matrix.	Bilayered matrix of bovine collagen I with fibroblasts.	Stored at 37°C	FDA approval for burns.

## 2.7 REFERENCES

1. Swanson J, Melton J. Anatomy and Histology of Normal Skin. Dermatology Atlas: Loyola University Dermatology Medical Education Website 1996.
2. Parenteau NL, Hardin-Young, J., and Ross, R.N. Skin. In: Vacanti J, editor. Principles of Tissue Engineering. San Diego: Academic Press; 2000.
3. Bush KA, Pins GD. Nano- and Microtechnologies for Development of Engineered Skin Substitutes. In: Khademhosseini A, Borenstein J, Toner M, Takayama S, editors. Micro and Nanoengineering of the Cell Microenvironment: Technologies and Applications. Boston: Artech House; 2008.
4. Harper RA, Grove G. Human skin fibroblasts derived from papillary and reticular dermis: differences in growth potential in vitro. *Science* 1979;204(4392):526-7.
5. Tajima S, Pinnell SR. Collagen synthesis by human skin fibroblasts in culture: studies of fibroblasts explanted from papillary and reticular dermis. *J Invest Dermatol* 1981;77(5):410-2.
6. Holbrook K. Ultrastructure of the epidermis. In: Leigh IM, Lane EB, Watt FM, editors. The Keratinocyte Handbook. New York: Press Syndicate of the University of Cambridge; 1994. p 3-39.
7. Potten CS, Morris RJ. Epithelial stem cells in vivo. *J Cell Sci Suppl* 1988;10:45-62.
8. Jones PH. Epithelial stem cells. *Bioessays* 1997;19(8):683-90.
9. Potten CS. Cell replacement in epidermis (keratopoiesis) via discrete units of proliferation. *Int Rev Cytol* 1981;69:271-318.
10. Jones PH, Watt FM. Separation of human epidermal stem cells from transit amplifying cells on the basis of differences in integrin function and expression. *Cell* 1993;73(4):713-24.
11. Jones PH, Harper S, Watt FM. Stem cell patterning and fate in human epidermis. *Cell* 1995;80(1):83-93.
12. Adams JC, Watt FM. Changes in keratinocyte adhesion during terminal differentiation: reduction in fibronectin binding precedes alpha 5 beta 1 integrin loss from the cell surface. *Cell* 1990;63(2):425-35.
13. Hotchin NA, Gandarillas A, Watt FM. Regulation of cell surface beta 1 integrin levels during keratinocyte terminal differentiation. *J Cell Biol* 1995;128(6):1209-19.
14. Gu LH, Coulombe PA. Keratin function in skin epithelia: a broadening palette with surprising shades. *Curr Opin Cell Biol* 2007;19(1):13-23.
15. Markova NG, Marekov LN, Chipev CC, Gan SQ, Idler WW, Steinert PM. Profilaggrin is a major epidermal calcium-binding protein. *Mol Cell Biol* 1993;13(1):613-25.
16. Holbrook KA. Biologic structure and function: perspectives on morphologic approaches to the study of the granular layer keratinocyte. *J Invest Dermatol* 1989;92(4 Suppl):84S-104S.
17. Potts RO, Francoeur ML. The influence of stratum corneum morphology on water permeability. *J Invest Dermatol* 1991;96(4):495-9.
18. Kligman AM. The biology of the stratum corneum. In: Montagna W, Lobitz WC, editors. The Epidermis. New York: Academic Press; 1964. p 387-433.
19. Holbrook KA. Ultrastructure of the epidermis. In: Leigh I, Lane B, Watt FM, editors. The Keratinocyte Handbook. New York: Cambridge University Press; 1994. p 3-39.
20. Martini F, Nath J. Fundamentals of Anatomy and Physiology (8th Edition) Benjamin Cummings; 2005, page 159.
21. Young B, Burkitt HG, Heath JW, Wheeler PR. Wheeler's Functional Histology: Figure 9.2.
22. Jastrow H. Workshop Anatomy for the Internet: Electron Microscopic Atlas of cells, tissues, and organs. Overview basement membrane and basal lamina Mainz, Germany; 1998.
23. Alberts ea. Molecular Biology of The Cell. New York: Garland Science; 2002.
24. Burgeson RE. Basement Membranes. Dermatology in General Medicine. New York, NY: McGraw-Hill; 1987. p 288-303.
25. Lavker RM, Sun TT. Heterogeneity in epidermal basal keratinocytes: morphological and functional correlations. *Science* 1982;215(4537):1239-41.
26. Lavker RM, Sun TT. Epidermal stem cells. *J Invest Dermatol* 1983;81(1 Suppl):121s-7s.

27. Carter WG, Symington BE, Kaur P. Cell adhesion and the basement membrane in early epidermal morphogenesis. In: Fleming TP, editor. *Epithelial Organization and Development*. London: Chapman and Hall; 1992. p 299-327.
28. Jensen UB, Lowell S, Watt FM. The spatial relationship between stem cells and their progeny in the basal layer of human epidermis: a new view based on whole-mount labelling and lineage analysis. *Development* 1999;126(11):2409-18.
29. Odland GF. The morphology of the attachment between the dermis and the epidermis. *Anat Rec* 1950;108(3):399-413.
30. Enoch S, Price P. Cellular, molecular and biochemical differences in the pathophysiology of healing between acute wounds, chronic wounds and wound in the aged. *World Wide Wounds (Online Publication)* 2004.
31. Clark RA, Singer AJ. *Wound Repair: Basic Biology to Tissue Engineering*. In: Lanza RP, Langer R, Vacanti J, editors. *Principles of Tissue Engineering, Second Edition*. Boston: Academic Press; 2000. p 857-878.
32. Clark RAF. *Wound Repair: Overview and General Considerations*. In: Clark RAF, editor. *The Molecular and Cellular Biology of Wound Repair (Second Edition)*. New York, NY: Plenum Press; 1995.
33. Clark RA, Lanigan JM, DellaPelle P, Manseau E, Dvorak HF, Colvin RB. Fibronectin and fibrin provide a provisional matrix for epidermal cell migration during wound reepithelialization. *J Invest Dermatol* 1982;79(5):264-9.
34. Singer AJ, Clark RA. Cutaneous wound healing. *N Engl J Med* 1999;341(10):738-46.
35. Krawczyk WS. A pattern of epidermal cell migration during wound healing. *J Cell Biology* 1971;49:247-263.
36. Nathan C, Sporn M. Cytokines in context. *J Cell Biol* 1991;113(5):981-6.
37. Clark R. *Wound Repair, Overview and General Considerations*. In: Clark R, editor. *The Molecular and Cellular Biology of Wound Repair (Second Edition)*. New York: Plenum Press; 1995. p 3-44.
38. Kurkinen M, Vaehri A, Roberts PJ, Stenman S. Sequential appearance of fibronectin and collagen in experimental granulation tissue. *Lab Invest* 1980;43(1):47-51.
39. Welch MP, Odland GF, Clark RA. Temporal relationships of F-actin bundle formation, collagen and fibronectin matrix assembly, and fibronectin receptor expression to wound contraction. *J Cell Biol* 1990;110(1):133-45.
40. Yamauchi M, London RE, Guenat C, Hashimoto F, Mechanic GL. Structure and formation of a stable histidine-based trifunctional cross-link in skin collagen. *J Biol Chem* 1987;262(24):11428-34.
41. Birk DE, Zycband EI, Winkelmann DA, Trelstad RL. Collagen fibrillogenesis in situ: fibril segments are intermediates in matrix assembly. *Proc Natl Acad Sci U S A* 1989;86(12):4549-53.
42. Singer, II, Kawka DW, Kazazis DM, Clark RA. In vivo co-distribution of fibronectin and actin fibers in granulation tissue: immunofluorescence and electron microscope studies of the fibronexus at the myofibroblast surface. *J Cell Biol* 1984;98(6):2091-106.
43. Levenson SM, Geever EF, Crowley LV, Oates JF, 3rd, Berard CW, Rosen H. *The Healing of Rat Skin Wounds*. *Ann Surg* 1965;161:293-308.
44. *Burn incidence and treatment in the United States: 1999 Fact Sheet*. Philadelphia, PA: The Burn Foundation; 1999.
45. Brigham PA, McLoughlin E. Burn incidence and medical care use in the United States: estimates, trends, and data sources. *J Burn Care Rehabil* 1996;17(2):95-107.
46. Saffle JR, Davis B, Williams P. Recent outcomes in the treatment of burn injury in the United States: a report from the American Burn Association Patient Registry. *J Burn Care Rehabil* 1995;16(3 Pt 1):219-32; discussion 288-9.
47. Supp DM, Boyce ST. Engineered skin substitutes: practices and potentials. *Clin Dermatol* 2005;23(4):403-12.
48. Rose JK, Herndon DN. Advances in the treatment of burn patients. *Burns* 1997;23 Suppl 1:S19-26.

49. Carlson B. BioMarket Trends: Phalanx of Treatments Propels Burn Market: Recombinant Growth Factor Therapies Are Predicted to Be Up-and-Coming Players. *Genetic Engineering and Biotechnology News* 2008.
50. Sheridan RL, Tompkins RG. Skin substitutes in burns. *Burns* 1999;25(2):97-103.
51. Boyce ST. Design principles for composition and performance of cultured skin substitutes. *Burns* 2001;27(5):523-33.
52. Bush KA, Pins GD. Nano- and Microtechnologies for the Development of Engineered Skin Substitutes. In: Khademhosseini A, Borenstein J, Toner M, Takayama S, editors. *Micro and Nanoengineering of the Cell Microenvironment*. Boston: Artech House; 2008. p 579-600.
53. Demling R. Use of the Temporary Skin Substitute, BIOBRANE® In the Management of Partial Thickness Burns and Wounds. *Journal of Burns and Wounds* (online journal).
54. Burn Care: Biobrane. UDL Laboratories, Inc. 2005.
55. Boyce ST. Cultures Skin Substitutes: A Review. *Tissue Eng* 1996;2:255-266.
56. Ghosh MM, Boyce S, Layton C, Freedlander E, Mac Neil S. A comparison of methodologies for the preparation of human epidermal-dermal composites. *Ann Plast Surg* 1997;39(4):390-404.
57. Wong T, McGrath JA, Navsaria H. The role of fibroblasts in tissue engineering and regeneration. *Br J Dermatol* 2007;156(6):1149-55.
58. Green H, Kehinde O, Thomas J. Growth of cultured human epidermal cells into multiple epithelia suitable for grafting. *Proc Natl Acad Sci U S A* 1979;76(11):5665-8.
59. Rheinwald JG, Green H. Formation of a keratinizing epithelium in culture by a cloned cell line derived from a teratoma. *Cell* 1975;6(3):317-30.
60. Clark RA, Ghosh K, Tonnesen MG. Tissue engineering for cutaneous wounds. *J Invest Dermatol* 2007;127(5):1018-29.
61. Compton CC, Gill JM, Bradford DA, Regauer S, Gallico GG, O'Connor NE. Skin regenerated from cultured epithelial autografts on full-thickness burn wounds from 6 days to 5 years after grafting. *Lab Invest* 1989;60:600-612.
62. Gallico 3rd GG, O'Connor NE, Compton CC, Kehinde O, Green H. Permanent coverage of large burn wounds with autologous cultured human epithelium. *N. Engl. J. Med.* 1984;311:448-451.
63. Sheridan RL, Tompkins RG. Cultured autologous epithelium in patients with burns of ninety percent or more of the body surface. *J Trauma* 1995;38:48-50.
64. Jones I, Currie L, Martin R. A guide to biological skin substitutes. *Br J Plast Surg* 2002;55(3):185-93.
65. Lam PK, Chan ESY, Liew CT, Lau CH, Yen SC, King WWK. Development and evaluation of a new composite Laserskin graft. *J Trauma* 1999;47:918-22.
66. Lam PK, Chan ESY, Liew CT, Lau CH, Yen SC, King WWK. Combination of a new composite biocompatible skin graft on the neodermis of artificial skin in an animal model. *ANZ Journal of Surgery* 2002;72:360-363.
67. Rennekampff HO, Kiessig V, Hansbrough JF. Current concepts in the development of cultured skin replacements. *J Surg Res* 1996;62(2):288-95.
68. Grant I, Warwick K, Marshall J, Green C, Martin R. The co-application of sprayed cultured autologous keratinocytes and autologous fibrin sealant in a porcine wound model. *Br J Plast Surg* 2002;55(3):219-27.
69. Ronfard V, Broly H, Mitchell V, Galizia JP, Hochart D, Chambon E, Pellerin P, Huart JJ. Use of human keratinocytes cultured on fibrin glue in the treatment of burn wounds. *Burns* 1991;17(3):181-4.
70. Ronfard V, Rives JM, Neveux Y, Carsin H, Barrandon Y. Long-term regeneration of human epidermis on third degree burns transplanted with autologous cultured epithelium grown on a fibrin matrix. *Transplantation* 2000;70(11):1588-98.
71. Cuono C, Langdon R, McGuire J. Use of cultured epidermal autografts and dermal allografts as skin replacement after burn injury. *Lancet* 1986;1(8490):1123-4.
72. Compton CC, Hickerson W, Nadire K, Press W. Acceleration of skin regeneration from cultured epithelial autografts by transplantation to homograft dermis. *J Burn Care Rehabil* 1993;14(6):653-62.



73. Orgill DP, Butler C, Regan JF, Barlow MS, Yannas IV, Compton CC. Vascularized collagen-glycosaminoglycan matrix provides a dermal substrate and improves take of cultured epithelial autografts. *Plast Reconstr Surg* 1998;102(2):423-9.
74. Kangesu T, Navsaria HA, Manek S, Shurey CB, Jones CR, Fryer PR, Leigh IM, Green CJ. A porcine model using skin graft chambers for studies on cultured keratinocytes. *Br J Plast Surg* 1993;46(5):393-400.
75. Navsaria HA, Kangesu T, Manek S, Green CJ, Leigh IM. An animal model to study the significance of dermis for grafting cultured keratinocytes on full thickness wounds. *Burns* 1994;20 Suppl 1:S57-60.
76. Coulomb B, Lebreton C, Dubertret L. Influence of human dermal fibroblasts on epidermalization. *J Invest Dermatol* 1989;92(1):122-5.
77. Coulomb B, Friteau L, Baruch J, Guilbaud J, Chretien-Marquet B, Glicenstein J, Lebreton-Decoster C, Bell E, Dubertret L. Advantage of the presence of living dermal fibroblasts within in vitro reconstructed skin for grafting in humans. *Plast Reconstr Surg* 1998;101(7):1891-903.
78. Yannas IV, Burke JF, Orgill DP, Skrabut EM. Wound tissue can utilize a polymeric template to synthesize a functional extension of skin. *Science* 1982;215(4529):174-6.
79. Yannas IV, Burke JF, Gordon PL, Huang C, Rubenstein RH. Design of an artificial skin. II. Control of chemical composition. *J Biomed Mater Res* 1980;14(2):107-32.
80. Heimbach D, Luterman A, Burke J, Cram A, Herndon D, Hunt J, Jordan M, McManus W, Solem L, Warden G and others. Artificial dermis for major burns. A multi-center randomized clinical trial. *Ann Surg* 1988;208(3):313-20.
81. Prunieras M, Regnier M, Woodley D. Methods for cultivation of keratinocytes with an air-liquid interface. *J Invest Dermatol* 1983;81(1 Suppl):28s-33s.
82. Andreadis ST, Hamoen KE, Yarmush ML, Morgan JR. Keratinocyte growth factor induces hyperproliferation and delays differentiation in a skin equivalent model system. *Faseb J* 2001;15(6):898-906.
83. Lattari V, Jones LM, Varcelotti JR, Latenser BA, Sherman HF, Barrette RR. The use of a permanent dermal allograft in full-thickness burns of the hand and foot: a report of three cases. *J Burn Care Rehabil* 1997;18(2):147-55.
84. Sheridan R, Choucair R, Donelan M, Lydon M, Petras L, Tompkins R. Acellular allodermis in burns surgery: 1-year results of a pilot trial. *J Burn Care Rehabil* 1998;19(6):528-30.
85. Wainwright DJ. Use of an acellular allograft dermal matrix (AlloDerm) in the management of full-thickness burns. *Burns* 1995;21(4):243-8.
86. Kealey GP, Aguiar J, Lewis RW, 2nd, Rosenquist MD, Strauss RG, Bale JF, Jr. Cadaver skin allografts and transmission of human cytomegalovirus to burn patients. *J Am Coll Surg* 1996;182(3):201-5.
87. Bell E, Ehrlich HP, Buttle DJ, Nakatsuji T. Living tissue formed in vitro and accepted as skin-equivalent tissue of full thickness. *Science* 1981;211(4486):1052-4.
88. Falanga VJ. Tissue engineering in wound repair. *Adv Skin Wound Care* 2000;13(2 Suppl):15-9.
89. Ramsey SD, Newton K, Blough D, McCulloch DK, Sandhu N, Reiber GE, Wagner EH. Incidence, outcomes, and cost of foot ulcers in patients with diabetes. *Diabetes Care* 1999;22(3):382-7.
90. Falanga V, Margolis D, Alvarez O, Auletta M, Maggiasco F, Altman M, Jensen J, Sabolinski M, Jardin-Young J. Rapid healing of venous ulcers and lack of clinical rejection with an allogeneic cultured human skin equivalent. *Arch Dermatol.* 1998;134:293-300.
91. Falanga V, Sabolinski M. A bilayered living skin construct (APLIGRAF) accelerates complete closure of hard-to-heal venous ulcers. *Wound Repair Regen* 1999;7(4):201-7.
92. Boyce ST, Christianson DJ, Hansbrough JF. Structure of a collagen-GAG dermal skin substitute optimized for cultured human epidermal keratinocytes. *J Biomed Mater Res* 1988;22(10):939-57.
93. Boyce ST, Hansbrough JF. Biologic attachment, growth, and differentiation of cultured human epidermal keratinocytes on a graftable collagen and chondroitin-6-sulfate substrate. *Surgery* 1988;103(4):421-31.

94. Hansbrough JF, Boyce ST, Cooper ML, Foreman TJ. Burn Wound Closure with Cultured Autologous Keratinocytes and Fibroblasts Attached to a Collagen-Glycosaminoglycan Substrate. *J Amer Med Assoc* 1989;262(15):2125-2130.
95. Boyce ST, Goretsky MJ, Greenhalgh DG, Kagan RJ, Rieman MT, Warden GD. Comparative assessment of cultured skin substitutes and native skin autograft for treatment of full-thickness burns. *Ann Surg* 1995;222(6):743-52.

---

---

## Chapter 3: Fibronectin Enhances Keratinocyte Attachment to Basal Lamina Analogs

---

### 3.1 INTRODUCTION

Bioengineered skin substitutes composed of biomaterials and cultured cells offer an advanced wound therapy to patients suffering from severe burns and chronic ulcers. Despite favorable results with these analogs, there is still a need to improve the rate at which autologous keratinocytes attach, populate, and epithelialize the surface of the biomaterial scaffold, as well as to improve the integration of the analog with the surrounding environment.<sup>1-4</sup> Optimizing current design strategies requires understanding the underlying mechanisms by which the biochemical composition of native skin modulates keratinocyte adhesion, proliferation, and differentiation.<sup>5-7</sup> Current knowledge indicates that during the initial phase of reepithelialization, basal and suprabasal keratinocytes interact directly with dermal collagens as well as with other extracellular matrix (ECM) proteins found in the wound environment.<sup>8,9</sup> These initial cell-ECM adhesions are responsible for initiating and controlling subsequent cellular signaling events.<sup>10-12</sup>

To elucidate relationships between ECM cues and keratinocyte functions related to epithelial morphogenesis, investigators have examined the mechanisms that modulate cell attachment, proliferation, and terminal differentiation in tissue culture models<sup>13-15</sup> and on engineered scaffolds.<sup>16-19</sup> Studies using bacteriological plastic have found that when type I collagen (CI), type IV collagen (CIV), laminin (LN), and fibronectin (FN) were present on the surfaces, the percentage of adherent keratinocytes depended on the concentration of the ECM protein used, with FN having a significantly greater effect on overall cellular attachment.<sup>21</sup> Collagen type I, CIV, LN, and FN have also been investigated on polystyrene, and a higher percentage

of basal keratinocytes adhered to CIV than to polystyrene, indicating a potential use of ECM proteins in selecting for discrete populations of keratinocytes. In addition to attachment studies, CI, LN, and FN have also been found to affect migration, proliferation, and differentiation of keratinocytes. Adsorption of CI on both poly(lactide-glycolide) (PLGA) and polystyrene substrates enhanced keratinocyte migration,<sup>16,19</sup> adsorption of LN on polystyrene stimulated keratinocyte migration and proliferation,<sup>19,22</sup> and adsorption of FN on polystyrene promoted keratinocyte migration and inhibited terminal differentiation (Table 3.1).<sup>16,23</sup> Additionally, keratinocyte attachment to biomaterial surfaces that have been conjugated with bioactive sequences that mimic cell binding domains of ECM proteins have been investigated. Sequences for LN were found to enhance keratinocyte attachment on polystyrene<sup>24</sup> and collagenous material modified with arginine-glycine-aspartic acid (RGD) peptides greatly promoted keratinocyte attachment.<sup>18</sup> Together, these studies demonstrate that biochemically modified substrates can be used to examine the mechanisms by which ECM proteins direct keratinocyte function. These findings also suggest that precisely designed biomaterials can be used to enhance the performance of bioengineered skin substitutes.

**Table 3.1. Effects of ECM on Keratinocyte Functions**

ECM PROTEIN	SUBSTRATE	RESPONSE
Fibronectin	<ul style="list-style-type: none"> <li>• Tissue culture polystyrene<sup>25</sup></li> <li>• Polyethylene glycol<sup>26</sup></li> </ul>	<ul style="list-style-type: none"> <li>• Attachment<sup>25</sup></li> <li>• Attachment and migration<sup>26</sup></li> </ul>
Collagen Type I	<ul style="list-style-type: none"> <li>• Poly(lactide-glycolide)<sup>19</sup></li> </ul>	<ul style="list-style-type: none"> <li>• Migration<sup>19</sup></li> </ul>
Collagen Type IV	<ul style="list-style-type: none"> <li>• Tissue culture polystyrene<sup>15</sup></li> </ul>	<ul style="list-style-type: none"> <li>• Attachment<sup>15</sup></li> </ul>
Laminin	<ul style="list-style-type: none"> <li>• Tissue culture polystyrene<sup>22</sup></li> </ul>	<ul style="list-style-type: none"> <li>• Proliferation and migration<sup>22</sup></li> </ul>

In a recent study we developed collagen-glycosaminoglycan (GAG) membrane that functioned as basal lamina analogs, providing an interface that facilitates the formation of an epidermal layer on the surface of a dermal analog.<sup>27,28</sup> A limitation of these membranes is that the surface biochemistry provides a limited number of cell-signaling cues that are known to promote reepithelialization. We hypothesize that by incorporating ECM proteins onto the surface of a collagenous biomaterial substrate, we can control keratinocyte attachment and subsequent cell-signaling that leads to rapid morphogenesis of a robust epidermal layer. Characterizing the ECM environment that influences keratinocyte attachment will also facilitate the design of bioengineered skin substitute with surfaces tailored to promote increased epithelialization rates, thereby enhancing their performance.

This chapter will discuss the methodology as well as results in establishing a quantitative link between keratinocyte attachment and ECM proteins coupled to collagen-GAG membranes. Briefly, a biomimetic design approach was used and we created basal lamina analogs that mimic the biochemical matrix composition of native tissue through passive adsorption of CI, CIV, LN, and FN. To characterize the relationship between keratinocyte attachment and protein binding, a high-throughput screening (HTS) device was developed that allows for keratinocytes to be seeded on the surface of collagen-GAG membranes and for examination of the effects of individual proteins at various concentrations. A tetrazolium-based colorimetric (MTT) assay was used to quantify attachment of viable keratinocytes. Comparative analysis of cellular attachment to the protein-conjugated surfaces suggests that keratinocyte attachment is enhanced when 0.1 mg/ml of FN is passively adsorbed to the surface of collagen-GAG membranes.

## 3.2 MATERIALS AND METHODS

### 3.2.1 High Throughput Screening (HTS) Device

To measure keratinocyte attachment on modified collagen-GAG membranes, a HTS device was developed by our laboratory (Figure 3.1<sup>20</sup>). This device consists of two machined Delrin™ plates that sandwich a rehydrated collagen-GAG membrane. The top Delrin™ plate of the device contains an array of 4.5 mm diameter through-holes. The through-holes are fitted with silicone o-rings to form sealed wells for protein and cell solutions when the plates and the membrane are sandwiched together.

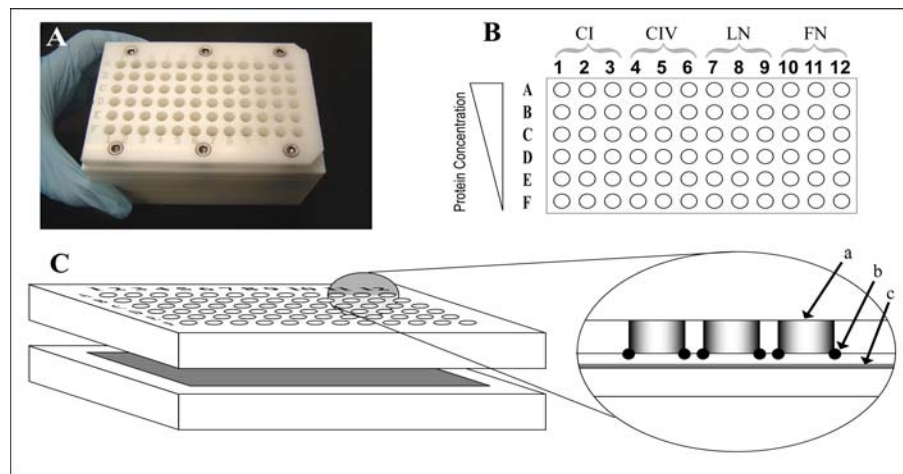


**Figure 3.1. High Throughput Screening (HTS) Device.** (A) Assembled HTS device unit with Delrin™ plates screwed together and sandwiching a rehydrated collagen-GAG membrane. (B) Collagen-GAG membranes were modified using a design of experiment scheme so that each concentration of collagen type I: CI, collagen type IV: CIV, laminin: LN, and fibronectin: FN were repeated in triplicate. (C) Schematic drawing of the assembly process with a) referring to individual wells, b) referring to silicone o-rings that form tight seals on c) collagen-GAG membranes when plates are screwed together.<sup>20</sup>

### 3.2.2 Collagen-GAG Membranes

#### 3.2.2.1 Collagen-GAG Dispersion

To produce collagen-GAG membranes, a collagen-GAG dispersion containing type I collagen (5 mg/ml) and GAG (0.18 mg/ml) was prepared according to previously described methods.<sup>29</sup> Briefly, 3.6 g of lyophilized bovine collagen (Semed S, Kensey Nash Corp.,

Exton, PA) was added to 500 ml of 0.05 M acetic acid (EMD Chemicals, Inc., Gibbstown, NJ) and blended at a constant temperature of 4°C for 90 minutes at 20,000 rpm in a refrigerated homogenizer. The collagen-GAG coprecipitate was formed by adding 100 ml of a 0.11% w/v solution of shark cartilage chondroitin 6-sulfate (Sigma, St. Louis, MI) to the blending collagen dispersion, then blending the collagen-GAG copolymer for an additional 90 minutes. Once fully blended, the collagen-GAG dispersion was degassed by centrifugation and stored at 4°C.

#### *3.2.2.2 Production of Collagen-GAG Membranes*

The collagen-GAG dispersion was cast onto flat 148.5 cm<sup>2</sup> molds made of polydimethylsiloxane silicone elastomer (PDMS, Sylgard 184, Dow Corning Corp., Midland, MI). The dispersion was air-dried for 48 hours in a laminar flow hood at room temperature and the resulting dried collagen-GAG membrane was gently peeled away from the PDMS surface.

#### *3.2.2.3 Dehydrothermal (DHT) Crosslinking of Collagen-GAG Membranes*

To stabilize the materials, dried collagen-GAG membranes were wrapped in aluminum foil, placed in an oven at room temperature, and subjected to a vacuum of less than 200 mTorr for 24 hours. The temperature within the vacuum oven was then increased to 105°C for 24 hours. Before removing membranes from the oven, the temperature was decreased to room temperature and the pressure was relieved. Membranes were then stored in aluminum foil in a desiccator.<sup>30</sup>

#### *3.2.2.4 Modification of Crosslinked Collagen-GAG Membranes*

Stock solutions (2 mg/ml) of human FN (BD Biosciences, Bedford, MA), rat tail collagen CI (purified by our laboratory by methods described by Elsdale and Bard<sup>31</sup>, rat tails were received from animals that were euthanized for other protocols, which were approved by Worcester Polytechnic Institute, Worcester, MA, Institutional Animal Care and Use

Committee), and mouse CIV and LN (BD Biosciences) were prepared as per manufacturer's instructions. Each protein was fluorescently labeled using a 594 Alexa Fluor Protein Labeling Kit (Molecular Probes, Eugene, OR) and purified by dialyzing against their natural buffer using a Slide-A-Lyzer cassette (Pierce, Rockford, IL).

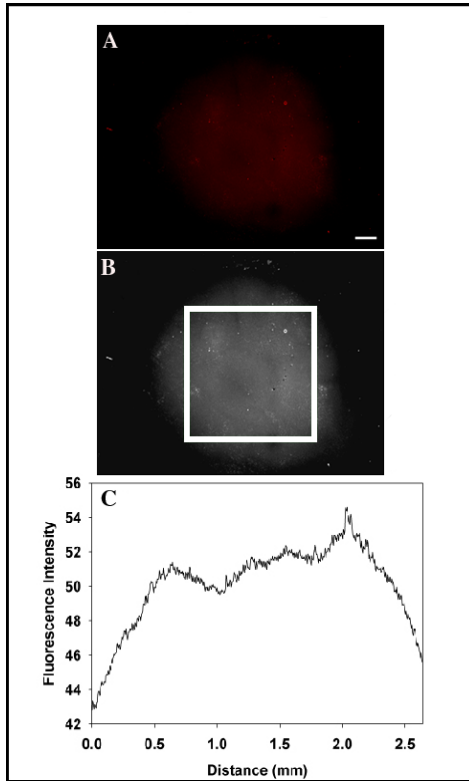


**Figure 3.2. Analysis of ECM Protein Conjugation to Collagen-GAG Membrane.** Extracellular matrix proteins were each conjugated to an Alexa Fluor dye, diluted, passively adsorbed to individual regions of a collagen-GAG membrane, and fluorescently imaged. Each photograph (A) was converted to 256 gray scale image (B) and fluorescence intensity of a 726 pixels by 696 pixels or 2.64 mm by 2.53 mm region of interest outlined in white was measured (C) using Scion Image. Scale bar in A = 0.5 mm.<sup>20</sup>

After the proteins were conjugated to the Alexa Fluor dye and purified, serial dilutions were made for final protein concentrations of 1 mg/ml, 0.3 mg/ml, 0.1 mg/ml, 0.03 mg/ml, 0 mg/ml using Dulbecco's phosphate buffer saline (dPBS, Hyclone, Logan, UT). Crosslinked membranes were placed on the HTS device as described, and 126  $\mu$ l of each protein concentration or dPBS (control sample) were placed in the wells in triplicate (Figure 3.1C<sup>20</sup>) overnight at 4°C to facilitate protein adsorption. After 18 hours, the wells were rinsed two times with dPBS to remove non-adherent protein.

### 3.2.2.5 Detection of Protein Modification

Fluorescent microscopy was used to evaluate the adsorption of the various concentrations of the proteins on the collagen-GAG membranes. The membranes were visualized for fluorescent emission at 594 nm using an upright Nikon Eclipse E400 Microscope (Nikon, Melville, NY) with a 2x objective. Images were captured with a RT Color Spot camera (Diagnostic Instruments, Inc Sterling



Heights, MI). All images in each protein group received the same exposure time using Spot Analysis 4.0.9 software (Diagnostic Instruments) in order to assess protein adsorption.

To determine the fluorescence intensity for each protein, each digital image was converted from 24 bit color (red channel only) (Figure 3.2A<sup>20</sup>) to 256 levels of gray using Scion Image Analysis Software (Figure 3.2B<sup>20</sup>) (Scion Corporation, Frederick, MD). Each image was scaled in the same manner, and a profile plot was taken of a rectangular region of interest (ROI) with dimensions of 2.64 mm by 2.53 mm (726 pixels by 696 pixels) (Figure 3.2B<sup>20</sup>). The profile plot was then inverted in order to report fluorescent intensity values of 0 representing black and 255 representing white (Figure 3.2C<sup>20</sup>).

### **3.2.3 Keratinocyte Attachment Assay**

#### *3.2.3.1 Modification of Crosslinked Collagen-GAG Membranes*

To modify the surfaces of the crosslinked collagen-GAG membranes, various concentrations of non-labeled solutions of the individual ECM proteins; CI, CIV, LN, or FN, were adsorbed to the membrane in different wells. Each protein was prepared at an initial concentration of 1 mg/ml per manufacturer's instructions, then passively adsorbed onto the membranes in triplicate overnight at 4°C at final concentrations of 0.3 mg/ml, 0.1 mg/ml, 0.03 mg/ml or 0.00 mg/ml (dPBS controls). After incubation, each well was rinsed twice with dPBS followed by addition of 200 µl of dPBS containing 0.5 mg/ml heat denatured bovine serum albumin (BSA, Sigma) for 1 hour. Each well was then rinsed twice with dPBS.

#### *3.2.3.2 Culture of Human Cells*

To measure keratinocyte attachment to the modified collagen-GAG membranes, the wells of the HTS device were seeded with human keratinocytes isolated from neonatal foreskins. Neonatal foreskins were obtained from non-identifiable discarded tissues from UMass Memorial Medical Center, Worcester, MA and were approved with exempt status from the New England Institutional Review Board. Keratinocyte isolations were performed using an

enzymatic treatment with a dispase (Gibco, Gaithersburg, MD) solution. The cells were propagated on a feeder layer of 3T3-J2 mouse fibroblasts (generously donated by Dr. Stelios Andreadis, State University of New York at Buffalo, Buffalo, NY) and cultured according to methods previously described<sup>28,32</sup> using keratinocyte media consisting of a 3:1 mixture of DMEM (high glucose) and Ham's F-12 medium (Life Technologies, Inc., Gaithersburg, MD) supplemented with 10% fetal bovine serum (FBS, Hyclone),  $10^{-10}$  M cholera toxin (Vibrio Cholerae, Type Inaba 569 B), 5  $\mu\text{g}/\text{ml}$  transferrin, 0.4  $\mu\text{g}/\text{ml}$  hydrocortisone (Calbiochem, La Jolla, CA), 0.13 U/ml insulin,  $1.4 \times 10^{-4}$  M adenine,  $2 \times 10^{-9}$  M triiodo-L-thyronine (Sigma), 1% penicillin/streptomycin (Invitrogen, Carlsbad, CA), and 0.01  $\mu\text{g}/\text{ml}$  epidermal growth factor (EGF, BD Biosciences). After 5 days of culture, cells were detached using 0.05% Trypsin-EDTA (Invitrogen) and then rinsed with serum free and EGF free keratinocyte media. Passage 2 keratinocytes were used in all experiments.

#### *3.2.3.3 Quantification of Keratinocyte Attachment*

To determine the number of viable attached keratinocytes in each well, a tetrazolium-based colorimetric (thiazoyl blue tetrazolium bromide, MTT, Sigma) assay was performed. The cells were seeded on protein modified collagen-GAG membranes (as previously described), with each well receiving 25,000 keratinocytes in serum free and epidermal growth factor free keratinocyte media for 3 hours at  $37^{\circ}\text{C}$  to facilitate attachment. Before adding the MTT solution, each well was rinsed twice with PBSABC (EMD Chemicals) to remove non-adherent cells. MTT was prepared at a final concentration of 10 mg/ml and added to each well for 2 hours at  $37^{\circ}\text{C}$ . After 2 hrs, the cells were rinsed twice with PBSABC and then dimethyl sulfoxide (DMSO, Sigma) was added to each well to lyse the cells. A SpectraMax 250 spectrophotometer (Molecular Devices, Sunnyvale, CA) was used along with Softmax Pro software version 3.1.2 (Molecular Devices) to determine the amount of dye absorbed by cells in each well using a protocol described previously by Ciapetti et. al.<sup>33</sup> Absorbance values from the experimental groups were compared to absorbance values from a standard curve of keratinocytes plated on tissue culture polystyrene.

### 3.2.5 Statistical Analyses

Sigma Stat Version 3.10 (Systat Software Inc., Richmond, CA) was used to determine statistical differences among the means of experimental groups. To determine if the means of two different samples were significantly different, a Student's t-test was performed when the samples were drawn from a normally distributed population with equal variance. Sigma Stat uses the Kolmogorov-Smirnov test to test for a normally distributed population and a P value  $> 0.05$  indicates normality. For all parametric tests, Sigma Stat assumes equal variance. When the data was not drawn from a normally distributed population (P value  $< 0.05$ ), a Mann-Whitney Rank Sum Test was used and a Levene Median test was used to determine equal variance with a P value  $> 0.05$  indicating equal variance. For both the Student's t-test and the Mann-Whitney Rank Sum Test, a p value  $< 0.05$  indicated a significant difference between the means of experimental groups.

To determine statistical differences among the means of three or more experimental groups a One Way Analysis of Variance (ANOVA) was used when the samples were drawn from a normally distributed population with equal variance (Kolmogorov-Smirnov test for normal distribution and equal variance was assumed). When the data was not normally distributed, a Kruskal-Wallis One way ANOVA on ranks was performed (Levene Median test to determine equal variance with a P  $> 0.05$  indicating equal variance). When a statistical difference was detected among the group means, a Tukey post-hoc analysis was performed for both the One Way ANOVA and Kruskal-Wallis One Way ANOVA on ranks. A p value  $< 0.05$ , for both variance tests, indicated a significant difference between the groups.

### 3.3 RESULTS

#### 3.3.1 Protein Adsorption

Examination of ECM proteins at each concentration through fluorescence microscopy allowed for the assessment of protein binding efficiency to the collagen-GAG membranes. To analyze the results we plotted the fluorescence intensity obtained at each concentration, of each protein (Figure 3.3<sup>20</sup>). A dose dependent increase in protein adsorption to the membranes was found for each protein examined. These increases are significantly different

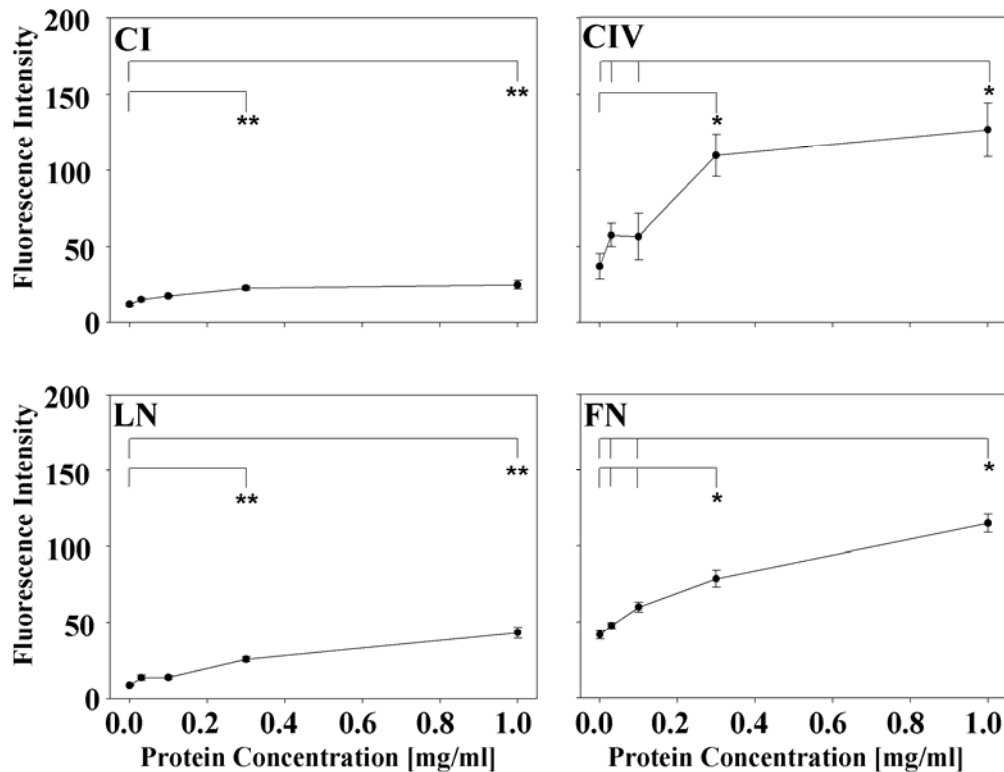


**Figure 3.3. ECM Protein Conjugation to Collagen-GAG Membrane.** Plots showing the average fluorescence intensities for regions of interest that were analyzed for each protein conjugation condition. Each data point represents the mean and standard error of the mean for two experiments, each having an  $n = 2$ . Statistical analyses were performed on membranes modified with collagen type I: CI, collagen type IV: CIV, laminin: LN, and fibronectin: FN amongst each concentration of 1 mg/ml, 0.3 mg/ml, 0.1 mg/ml, 0.03 mg/ml, and for unmodified membranes. \* indicates  $p < 0.05$  using One-way ANOVA with a Tukey Test and \*\* indicates  $p < 0.05$  using Kruskal-Wallis one-way ANOVA on ranks with a Tukey Test. Error bars indicate standard error.<sup>20</sup>

between protein concentrations of 0.3 mg/ml and non-modified membranes and between 1 mg/ml and non-modified membranes for all proteins examined. Fibronectin and CIV showed significant increases in protein binding efficiency between multiple concentrations, except between the two highest concentrations (0.3 mg/ml vs. 1.0 mg/ml). This phenomenon was also observed during the CI and LN studies. Based on this data, keratinocyte attachment studies were only conducted on adsorbed protein concentrations ranging from 0 to 0.3 mg/ml.

### **3.3.2 Keratinocyte Attachment to ECM Modified Collagen-GAG Membranes**

To characterize keratinocyte attachment to ECM proteins, cells were allowed to adhere for 3 hrs to regions of collagen-GAG membranes that had been conjugated with a range of concentrations of CI, CIV, LN, and FN. Attached viable cells were quantified through absorbance value measurements of solubilized tetrazolium crystals from the cell lysate.

A standard curve of absorbance values from a given cell number was used to calculate the attached cells based on the absorbance value recorded. The results of this study indicated that keratinocyte attachment was significantly enhanced by the type and concentration of ECM protein adsorbed to the surfaces of collagen-GAG membranes (Figure 3.4<sup>20</sup>). This effect was most pronounced when cells were attached to CIV and FN, when comparing the highest concentration studied (0.3 mg/ml) to unmodified membranes. Cell attachment to 0.1 mg/ml of FN was statistically greater than cell attachment to the unmodified membranes. There were no significant differences between keratinocytes attached to 0.1 mg/ml and 0.3 mg/ml of FN. Neither CI nor LN, at any studied concentration, promoted increased keratinocyte attachment to the collagen-GAG membrane over the baseline value for the unmodified membranes.

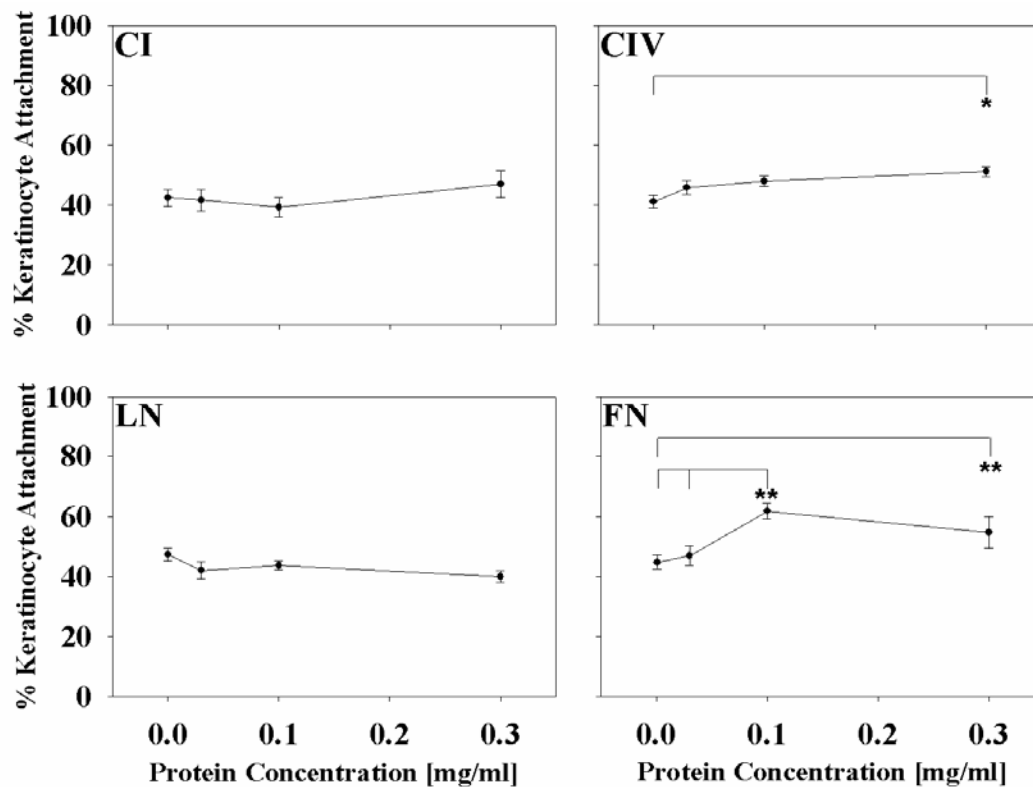


**Figure 3.4. Percent Keratinocyte Attachment on Biochemically Modified Collagen-GAG Membranes.** Keratinocyte attachment values were measured on extracellular matrix modified collagen-GAG membranes. Each data point represents the mean and standard error of the mean for three experiments, each having  $n = 6$ . Statistical analyses were performed on membranes modified with collagen type I: CI, collagen type IV: CIV, laminin: LN, and fibronectin: FN amongst each concentration of 0.3 mg/ml, 0.1 mg/ml, 0.03 mg/ml, and for unmodified membranes. \* indicates  $p < 0.05$  using One-way ANOVA with a Tukey Test and \*\* indicates  $p < 0.05$  using Kruskal-Wallis one-way ANOVA on ranks with a Tukey Test. Error bars indicate standard error.<sup>20</sup>

To compare the effects of protein concentrations on cell attachment, statistical analyses were performed at each of the varying concentrations. At 0.03 mg/ml of protein modification, there were no statistical differences found between the various proteins or the unmodified membranes (Figure 3.5A<sup>20</sup>). Increasing the protein concentration to 0.1 mg/ml induced changes from that seen for keratinocyte attachment on the unmodified membranes and the initial concentration examined (0.03 mg/ml) (Figure 3.5B<sup>20</sup>). At the protein concentration of

0.1 mg/ml, FN significantly increased keratinocyte attachment in comparison to the other proteins studied. It was found that keratinocyte attachment was 13% greater on FN than on CIV, 18% greater than on LN, and 22% greater than on CI. When the protein concentration was increased to 0.3 mg/ml, cell attachment to LN was found to be significantly lower than FN (Figure 3.5C<sup>20</sup>). Overall, a concentration of 0.1 mg/ml of FN induced the greatest keratinocyte attachment for all of the protein concentrations evaluated.

### 3.4 DISCUSSION

The goal of this study was to investigate the relationship between biochemical modifications of crosslinked collagen-GAG membranes and keratinocyte attachment as a function of protein composition and concentration in order to improve the rate of epithelialization of bioengineered skin substitutes. A HTS device was developed by our laboratory to facilitate examination of passive adsorption of multiple proteins at varying concentrations on a collagen-GAG membrane as well as the attachment of viable keratinocytes. This system allows for

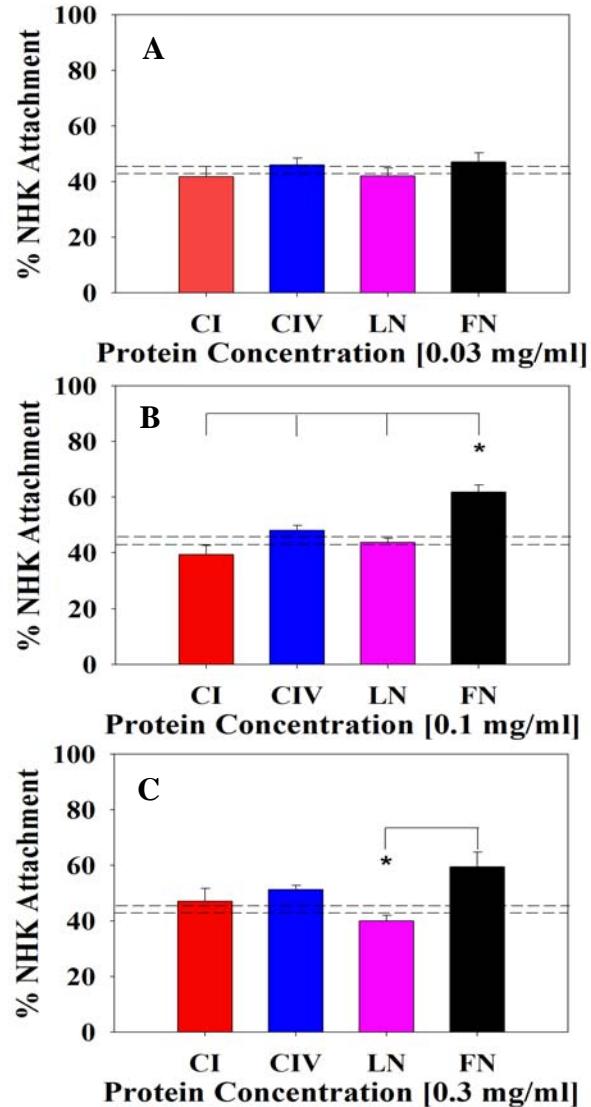


**Figure 3.5. Effects of Protein Concentration on Percent Keratinocyte Attachment.** Keratinocyte attachment values were compared at 0.03 mg/ml (A), 0.1 mg/ml (B), and 0.3 mg/ml (C) CI, CIV, LN, and FN. Three experiments, each having  $n = 6$  for each condition were evaluated. The baseline value for percent keratinocyte attachment to unmodified collagen-GAG membranes was found to be 44.03% and the dotted lines represent the standard error of  $\pm$  of 1.3 from this baseline value. \* indicates  $p < 0.05$  using One-way ANOVA with a Tukey Test. Error bars indicate standard error.<sup>20</sup>

a minimization in variability for each experiment since one membrane and keratinocytes from the same culture can be used to examine large numbers of cell-protein interactions simultaneously. Protein binding efficiency to the collagen-GAG membranes was determined as a function of concentration by means of fluorescent microscopy coupled with image analysis. Viable keratinocyte attachment was evaluated using a MTT-attachment assay. The results of our study indicate that keratinocyte attachment to basal lamina analogs is enhanced by passively adsorbing FN at 0.1 mg/ml to the surfaces of the membranes.

Previous studies have demonstrated that collagen-GAG biomaterials prevent wound contraction, enhance the growth rate of keratinocytes, and lead to the regeneration of connective tissue.<sup>34,35</sup> Crosslinking collagenous biomaterials with DHT has shown to increase the strength and decrease the reabsorption rate of these implant materials without introducing cytotoxic chemicals into the system.<sup>30,36</sup> However, a limitation of using DHT crosslinking is that cellular attachment is compromised. It has been suggested that DHT masks integrin binding sites that promote cellular attachment.<sup>37</sup> We found that passively adsorbing ECM proteins to the surface of the DHT crosslinked collagen-GAG membrane significantly increased its ability to support cellular attachment. Collagen type IV and FN provided an increase of 10% and 18% cellular attachment, respectively.

The results of this study demonstrate a strong relationship between the ECM protein conjugated to the surface of a collagenous biomaterial and the specific cellular-matrix interactions that occur during keratinocyte attachment. Protein conjugation results show an increase in fluorescence intensity for each protein as the concentrations increased to 0.3 mg/ml, however CI and LN were found to have no significant effect on increasing keratinocyte attachment even at the highest concentrations. These trends are consistent with previous studies performed by Adams et al. on bacteriological plastic,<sup>21</sup> and can be explained by the integrin expression profile of cultured keratinocytes that facilitates for cell-ECM attachment.



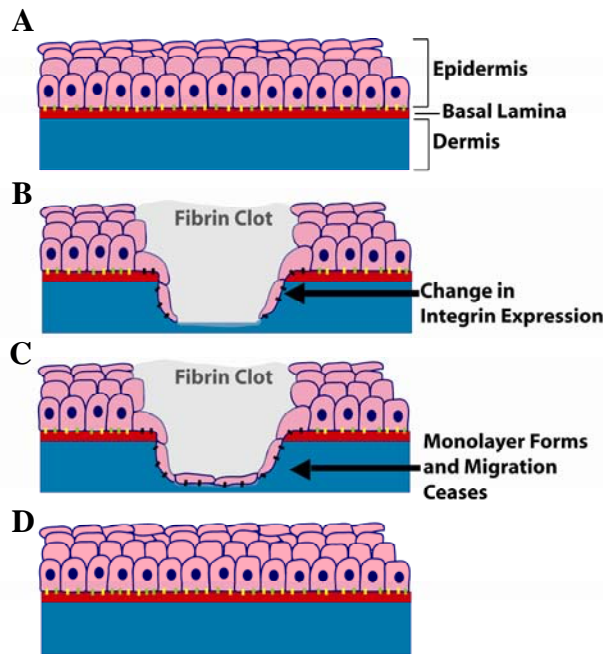


**Figure 3.6. Reepithelialization of Wound in Native Skin.** (A) depicts native healthy skin with the two main layers, the epidermis and dermis uninjured. At the dermal-epidermal junction is the basal lamina. When a wound occurs (B) a fibrin clot forms and keratinocytes at the wound margin become activated and undergo a change in integrin expression. (C) The activated keratinocytes begin to migrate until a monolayer of cells is formed. When a monolayer is formed, keratinocytes begin to proliferate and differentiate to fill the wound site and native physiology is returned (D).

The principle integrins on the surface of keratinocytes in non-wounded skin are  $\alpha_2\beta_1$ , which bind cells to dermal collagens,<sup>21,38-40</sup> and  $\alpha_3\beta_1$ , which bind cells to LN (Figure 3.6A).<sup>41</sup> After wounding, changes in the expression profile of integrins on the wound edge keratinocytes allow for dynamic interactions with the dermal ECM as well as with components of the provisional matrix supplied by the fibrin clot and endogenous protein secretion (Figure 3.6B).<sup>9</sup> During this reepithelialization process, keratinocytes located at the margin of the wound, transition from a stationary to a migratory phenotype characterized by a flat and elongated morphology, reorganization of cytoskeletal and

junctional complexes, and a change in integrin expression.<sup>42-47</sup> Most notably, the change in integrin expression can be characterized by the induction of  $\alpha_5\beta_1$ , an integrin responsible for binding cells to FN via the RGD sequence in the central cell binding domain of the molecule.<sup>9,21,39,45,48</sup> Concomitant with this transition, keratinocytes detach from the basal lamina and migrate laterally by dynamically interacting with the dermal ECM as well as with the components of the provisional matrix supplied by the fibrin clot and endogenous protein secretion, through integrin based mechanisms.<sup>8-11</sup> Studies investigating wound healing phenomenon *in vivo* have found FN present under the tip of a migrating epithelial tongue and

an absence of both LN and CIV, which are known to be present at greater levels in the basal lamina, of healthy tissue. Once the wound surface has been covered with a monolayer of keratinocytes and migration has ceased (Figure 3.6C), native basement membrane proteins, notably LN and CIV, reappear in a very ordered sequence from the margin of the wound inward, and keratinocytes return to the standard proliferation and differentiation program of the cell (Figure 6D).<sup>49,50</sup> When keratinocytes are harvested and cultured *in vitro*, they exhibit the same change in expression profile of integrins as wounded keratinocytes and develop the ability to attach to FN.<sup>51</sup> Together these findings demonstrate that FN based cellular adhesions as well as interactions with dermal collagens can be used to direct the spatial organization, migration, proliferation, and differentiation of keratinocytes and enhance the rate of reepithelialization of crosslinked collagenous biomaterials.<sup>9,10,52</sup>

Characterizing the composition of ECM proteins that enhance keratinocyte attachment on collagen-GAG membranes is an important feature that can be leveraged for the design of bioengineered skin substitutes. Increased attachment of keratinocytes is thought to facilitate a more rapid regeneration of the wound environment through outside-in signaling events that are controlled by cellular-integrin-ECM adhesions. These signals are responsible for triggering migration, proliferation, and differentiation.<sup>53</sup> To further test the hypothesis of this study the next step in our research plan is to build on our current results by establishing a quantitative link between the ECM composition of our basal lamina analogs and the formation of an epidermal layer. Before doing so, we will first investigate the presentation of FN on our dermal scaffolds and study the effects of modification strategies on its presentation and overall bioactivity. We believe that understanding how to strategically modify a biomaterial surface to increase its bioactivity is of great importance for enhancing epithelialization as well for engineering other functional tissues.

### 3.5 ACKNOWLEDGEMENTS

This work was funded by a grant from the Whitaker Foundation (GDP). I would like to thank The Department of Obstetrics and Gynecology at UMMS (Worcester, MA) for providing us with neonatal foreskins and Russell Kronengold at Kensey Nash Corp. (Exton, PA) for his generous donations of the collagen materials that were used to produce the dermal analogs. I would like to thank the co-authors of this work, Brett Downing, Sarah Walsh and my advisor George Pins. Also, I would like to thank Jenna Balestrini, Kevin Cornwell, Stuart Howes, Donna Davidson, and Gharam Han for their technical assistance.

### 3.6 REFERENCES

1. Boyce ST, Goretsky MJ, Greenhalgh DG, Kagan RJ, Rieman MT, Warden GD. Comparative assessment of cultured skin substitutes and native skin autograft for treatment of full-thickness burns. *Ann Surg* 1995;222(6):743-52.
2. Bell E, Ehrlich HP, Buttle DJ, Nakatsuji T. Living tissue formed in vitro and accepted as skin-equivalent tissue of full thickness. *Science* 1981;211(4486):1052-4.
3. Yannas IV, Burke JF, Orgill DP, Skrabut EM. Wound tissue can utilize a polymeric template to synthesize a functional extension of skin. *Science* 1982;215(4529):174-6.
4. Supp DM, Boyce ST. Engineered skin substitutes: practices and potentials. *Clin Dermatol* 2005;23(4):403-12.
5. Boyce ST. Cultures Skin Substitutes: A Review. *Tissue Eng* 1996;2:255-266.
6. Sheridan RL, Tompkins RG. Skin substitutes in burns. *Burns* 1999;25(2):97-103.
7. Parenteau NL, Hardin-Young, J., and Ross, R.N. Skin. In: Vacanti J, editor. *Principles of Tissue Engineering*. San Diego: Academic Press; 2000.
8. Garlick JA, Taichman LB. Fate of human keratinocytes during reepithelialization in an organotypic culture model. *Lab Invest* 1994;70(6):916-24.
9. Grinnell F. Wound repair, keratinocyte activation and integrin modulation. *J Cell Sci* 1992;101 ( Pt 1):1-5.
10. Clark RA. Fibronectin matrix deposition and fibronectin receptor expression in healing and normal skin. *J Invest Dermatol* 1990;94(6 Suppl):128S-134S.
11. Larjava H, Salo T, Haapasalmi K, Kramer RH, Heino J. Expression of integrins and basement membrane components by wound keratinocytes. *J Clin Invest* 1993;92(3):1425-35.
12. Alberts ea. *Molecular Biology of The Cell*. New York: Garland Science; 2002.
13. Watt FM, Jordan PW, O'Neill CH. Cell shape controls terminal differentiation of human epidermal keratinocytes. *Proc Natl Acad Sci U S A* 1988;85(15):5576-80.
14. Watt FM. Cell culture models of differentiation. *FASEB J* 1991;5(3):287-94.
15. Bickenbach JR, Chism E. Selection and extended growth of murine epidermal stem cells in culture. *Exp Cell Res* 1998;244(1):184-95.
16. Guo M, Toda K, Grinnell F. Activation of human keratinocyte migration on type I collagen and fibronectin. *J Cell Sci* 1990;96 ( Pt 2):197-205.
17. Tinois E, Tiollier J, Gaucherand M, Dumas H, Tardy M, Thivolet J. In vitro and post-transplantation differentiation of human keratinocytes grown on the human type IV collagen film of a bilayered dermal substitute. *Exp Cell Res* 1991;193(2):310-9.

18. Grzesiak JJ, Pierschbacher MD, Amodeo MF, Malaney TI, Glass JR. Enhancement of cell interactions with collagen/glycosaminoglycan matrices by RGD derivatization. *Biomaterials* 1997;18(24):1625-32.
19. Tjia JS, Aneskievich BJ, Moghe PV. Substrate-adsorbed collagen and cell secreted fibronectin concertedly induce cell migration on poly(lactide-glycolide) substrates. *Biomaterials* 1999;20(23-24):2223-33.
20. Bush KA, Downing BR, Walsh SE, Pins GD. Conjugation of extracellular matrix proteins to basal lamina analogs enhances keratinocyte attachment. *J Biomed Mater Res A* 2007;80(2):444-52.
21. Adams JC, Watt FM. Expression of beta 1, beta 3, beta 4, and beta 5 integrins by human epidermal keratinocytes and non-differentiating keratinocytes. *J Cell Biol* 1991;115(3):829-41.
22. Pouliot N, Saunders NA, Kaur P. Laminin 10/11: an alternative adhesive ligand for epidermal keratinocytes with a functional role in promoting proliferation and migration. *Exp Dermatol* 2002;11(5):387-97.
23. Adams JC, Watt FM. Fibronectin inhibits the terminal differentiation of human keratinocytes. *Nature* 1989;340(6231):307-9.
24. Wilke MS, Skubitz AP. Human keratinocytes adhere to multiple distinct peptide sequences of laminin. *J Invest Dermatol* 1991;97(1):141-6.
25. Watt FM. Influence of cell shape and adhesiveness on stratification and terminal differentiation of human keratinocytes in culture. *J Cell Sci Suppl* 1987;8:313-26.
26. Tziampazis E, Kohn J, Moghe PV. PEG-variant biomaterials as selectively adhesive protein templates: model surfaces for controlled cell adhesion and migration. *Biomaterials* 2000;21(5):511-20.
27. Downing BR, Cornwell K, Toner M, Pins GD. The influence of microtextured basal lamina analog topography on keratinocyte function and epidermal organization. *J Biomed Mater Res A* 2005;72(1):47-56.
28. Pins GD, Toner M, Morgan JR. Microfabrication of an analog of the basal lamina: biocompatible membranes with complex topographies. *Faseb J* 2000;14(3):593-602.
29. Jones PH, Harper S, Watt FM. Stem cell patterning and fate in human epidermis. *Cell* 1995;80(1):83-93.
30. Weadock K, Olson RM, Silver FH. Evaluation of collagen crosslinking techniques. *Biomater Med Devices Artif Organs* 1983;11(4):293-318.
31. Elsdale T, Bard J. Collagen substrata for studies on cell behavior. *J Cell Biol* 1972;54(3):626-37.
32. Carter WG, Symington BE, Kaur P. Cell adhesion and the basement membrane in early epidermal morphogenesis. In: Fleming TP, editor. *Epithelial Organization and Development*. London: Chapman and Hall; 1992. p 299-327.
33. Ciapetti G, Cenni E, Pratelli L, Pizzoferrato A. In vitro evaluation of cell/biomaterial interaction by MTT assay. *Biomaterials* 1993;14(5):359-64.
34. Yannas IV, Burke JF, Gordon PL, Huang C, Rubenstein RH. Design of an artificial skin. II. Control of chemical composition. *J Biomed Mater Res* 1980;14(2):107-32.
35. Boyce ST, Christianson DJ, Hansbrough JF. Structure of a collagen-GAG dermal skin substitute optimized for cultured human epidermal keratinocytes. *J Biomed Mater Res* 1988;22(10):939-57.
36. Wang MC, Pins GD, Silver FH. Collagen fibres with improved strength for the repair of soft tissue injuries. *Biomaterials* 1994;15(7):507-12.
37. Cornwell KG, Downing BR, Pins GD. Characterizing fibroblast migration on discrete collagen threads for applications in tissue regeneration. *J Biomed Mater Res A* 2004;71(1):55-62.
38. Staquet MJ, Levarlet, B., Dezutter-Dambuyant, C., Schmidt, D., and Thivolet, J. Indification of specific human epithelial cell integrin receptors as VLA proteins. *Experimental Cell Research* 1990;187:277-83.
39. Carter WG, Wayner EA, Bouchard TS, Kaur P. The role of integrins alpha 2 beta 1 and alpha 3 beta 1 in cell-cell and cell-substrate adhesion of human epidermal cells. *J Cell Biol* 1990;110(4):1387-404.
40. Emsley J, Knight CG, Farndale RW, Barnes MJ, Liddington RC. Structural basis of collagen recognition by integrin alpha2beta1. *Cell* 2000;101(1):47-56.

41. De Luca M, Tamura RN, Kajiji S, Bondanza S, Rossino P, Cancedda R, Marchisio PC, Quaranta V. Polarized integrin mediates human keratinocyte adhesion to basal lamina. *Proc Natl Acad Sci U S A* 1990;87(17):6888-92.
42. Nguyen BP, Ren XD, Schwartz MA, Carter WG. Ligation of integrin alpha 3beta 1 by laminin 5 at the wound edge activates Rho-dependent adhesion of leading keratinocytes on collagen. *J Biol Chem* 2001;276(47):43860-70.
43. Odland G, Ross R. Human wound repair. I. Epidermal regeneration. *J Cell Biol* 1968;39(1):135-51.
44. Stenn KS, and L, Depalma. Re-epithelialization. In: Clark RA, Hensen PM, editors. *The Molecular and Cellular Biology of Wouond Repair*, 1st edition. New York: Plenum Press; 1988. p 321-325.
45. Martin P. Wound healing-aiming for perfect skin regeneration. *Science* 1997;276(5309):75-81.
46. Knust E. Control of epithelial cell shape and polarity. *Curr Opin Genet Dev* 2000;10(5):471-5.
47. Clark R. Wound Repair, Overview and General Considerations. In: Clark R, editor. *The Molecular and Cellular Biology of Wound Repair (Second Edition)*. New York: Plenum Press; 1995. p 3-44.
48. Adams JC, Watt FM. Changes in keratinocyte adhesion during terminal differentiation: reduction in fibronectin binding precedes alpha 5 beta 1 integrin loss from the cell surface. *Cell* 1990;63(2):425-35.
49. Clark RA, Lanigan JM, DellaPelle P, Manseau E, Dvorak HF, Colvin RB. Fibronectin and fibrin provide a provisional matrix for epidermal cell migration during wound reepithelialization. *J Invest Dermatol* 1982;79(5):264-9.
50. Clark RA, Winn HJ, Dvorak HF, Colvin RB. Fibronectin beneath reepithelializing epidermis in vivo: sources and significance. *J Invest Dermatol* 1983;80 Suppl:26s-30s.
51. Takashima A, Grinnell F. Fibronectin-mediated keratinocyte migration and initiation of fibronectin receptor function in vitro. *J Invest Dermatol* 1985;85(4):304-8.
52. Watt FM, Hertle, M.D. Keratinocyte integrins. In: Leigh I, Birgitte, L, and Watt, F., editor. *The Keratinocyte Handbook*. New York, New York: Press Syndicate of the University of Cambridge; 1994.
53. Hynes RO. Integrins: versatility, modulation, and signaling in cell adhesion. *Cell* 1992;69(1):11-25.

---

---

## Chapter 4: Fibronectin Cellular Binding Site Availability

---

### 4.1 INTRODUCTION

The role of extracellular matrix (ECM) proteins in directing keratinocyte function has been studied extensively during the reepithelialization phase of wound healing,<sup>1-3</sup> in tissue culture models,<sup>4,5</sup> and on the surfaces of biomaterials.<sup>6-8</sup> Specifically, the ECM protein fibronectin (FN) plays an integral role in the attachment of keratinocytes and the regeneration of an epidermal layer in the wound healing environment. Fibronectin is part of the provisional matrix that interacts with dermal collagens and provides signaling cues to direct reepithelialization. The FN interactions with collagen are mediated by specific domains on the surfaces of collagen molecules that produce oriented FN binding, in a manner that presents FN binding sites for cellular interactions. Specifically, the principle collagen found in the dermis is collagen type I (CI), and the FN binding site is found on the  $\alpha 1(I)$  chain between amino acid residues 757-791.<sup>9</sup>

Fibronectin is a high molecular weight glycoprotein that is found in the ECM as well as in blood plasma (Figure 4.1<sup>10</sup>). Fibronectin is composed of three types of

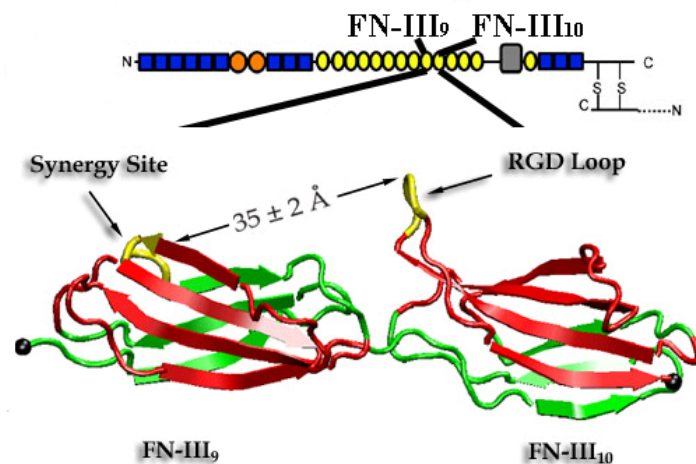


**Figure 4.1. Structure of FN Monomer.** Fibronectin monomer with expanded view of the 9<sup>th</sup> and 10<sup>th</sup> type III repeat. Integrin binding motif is displayed in yellow.<sup>10</sup>

repeating modules. There are 12 type I repeats (~45 amino acids long), two adjacent type II repeats (60 amino acids long), and 15-17 type III repeats (~90 amino acids long). The repeating modules of FN fold independently with 20-35%  $\beta$ -structure and no  $\alpha$ -helix. When assembled in ECM fibrils, the subunits unfold into elongated forms 2-3 nm in diameter and each subunit 60-70 nm in length.<sup>11,12</sup>

Fibronectin contains an arginine-glycine-aspartic acid (RGD) binding domain that acts as a ligand for integrin receptors found on the surfaces of keratinocytes and other cells.<sup>13,14</sup> Studies have demonstrated that the conformation of adsorbed FN affects the availability of these ligand domains for integrin binding. Furthermore, the presence of these domains directs specific functions of fibroblast,<sup>15</sup> osteoblast,<sup>16</sup> myoblast,<sup>17</sup> and endothelial cells.<sup>18</sup> Although many research efforts have elucidated the importance of FN in controlling keratinocyte attachment, migration, proliferation, and differentiation,<sup>19-22</sup> little research has been conducted to evaluate the roles of biomaterial substrate properties, including chemistry and hydrophobicity, on FN conformation and subsequent FN mediated keratinocyte functions.

Understanding how to engineer biomaterial surfaces with the appropriate properties to present tailored biochemical signaling cues to keratinocytes, will ultimately lead to the design of dermal scaffolds that promote rapid reepithelialization and improve the performance of tissue engineered skin substitutes. Self-assembled monolayers (SAMs) of alkanethiols on gold substrates offer an excellent model system to evaluate the effect of biomaterial surface properties on protein conformation and subsequent cellular interactions, due to their ease of fabrication and ability to present homogenous surface chemistries.<sup>23,24</sup> Various surface chemistries can be created by modifying the terminal functional group of alkanethiol molecules without altering other surface variables, such as roughness or topology. Previous studies have demonstrated that both the hydrophobicity and charge of a SAM surface directly affect protein conformation and concentration and modulate cellular

signaling and subsequent cellular functions.<sup>15,16,23,25-28</sup>

The purpose of this chapter was to evaluate the effect of FN concentration and conformation on keratinocyte attachment, morphology, and differentiation. Using SAMs as model biomaterial surfaces, we analyzed FN adsorption and conformation at both low and saturated FN surface densities, as a function of different surface chemistries. Low FN surface density experiments were conducted to compare the effects of each surface chemistry on FN conformation and subsequent cellular functions, since each surface had the same amount of protein adsorbed. Saturated FN surface density experiments were conducted to analyze the effects of surface chemistry on FN conformation and concentration as well as their roles on keratinocyte functions. The availability of cellular binding sites was evaluated and correlated with keratinocyte attachment, morphology, differentiation, as well as focal adhesion (FA) formation. Comparative analyses of keratinocyte function on FN coated SAMs suggest that NH<sub>2</sub> and CH<sub>3</sub> terminated surfaces at saturated FN densities increase binding domain availability which correlates directly with increased control of keratinocyte attachment, morphology, and decreased differentiation through integrin mediated signaling mechanisms.

## **4.2 MATERIALS AND METHODS**

### **4.2.1 Preparation of SAMs**

Gold surfaces on glass substrates were obtained commercially from Evaporated Metal Films (Ithaca, NY). For monolayer formation, slides were cleaned and immersed in 1 mM alkanethiol solutions in absolute ethanol of dodecanethiol (CH<sub>3</sub> surface, Alfa Aesar, Ward Hill, MA), 11-mercaptoundecanoic acid (COOH surface, Aldrich, Milwaukee, WI), 11-mercapto-1-undecanol (OH surface, Aldrich), and 11-amino-1-undecanethiol, hydrochloride (NH<sub>2</sub> surface, Dojindo Laboratories, Kumamoto, Japan) for 18 hours. After a packed monolayer formed, the slides were removed from solution, rinsed with ethanol, and dried with nitrogen following protocols previously described.<sup>25,29</sup> New films were prepared immediately prior to each characterization and cellular experiment.



#### **4.2.2 Characterization of SAMs**

To measure the contact angle for each SAM surface, sessile drop measurements were obtained using a 100-00 Goniometer (Rame-Hart Netcong, NJ) with a protractor mounted in the eyepiece on 1  $\mu$ l droplets of deionized water that were applied to the surface. A minimum of four measurements were taken on each surface and the results were averaged. These measurements were repeated for each surface.

To determine the thickness of the SAM layers on the surface of each substrate, ellipsometry measurements were obtained with a manual null ellipsometer (Rudolph, Denville, NJ). Film thickness values were determined using regression algorithms with constant values of 1.457 for the index of refraction of the film, 3.50 for the substrate absorption, and varying the index of refraction of the substrate from 0.15 – 0.30 in 0.05 increments. For each SAM surface 5 measurements were made.

#### **4.2.3 Culture of Neonatal Human Keratinocytes**

Neonatal foreskins were obtained from non-identifiable discarded tissues from UMass Memorial Medical Center, Worcester, MA and were approved with exempt status from the New England Institutional Review Board. Keratinocyte isolations were performed using an enzymatic treatment with a dispase (Gibco, Gaithersburg, MD) solution. The cells were propagated on a feeder layer of 3T3-J2 mouse fibroblasts (generously donated by Dr. Stelios Andreadis, State University of New York at Buffalo, Buffalo, NY) and cultured according to methods previously described<sup>30,31</sup> using keratinocyte media consisting of a 3:1 mixture of Dulbecco's Modified Eagle's Medium (DMEM high glucose) and Ham's F-12 medium (Life Technologies, Inc., Gaithersburg, MD) supplemented with 10% fetal bovine serum (FBS, Hyclone, Logan, UT),  $10^{-10}$  M cholera toxin (Vibrio Cholerae, Type Inaba 569 B), 5  $\mu$ g/ml transferrin, 0.4  $\mu$ g/ml hydrocortisone (Calbiochem, La Jolla, CA), 0.13 U/ml insulin,  $1.4 \times 10^{-4}$  M adenine,  $2 \times 10^{-9}$  M triiodo-L-thyronine (Sigma, St. Louis, MI), 1% penicillin/streptomycin (Invitrogen, Carlsbad, CA), and 0.01  $\mu$ g/ml epidermal growth factor (EGF, BD Biosciences,

Bedford, MA). After 5 days of culture, cells were detached using 0.05% Trypsin-EDTA (Invitrogen) and then rinsed with serum free and EGF free keratinocyte media KCM(-S-GF). For all cellular experiments, keratinocytes were seeded in KCM(-S-GF) and passage 2-4 keratinocytes were used for all experiments.

#### **4.2.4 FN Adsorption on SAM Surfaces**

To create individual wells for cellular assays, 9 mm inner diameter adhesive silicone isolators (Grace BioLabs, Bend, OR) were affixed to SAM surfaces or tissue culture polystyrene cover slips (positive controls) (TCPS, Thermanox, Nunc, Rochester, NY). Fibronectin (FN, BD Biosciences) was then passively adsorbed at low surface density or saturated surface density for 1 hour at room temperature. Based on the results of previous studies 40 ng/cm<sup>2</sup> of FN for each surface was used as the low surface density to achieve the same surface density of FN on each SAM surface. This density was achieved by using 10 µg/ml of FN for the OH surface, 2 µg/ml of FN for the CH<sub>3</sub>, COOH, and NH<sub>2</sub> surfaces, and 1 µg/ml of FN for the TCPS surface.<sup>17,29</sup> Saturated surface densities were achieved using 25 µg/ml of FN, based on our ellipsometry data as well as previously reported values for SAM surfaces.<sup>24,29</sup> This concentration produced surfaces with FN surface densities of approximately 110 ng/cm<sup>2</sup>, 360 ng/cm<sup>2</sup>, 280 ng/cm<sup>2</sup>, 410 ng/cm<sup>2</sup>, and 400 ng/cm<sup>2</sup> for OH, CH<sub>3</sub>, COOH, NH<sub>2</sub>, and TCPS surfaces, respectively.<sup>17,29</sup> After FN adsorption, each well was blocked for non-specific binding using 1% heat denatured bovine serum albumin (BSA, Sigma) in dPBS (Hyclone).

#### **4.2.5 Determining Saturation Density of Adsorbed FN using Ellipsometry**

The thickness of the adsorbed FN on the SAM surfaces was quantified using ellipsometry methods previously described.<sup>24</sup> Self-assembled monolayer substrates were prepared and individual wells were created on each surface. Stock solutions of 0, 5, 25, and 100 µg/ml of FN were added to each well in dPBS for 1 hour or 4 hours at room temperature. Each well was measured three times and average film thickness was recorded and compared with the initial value, determined during characterization of the untreated surfaces, to give the

thickness of adsorbed protein on each SAM surface. This analysis was performed on each surface in triplicate and averages with standard deviations were reported.

#### **4.2.6 SAM Mediated Changes in FN Conformation**

To measure SAM dependent changes in adsorbed FN conformation and the availability of the central cellular binding domain on FN, a monoclonal antibody directed towards this domain (HFN 7.1, Developmental Studies Hybridoma Bank, Iowa City, IA) was used.<sup>32</sup> Low surface density and saturated surface density FN treated SAM surfaces as well as TCPS surfaces were blocked using 1% heat denatured BSA (in dPBS) then incubated with HFN 7.1 for 1 hour in 10% CO<sub>2</sub> at 37°C. Each surface was then rinsed in blocking buffer (0.05% Tween-20 (Sigma) and 0.25% BSA in dPBS) and incubated with 546 Alexa Fluor conjugated goat anti-mouse IgG (1:200 in blocking buffer, Molecular Probes, Eugene, OR ) for 1 hour in 10% CO<sub>2</sub> at 37°C. Slides were then rinsed with dPBS, and images were captured using an RT Color Spot camera (Spot Diagnostics, Sterling Heights, MI). Image J Analysis software (downloaded from <http://rsb.info.nih.gov/ij/>) was used to determine the relative amount of cellular binding sites on each FN treated SAM and control surface. The total area of fluorescent pixels was calculated, normalized against the total area of each well examined, and the values are reported as HFN 7.1 percent positive area. This assay was performed four times for each surface at each surface density. Results are reported as averages and standard deviations.

#### **4.2.7 Cell Spreading**

To quantify the effect of FN treated SAM surfaces on keratinocyte morphology, cell spreading was measured using fluorescein-5-maleimide, as previously described.<sup>33</sup> Keratinocytes were seeded at a density of 5000 cells/well in KCM(-S-GF) and allowed to attach for 3 hours in 10% CO<sub>2</sub> at 37°C. After attachment, the wells were rinsed using PBSABC (EMD Chemicals, Gibbstown, NJ), fixed using 16% formaldehyde (Ted Pella, Inc., Redding, CA), and then permeated using 0.1% Triton X-100 (Sigma). Fluorescein-5-

maleimide (Molecular Probes) at 0.6 mM was added to the cells for 1 hour at room temperature. This fluorescent compound becomes covalently coupled to functional groups of proteins found in the cell membrane. After 1 hour, cells were rinsed with dPBS and cell nuclei were stained with a 0.06 mM solution of Hoechst nuclear reagent (Molecular Probes) for 5 minutes at 37°C. All images of stained cells were thresholded using the same image analysis protocol to clearly define cellular areas. Each cell was traced and its area was calculated with Image J software. For each surface condition, 15 random cells were analyzed.

#### **4.2.8 Analysis of Keratinocyte Attachment**

Keratinocytes were seeded at a density of 5000 cells/well in KCM(-S-GF) and allowed to attach for 3 hours in 10% CO<sub>2</sub> at 37°C on each FN treated surface. The wells were then rinsed using PBSABC and the cell nuclei were stained Hoechst nuclear reagent. Images were captured to determine the number of attached cells in a defined region. Assuming the cells were homogenously dispersed in each well, this value was used to extrapolate the total number of attached cells per well and normalized to the initial number of cells seeded. For each surface condition examined, 3 separate wells were imaged and each experimental surface condition was assayed in duplicate. Values are reported as percent keratinocyte attachment.

#### **4.2.9 Analysis of Keratinocyte Differentiation**

The percentage of involucrin positive keratinocytes was detected by immunofluorescence staining using methods previously described.<sup>34</sup> Involucrin is expressed by keratinocytes that have committed to terminal differentiation.<sup>35,36</sup> Keratinocytes were allowed to attach on FN treated surfaces for 3 hours in KCM(-S-GF) in 10% CO<sub>2</sub> at 37°C. Following incubation, the wells were rinsed with PBSABC, fixed with 4% formaldehyde, and then permeabilized with 0.5% Triton X-100 in dPBS. The cells were treated with a monoclonal mouse anti-human

involucrin antibody (Clone SY5, Sigma) (1:50 dilution in blocking buffer; 0.05% Tween 20 and 0.25% BSA in dPBS) for 1 hour at room temperature.

Cells were then rinsed with blocking buffer and incubated with an Alexa Fluor 546 conjugated goat anti-mouse secondary antibody (1:200 dilution in blocking buffer) for 45 minutes in 10% CO<sub>2</sub> at 37°C. Immunofluorescence images were converted to binary images by thresholding to 50% of maximum intensity. Thresholded cells that exhibited a fluorescent area greater than 100 μm<sup>2</sup> were marked involucrin positive. The total cell number was also evaluated for each image and the percentage of involucrin positive cells for each image was reported. For each surface condition, 4 samples were evaluated and each experimental surface condition was assayed in duplicate.

#### 4.2.10 Fluorescence Assessment of FA Formation

To further evaluate keratinocyte attachment on precisely tailored SAM surfaces, quantitative immunolocalization studies were used to evaluate the expression of the FA protein vinculin within the cells following a previously published method.<sup>37</sup> Keratinocytes were seeded on FN treated surfaces for 3 hours in 10% CO<sub>2</sub> at 37°C. Each of the cell seeded surfaces was then rinsed with PBSABC, treated for 10 minutes with a solution to fix and permeabilize the cells (4% formaldehyde, 0.2% Triton X-100

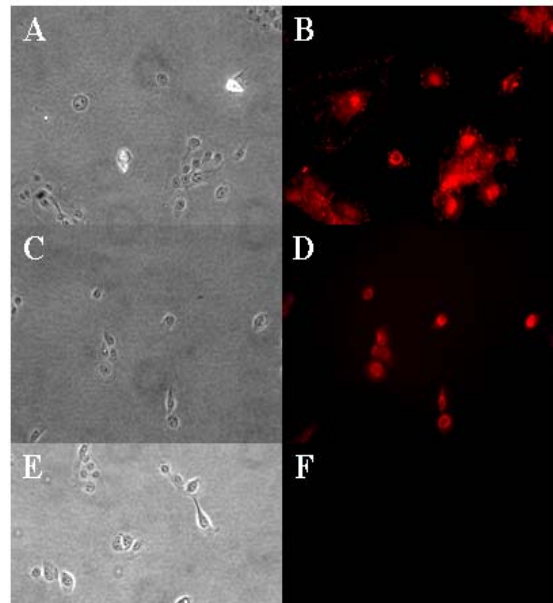


**Figure 4.2. FA Validation on Tissue Culture Plastic.** An anti-vinculin antibody was used to determine presence of peripheral FAs. Keratinocytes were cultured on tissue culture plastic for 3 hours. A and B represent cells that received both primary and secondary antibodies. A is the brightfield image, and B is the fluorescent image to detect vinculin. Note the punctuate staining at the cell peripheries in B. C and D represent cells that received only the labeled secondary antibody. C is the brightfield image, and D is the fluorescent image to detect vinculin. E and F represent cells that received neither the primary nor the secondary antibody. E is the brightfield image, and F is the fluorescent image to detect vinculin. Scale bar represents 100 μm.

in dPBS), and then treated for 10 minutes with a blocking solution (1% BSA in dPBS) to minimize nonspecific binding. The cells were then incubated with mouse anti-human vinculin primary antibody (Clone HVIN-1, Sigma) (1:100 dilution in blocking solution) for 45 minutes in 10% CO<sub>2</sub> at 37°C. Following primary incubation, the surfaces were rinsed in 1% BSA and incubated with Alexa Fluor 546 conjugated goat anti-mouse secondary antibody (1:100 in blocking solution) for 30 minutes in 10% CO<sub>2</sub> at 37°C. Figure 4.2 displays validation of focal adhesion staining. Figure 4.2A and 4.2B represent cells that received both primary and secondary antibodies. In the fluorescent image (Figure 4.2B) punctate staining of vinculin is located at the edges of the cells, where focal adhesions are located. Figures 4.2C and 4.2D represent cells that received only the labeled secondary, and it can be seen in 4.2D that there is no punctate staining at the edges of the cells. Figures 4.2E and 4.2F are images that received neither primary nor secondary antibodies. Images were all exposed to the same fluorescence intensity to allow for quantification of FAs. Using Image J analysis software, the area of each individual FA was measured and the total area of FAs was summed for each individual cell. This value was then normalized to the area of the corresponding cell to calculate the area density of focal adhesions for each cell. For each surface condition, 10 cells were analyzed.

#### **4.2.11 Statistical Analyses**

Sigma Stat Version 3.10 (Systat Software Inc., Richmond, CA) was used to determine statistical differences among the means of experimental groups. To determine if the means of two different samples were significantly different, a Student's t-test was performed when the samples were drawn from a normally distributed population with equal variance. Sigma Stat uses the Kolmogorov-Smirnov test to test for a normally distributed population and a P value > 0.05 indicates normality. For all parametric tests, Sigma Stat assumes equal variance. When the data was not drawn from a normally distributed population (P value < 0.05), a Mann-Whitney Rank Sum Test was used and a Levene Median test was used to determine equal variance with a P value > 0.05 indicating equal variance. For both the

Student's t-test and the Mann-Whitney Rank Sum Test, a p value < 0.05 indicated a significant difference between the means of experimental groups.

To determine statistical differences among the means of three or more experimental groups a One Way Analysis of Variance (ANOVA) was used when the samples were drawn from a normally distributed population with equal variance (Kolmogorov-Smirnov test for normal distribution and equal variance was assumed). When the data was not normally distributed, a Kruskal-Wallis One way ANOVA on ranks was performed (Levene Median test to determine equal variance with a P > 0.05 indicating equal variance). When a statistical difference was detected among the group means, a Tukey post-hoc analysis was performed for both the One Way ANOVA and Kruskal-Wallis One Way ANOVA on ranks. A p value < 0.05, for both variance tests, indicated a significant difference between the groups.

## 4.3 RESULTS

### 4.3.1 Model Surfaces with Precisely Tailored Surface Chemistries

Self-assembled monolayer surfaces presenting nonpolar hydrophobic (CH<sub>3</sub>), negatively charged (COOH), neutral hydrophilic (OH), and positively charged (NH<sub>2</sub>) surfaces were produced at physiological conditions (pH 7.4) (Figure 4.3).

Contact angles obtained from this study were  $112 \pm 1^\circ$  for CH<sub>3</sub>,  $20 \pm 2^\circ$  for OH,  $29 \pm 2^\circ$  for COOH, and  $46 \pm 2^\circ$  for NH<sub>2</sub> (Table 4.1) and are comparable to previously reported values for the same or similar alkanethiols.<sup>29,38</sup>

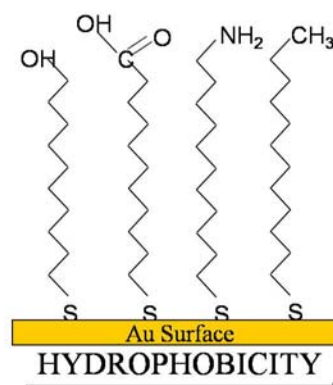


**Figure 4.3 SAMs on Gold Surface.** Cartoon depicts alkanethiols with different functional end groups to obtain different chemistries on a gold surface. The hydrophobicity of each alkanethiol increases going from left to right.

**Table 4.1 Contact Angle and Characteristic Properties of SAMs**

	Chemical Name	Contact Angle	Property
OH	11-mercapto-1-undecanol	20+/-2	Hydrophilic neutral
COOH	11-mercaptopundecanoic acid	29+/-2	Negatively charged
NH <sub>2</sub>	11-amino-1-undecanethiol	46+/-2	Positively charged
CH <sub>3</sub>	1-dodecanethiol	112+/-1	Hydrophobic

### 4.3.2 Determining Saturation Levels of FN

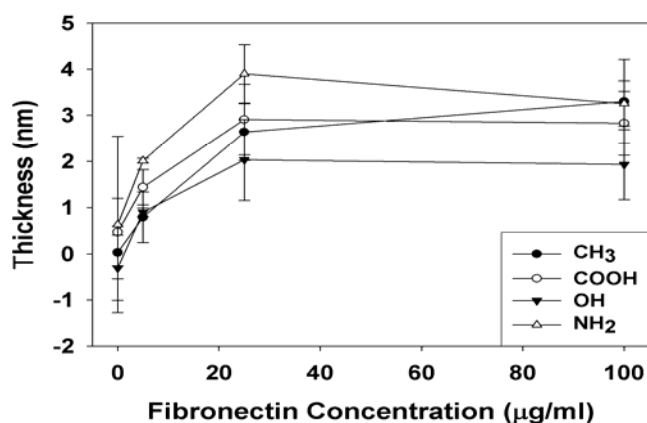


**Figure 4.4. Relationship Between FN Concentration and Thickness on SAM Surfaces.** Ellipsometry was used to determine saturation levels of adsorbed FN on CH<sub>3</sub>, COOH, OH, and NH<sub>2</sub> terminated SAM surfaces. FN concentrations of 0, 5, 25, and 100 µg/ml were passively adsorbed for 1 hour. It was found that saturation was achieved for all surfaces at 25 µg/ml. No statistical differences were found between 25 µg/ml and 100 µg/ml on each SAM surface or between different SAM surfaces at 25 µg/ml (One way ANOVA with Tukey post-hoc analysis). For each surface condition 4 samples were evaluated at each concentration. Data is plotted as mean ± standard deviations.<sup>39</sup>

At 1 hour, ellipsometry showed that the thickness of adsorbed FN increased between the surfaces treated with 5 µg/ml and 25 µg/ml and plateaued at a concentration of 25 µg/ml on all SAM surfaces. No statistical differences were observed between 25 µg/ml and 100 µg/ml on any surface examined (Figure 4.4<sup>39</sup>). When FN was adsorbed onto SAM surfaces for 4 hours, the thicknesses of the FN were comparable to those measured at 1 hr (data not included).

When comparing the thicknesses of FN on each SAM surface after 25 µg/ml was adsorbed, no statistical differences were found. Based on our ellipsometry data, we chose to use 25 µg/ml as our FN concentration to saturate each SAM surface.



### 4.3.3 Analysis of SAM Directed Changes in FN Conformation

Analyses of fluorescent images indicated that at low surface density, FN treated OH surfaces exhibited a statistically greater HFN 7.1 positive area than the other surfaces evaluated (Figure 4.5<sup>39</sup>). When surfaces were treated with saturated surface densities of FN, HFN 7.1 positive areas on CH<sub>3</sub>, and NH<sub>2</sub> functionalized substrates as well as TCPS were statistically greater than the OH and COOH functionalized surfaces.

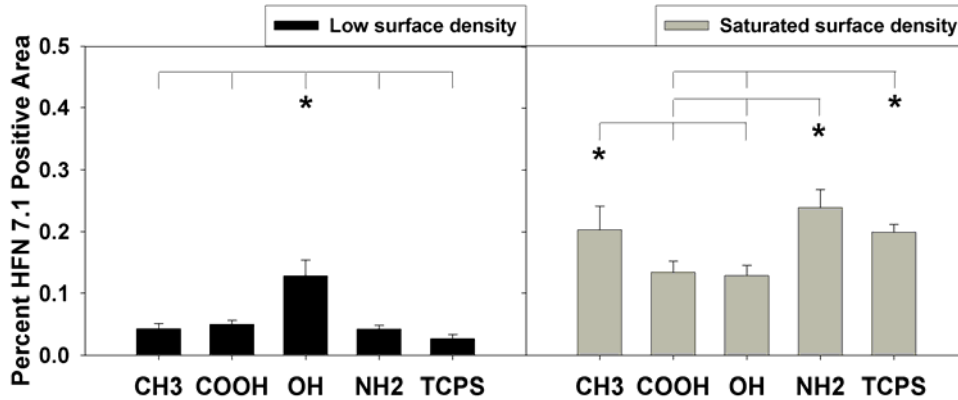


**Figure 4.5. Analysis of Changes in FN Conformation on SAM Surfaces.** To determine the relative quantity of cell binding sites of FN an antibody directed towards the RGD and PHSRN sites of was used. At low FN surface density, OH terminated surfaces promoted a significant increase in positive HFN 7.1 area and at saturated FN surface densities, CH<sub>3</sub>, NH<sub>2</sub>, and TCPS surfaces facilitated a significant increase in positive HFN 7.1 area. For both low and saturated surface densities \* indicates statistical difference using One way ANOVA with Tukey post hoc analysis  $p < 0.05$ . Sample values of  $n = 4$  and data is plotted as mean  $\pm$  standard deviations.<sup>39</sup>

### 4.3.4 SAM Dependent Changes in FN Treated Surfaces Direct Keratinocyte Attachment

The percentage of keratinocyte attachment at low FN surface density was found to be significantly higher on OH terminated SAM surfaces (25%) than other surfaces evaluated (14 – 18%) (Figure 4.6<sup>39</sup>). When comparing keratinocyte attachment at low surface density and saturated surface densities of FN for each surface condition, a statistically significant increase was found for all surfaces except for OH terminated surfaces. At saturated surface densities of FN, keratinocyte attachment values on CH<sub>3</sub>, NH<sub>2</sub>, and TCPS surfaces were comparable to each other and significantly greater than on the other surfaces, 55% vs. 25%,

respectively. These findings exhibit a trend that is consistent with the results of analyses of available cell binding epitopes for FN treated SAM surfaces.

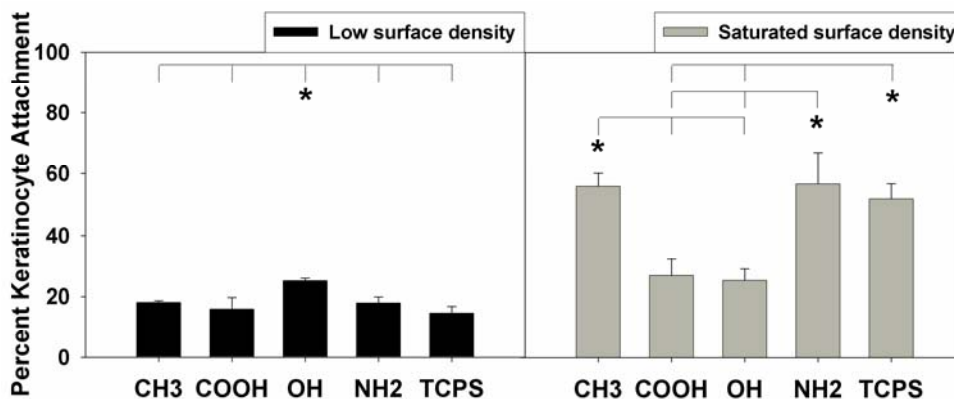


**Figure 4.6. Keratinocyte Attachment on FN Treated SAM Surfaces.** Cell nuclei were stained to determine attachment percentage of keratinocytes on various SAM surfaces. Results indicate that at low surface density OH terminated surfaces promoted a significant increase in percent keratinocyte attachment and at saturated surface densities there was a statistically significant increase in percent keratinocyte attachment on CH<sub>3</sub>, NH<sub>2</sub>, and TCPS surfaces. For both low and saturated surface densities \* indicates statistical difference using One way ANOVA with Tukey post hoc analysis  $p < 0.05$ . Sample values of  $n = 3$  and data is plotted as mean  $\pm$  standard deviations.<sup>39</sup>

#### 4.3.5 SAM Dependent Changes in Fibronectin Treated Surfaces Direct Keratinocyte Morphology

At low FN surface densities, OH terminated SAM surfaces facilitated a statistically significant increase in cell spreading relative to all other surfaces analyzed (Figure 4.7<sup>39</sup>). In comparing keratinocyte spreading at low surface density and saturated surface densities of FN for each surface condition, a statistically significant increase was found for all surfaces except for OH terminated surfaces. When we evaluated the effects of FN treated SAM substrates at saturated surface densities, it was found that NH<sub>2</sub>, CH<sub>3</sub>, and TCPS surfaces mediated the same amount of keratinocyte spreading, and all of these surfaces promoted significantly greater keratinocyte spreading than OH and COOH functionalized surfaces.

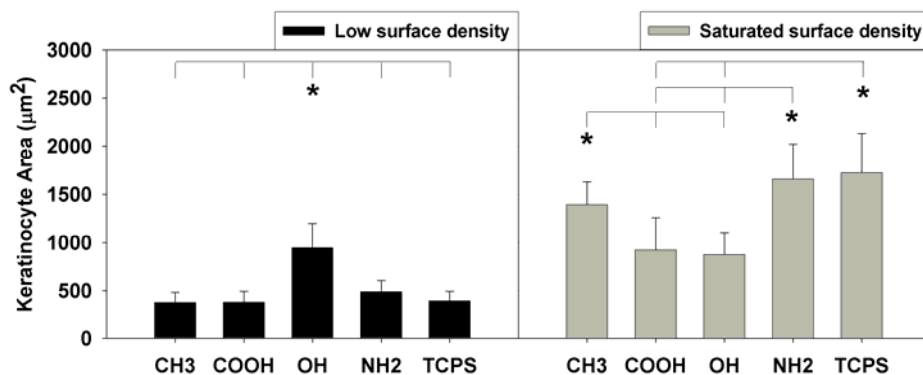


**Figure 4.7. Keratinocyte Spreading Area on FN Treated SAM Surfaces.** For morphological assessment of keratinocytes, cell spreading area was analyzed. At low FN surface density, OH terminated surfaces promoted a significant increase in keratinocyte spreading and at saturated FN surface densities, CH<sub>3</sub>, NH<sub>2</sub>, and TCPS surfaces facilitated a significant increase in cell spreading. For low surface density \* indicates statistical difference using One way ANOVA with Tukey post hoc analysis  $p < 0.05$  and for saturated surface density \* indicates statistical difference using Kruskal-Wallis One way ANOVA on ranks with Tukey post hoc analysis  $p < 0.05$ . Sample values of  $n = 15$  and data is plotted as mean  $\pm$  standard deviations.<sup>39</sup>

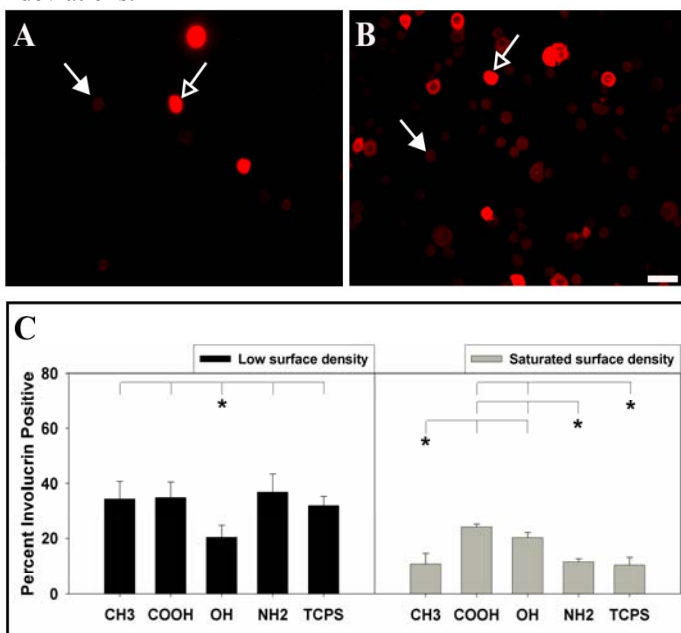
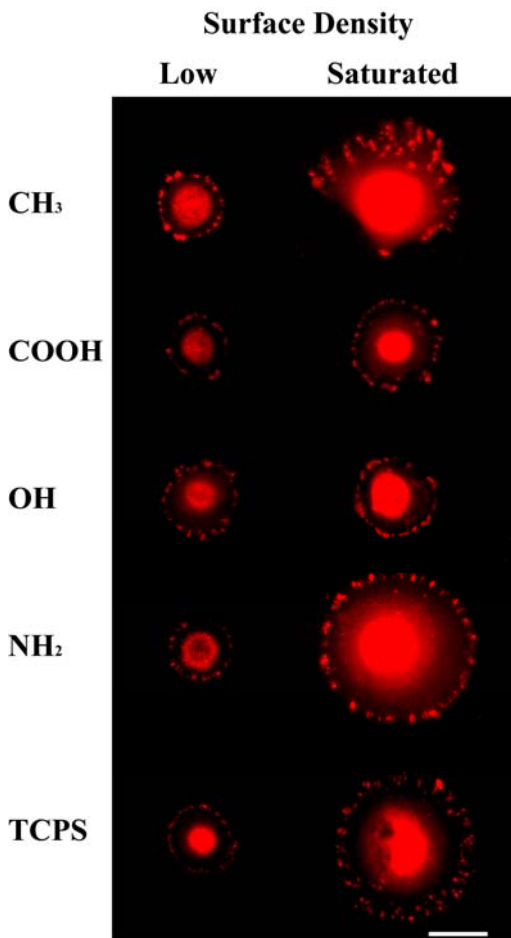


**Figure 4.8. The Effect of SAM Dependent Changes in FN on Keratinocyte Differentiation.** Keratinocytes expressing involucrin were considered differentiated and can be seen as the cells that are stained positive (open arrows), whereas keratinocytes that did not express the protein were considered to stain negative (closed arrows). Fluorescent images of keratinocytes on NH<sub>2</sub> surface at A) low surface density and B) at saturated surface densities. A greater percentage of cells stained positive on the low surface density (A), in comparison to the percentage of cells that stained positive on the saturated surface densities (B). At low surface density, the OH SAM has statistically lower amounts of positive involucrin expression than the other surfaces evaluated. At saturated surface densities, CH<sub>3</sub>, NH<sub>2</sub>, and TCPS surfaces have statistically lower amounts of positive involucrin expression than COOH or OH terminated surfaces (C). For both low and saturated surface densities \* indicates statistical difference using One way ANOVA with Tukey post hoc analysis  $p < 0.05$ . Scale bar represents 50  $\mu\text{m}$ . Sample values of  $n = 4$  and data is plotted as mean  $\pm$  standard deviations.<sup>39</sup>

involucrin expression decreased significantly for all surfaces except OH terminated surfaces. Additionally, CH<sub>3</sub>, NH<sub>2</sub>, and TCPS surfaces were shown to have the lowest levels of involucrin positive expression (~11%).

#### 4.3.7 Quantification of FA on FN Treated SAM Surfaces



Fluorescent images of keratinocytes on OH surfaces at low FN surface density suggest these cells had a greater spreading area and appeared to express more FAs than cells on the other surfaces. At saturated FN surface densities, cells cultured on CH<sub>3</sub>, NH<sub>2</sub>, and TCPS surfaces displayed larger spreading areas and appeared to have more FAs than cells cultured on COOH and OH surfaces (Figure 4.9<sup>39</sup>). Qualitative analyses showed that at a low FN surface density, the area density of FAs in each cell on OH terminated surfaces was statistically greater than on other surfaces. At saturated FN surface densities, all surfaces except for the OH surface exhibited an increase in area density of FAs when compared to low FN surface densities and the area density of FAs on NH<sub>2</sub>, CH<sub>3</sub>, and TCPS surface was significantly greater than on the OH and COOH

**Figure 4.9. FA Analysis on SAM Surfaces.** An anti-vinculin antibody was used to determine presence of FAs. Keratinocytes cultured on OH at low FN surface density appeared to have more FAs than on the other surfaces evaluated. Cells cultured on CH<sub>3</sub>, NH<sub>2</sub>, and TCPS at saturated FN surface densities exhibited larger spreading areas and appeared to have more FA than the COOH and OH surfaces. Additionally, when comparing FAs at low and saturated surface densities, CH<sub>3</sub>, COOH, NH<sub>2</sub>, and TCPS surfaces exhibited a difference in the size and number of FAs. Scale bar represents 25 μm.<sup>39</sup>

surfaces (Figure 4.10<sup>39</sup>). Additionally, at saturated FN surface densities, we observed that the size and amount of FAs were greater on the NH<sub>2</sub>, CH<sub>3</sub>, and TCPS surfaces.

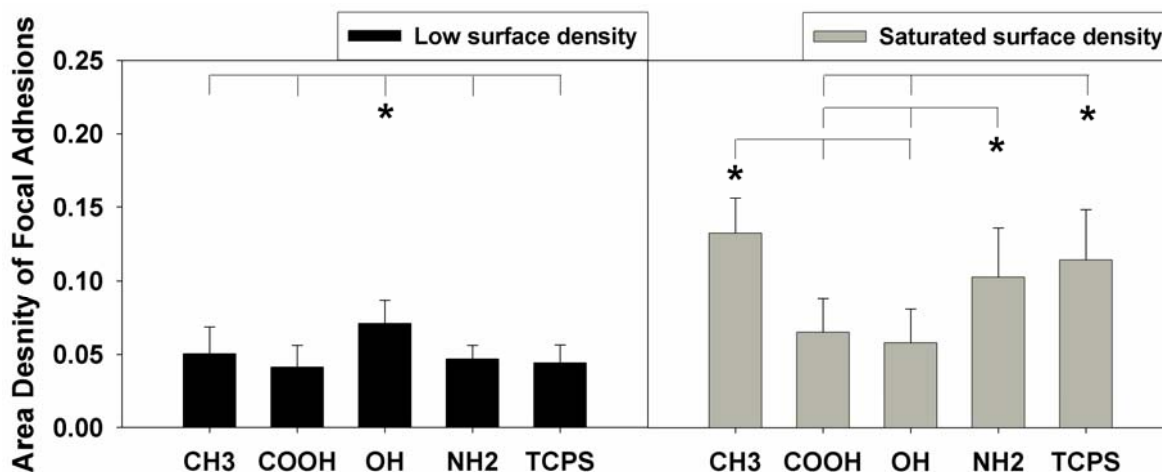


**Figure 4.10. FA Area Density Measurements.** The area density of FAs was determined using immunostaining techniques coupled with fluorescent microscopy. Keratinocytes cultured on OH at low FN surface density exhibited increased area density of FAs in comparison with the other surfaces examined. At high FN surface density, increased area density of FAs were expressed on CH<sub>3</sub>, NH<sub>2</sub>, and TCPS surfaces in comparison with the OH and COOH surfaces. For both low and saturated surface densities \* indicates statistical difference using One way ANOVA with Tukey post hoc analysis  $p < 0.05$ . Sample values of  $n = 10$  and data is plotted as mean  $\pm$  standard deviations.<sup>39</sup>

#### 4.4 DISCUSSION

A critical component in the advancement of tissue engineered skin substitutes is the development of biomaterials that are tailored to include specific biochemical cues which direct cellular signaling and subsequent physiological functions. In the present study, we used SAMs as model biomaterial surfaces to examine the role of surface chemistry on mediating the conformations and concentrations of adsorbed FN, as well as on directing keratinocyte functions that guide reepithelialization of dermal equivalents. Overall, our results indicate the NH<sub>2</sub> and CH<sub>3</sub> functional groups at saturation densities facilitate the largest quantity of FN to be adsorbed, in a manner that promotes cell binding. We also showed that the availability of synergy sites correlates with the number of FAs and

hypothesize that integrin mediated mechanisms modulate keratinocyte spreading, attachment, and differentiation.

The availability of the central cellular binding domain of FN, which spans the 9<sup>th</sup> and 10<sup>th</sup> type III repeats of the molecule, is known to play a major role in cellular attachment. This FN domain encompasses the RGD and PHSRN binding sites which are critical for integrin binding and subsequent cellular signaling.<sup>40-42</sup> Availability of this region, and the biological activity of the protein, is highly dependent on the proper structural orientation of the protein. The results of our studies indicate structural orientation and biological activity of FN is modulated by the surface chemistry of the substrate in a manner that is consistent with the results of previous research.<sup>17</sup>

Low FN density experiments were carried out to evaluate the effects of conformation of FN since at low density the same amount of FN was adsorbed on each surface (40 ng/cm<sup>2</sup>). Our results indicate at low FN surface density, FN adsorbed on the OH terminated SAM exhibited a conformation that provided an increase in available cell binding sites, relative to the other SAMs and the control surface. When evaluating keratinocyte spreading and attachment at the low surface density, we found a direct relationship between the number of available binding sites and keratinocyte spreading and attachment and an inverse relationship for keratinocyte differentiation.

Saturated FN density experiments were also performed to analyze the effects of surface chemistry on conformation and concentration of FN. At saturation densities, the OH surface exhibited the same amount of binding sites as the low density of FN on the OH surface, suggesting that the surface was saturated at both densities that were analyzed. When characterizing the relative number of binding sites on FN on the CH<sub>3</sub>, NH<sub>2</sub>, COOH, and TCPS surfaces, an increase was found between low and saturated densities. Fibronectin treated CH<sub>3</sub>, NH<sub>2</sub>, and TCPS surfaces at saturation densities exhibited a greater number of

binding sites than the COOH or OH surfaces. In a previous study, Keselowsky et al., reported that the density of FN on CH<sub>3</sub> and NH<sub>2</sub> surfaces was not statistically different from COOH SAM surfaces, at theoretical saturation densities.<sup>29</sup> Our data indicates a less preferential cellular binding conformation was achieved on the COOH surface relative to the CH<sub>3</sub> and NH<sub>2</sub> surfaces. This study also showed that there was a significant difference between the density of FN on OH and COOH surfaces at saturation densities. However, in our studies, there were no differences in available binding sites or functional measurements between these surfaces. Together, these observations indicate that even though a greater FN density was achieved on the COOH surface, it does not yield a preferential cellular binding conformation in comparison with the NH<sub>2</sub> and CH<sub>3</sub> surfaces. In addition, although the OH surface at the low surface density had increased cellular binding sites in comparison to the other surfaces, when the CH<sub>3</sub> and NH<sub>2</sub> surfaces received their saturation density of FN, they exhibited more binding sites. It cannot be determined however, if the increased binding sites on the CH<sub>3</sub> and NH<sub>2</sub> surfaces in comparison to the OH surfaces were due to conformation or concentration, or a combination of the two, since more FN was adsorbed at the saturated densities on the CH<sub>3</sub> and NH<sub>2</sub> surfaces.

One proposed mechanism to explain non-specific protein adsorption on well defined SAM surfaces is the hydrophobicity, or the wettability of the surface. It has been reported that as a surface decreases in wettability (greater contact angle), an increase in non-specific protein adsorption occurs.<sup>23</sup> Other findings suggest other mechanisms such as adsorption by charge-charge interactions as well as specific structural features of the surface, are necessary to consider for the adsorption of high molecular weight proteins, such as FN.<sup>43-45</sup> Evaluating the wettability and charge of the SAMs used in this study, we found the same relative amount of FN binding site presentation on CH<sub>3</sub> and NH<sub>2</sub> surfaces, which are hydrophobic (contact angle 112°) and neutral, and hydrophilic (contact angle 46°) and positive, respectively. These results suggest that a combination of mechanisms govern non-specific FN adsorption.

The differences in FN conformation and availability of binding sites coupled with variations in cellular responses on SAMs indicated that increased binding site presentation had a direct effect on controlling cellular processes on model biomaterial substrates. To examine the role by which the surface properties contribute to directing cellular attachment, spreading, and differentiation, we measured changes in FA formations by probing the expression of vinculin in FA complexes. Our FA data directly correlated with the number of binding sites as well as the up and down regulation of the cellular processes we examined. Focal adhesion complexes facilitate the transmission of information between the intra- and extracellular environments through integrin based mechanisms. Although we did not specifically probe for integrin subunits in this study, the strong correlations between FA expression and changes in cellular attachment, spreading, and differentiation to FN treated surfaces suggest these cellular functions were governed by integrin mediated signaling mechanisms. Previous studies examining integrin expression profiles of activated keratinocytes, both in the wound environment and culture conditions, suggest that  $\alpha_5\beta_1$  is a principle integrin that interacts with the FN and transmits information that directs cellular processes involved in reepithelialization.<sup>5,46,47</sup> These observations, together with the findings in this study, suggest that FN mediated regulation of keratinocyte functions is directed through the  $\alpha_5\beta_1$  integrin signaling pathway. In future studies, we plan to develop quantitative relationships between keratinocyte functions, specific integrin signaling pathways, and the conformation of FN. These studies will yield a series of design parameters that will enhance the ability of biomaterials to control keratinocyte functionality for use as dermal equivalents. Similarly, these design parameters will be applied to the development of percutaneous devices such as catheters and prosthesis attachments, which depend upon the rapid formation of a robust cutaneous seal with the surrounding epithelial tissue to prevent infections and implant failure.

To improve the design of dermal analogs, it is essential to develop relationships characterizing keratinocyte interactions with FN moieties, presented at different surface densities and different conformations on the surfaces of biomaterials. In the wound healing



environment, FN is part of the provisional matrix that interacts with dermal collagens and provides signaling cues to direct re-epithelialization. These FN interactions with collagen are mediated by specific domains on the surfaces of collagen molecules that produce oriented FN binding, in a manner that presents FN binding sites for cellular interactions. Specifically, the main collagen found in the dermis is collagen type I, and the FN binding site is found on the  $\alpha 1(I)$  chain between amino acid residues 757-791.<sup>9</sup> In a study comparing the effects of adsorbed FN conformation on tissue culture polystyrene and collagen coated polystyrene, it was shown that the saturation density of FN on collagen was approximately half the amount of that on tissue culture polystyrene. Additionally, when the surfaces were immunoprobed for quantities of cell binding domains at saturation densities, FN treated tissue culture polystyrene exhibited an increase in fluorescence intensity for HFN 7.1 binding relative to the values observed on FN treated collagen surfaces. Furthermore, when equal surface densities of FN were adsorbed to tissue culture polystyrene and collagen surfaces, minimal myoblast differentiation was found on the tissue culture polystyrene surface in comparison with the collagen surface.<sup>17</sup> These findings suggest that passively adsorbing FN to collagen surfaces and collagen membranes represents a promising, but suboptimal approach to directing keratinocyte functions on engineered biomaterials. Additionally, the results of our present study suggest that strategically conjugating FN to the collagen membranes by functionalizing the surface of the collagen with a  $\text{NH}_2$  or  $\text{CH}_3$  terminated ligand will increase the availability of the FN synergy sites and will significantly enhance keratinocyte attachment and reepithelialization of collagen based dermal equivalents.

#### **4.5 ACKNOWLEDGMENTS**

This work was funded in part by a grant from the WPI Research Development Council, the Bioengineering Institute at WPI, NIH Grant EB-005645 (GDP), and the U.S. Army Medical Research and Material Command (USAMRC); grant W81XWH-08-01-0422. The views, opinions, and/or findings and information contained this manuscript are those of the authors and should not be construed as an official Department of Defense position or policy, unless

so designated by other documentation. No official endorsement should be made. The HFN 7.1 hybridoma supernatant was obtained from the Developmental Studies Hybridoma Bank developed under the auspices of the NICHD and maintained by the University of Iowa, Department of Biological Sciences, Iowa City, IA: R.J. Klebe, contributor. I would like to thank The Department of Obstetrics and Gynecology at UMMS (Worcester, MA) for providing neonatal foreskins for keratinocyte isolations. Additionally, I would like to thank the co-authors of this work including Pete Driscoll, Ernesto Soto, Chris Lambert, Grant McGimpsey, and my advisor George Pins. Also I would like to thank Kevin Cornwell, and Donna Davidson for their technical assistance.

#### 4.6 REFERENCES

1. Clark RA, Lanigan JM, DellaPelle P, Manseau E, Dvorak HF, Colvin RB. Fibronectin and fibrin provide a provisional matrix for epidermal cell migration during wound reepithelialization. *J Invest Dermatol* 1982;79(5):264-9.
2. Larjava H, Salo T, Haapasalmi K, Kramer RH, Heino J. Expression of integrins and basement membrane components by wound keratinocytes. *J Clin Invest* 1993;92(3):1425-35.
3. Clark RA, Winn HJ, Dvorak HF, Colvin RB. Fibronectin beneath reepithelializing epidermis in vivo: sources and significance. *J Invest Dermatol* 1983;80 Suppl:26s-30s.
4. Bickenbach JR, Chism E. Selection and extended growth of murine epidermal stem cells in culture. *Exp Cell Res* 1998;244(1):184-95.
5. Adams JC, Watt FM. Expression of beta 1, beta 3, beta 4, and beta 5 integrins by human epidermal keratinocytes and non-differentiating keratinocytes. *J Cell Biol* 1991;115(3):829-41.
6. Bush KA, Downing BR, Walsh SE, Pins GD. Conjugation of extracellular matrix proteins to basal lamina analogs enhances keratinocyte attachment. *J Biomed Mater Res A* 2007;80(2):444-52.
7. Boyce ST, Hansbrough JF. Biologic attachment, growth, and differentiation of cultured human epidermal keratinocytes on a graftable collagen and chondroitin-6-sulfate substrate. *Surgery* 1988;103(4):421-31.
8. Tinois E, Tiollier J, Gaucherand M, Dumas H, Tardy M, Thivolet J. In vitro and post-transplantation differentiation of human keratinocytes grown on the human type IV collagen film of a bilayered dermal substitute. *Exp Cell Res* 1991;193(2):310-9.
9. Kleinman HK, McGoodwin EB, Martin GR, Klebe RJ, Fietzek PP, Woolley DE. Localization of the binding site for cell attachment in the alpha1(I) chain of collagen. *J Biol Chem* 1978;253(16):5642-6.
10. Kaur P. Interfollicular epidermal stem cells: identification, challenges, potential. *J Invest Dermatol* 2006;126(7):1450-8.
11. Erickson HP, Carrell NA. Fibronectin in extended and compact conformations. Electron microscopy and sedimentation analysis. *J Biol Chem* 1983;258(23):14539-44.
12. Hynes R. Fibronectin. In: Kreis T, Vale R, editors. *Guidebook to the Extracellular Matrix and Adhesion Proteins*. New York: Oxford University Press; 1993.
13. Ruoslahti E, Pierschbacher MD. Arg-Gly-Asp: a versatile cell recognition signal. *Cell* 1986;44(4):517-8.

14. Pierschbacher MD, Ruoslahti E, Sundelin J, Lind P, Peterson PA. The cell attachment domain of fibronectin. Determination of the primary structure. *J Biol Chem* 1982;257(16):9593-7.
15. McClary KB, Ugarova T, Grainger DW. Modulating fibroblast adhesion, spreading, and proliferation using self-assembled monolayer films of alkylthiolates on gold. *J Biomed Mater Res* 2000;50(3):428-39.
16. Keselowsky BG, Collard DM, Garcia AJ. Integrin binding specificity regulates biomaterial surface chemistry effects on cell differentiation. *Proc Natl Acad Sci U S A* 2005;102(17):5953-7.
17. Garcia AJ, Vega MD, Boettiger D. Modulation of cell proliferation and differentiation through substrate-dependent changes in fibronectin conformation. *Mol Biol Cell* 1999;10(3):785-98.
18. Koenig AL, Gambillara V, Grainger DW. Correlating fibronectin adsorption with endothelial cell adhesion and signaling on polymer substrates. *J Biomed Mater Res A* 2003;64(1):20-37.
19. Watt FM, Jordan PW, O'Neill CH. Cell shape controls terminal differentiation of human epidermal keratinocytes. *Proc Natl Acad Sci U S A* 1988;85(15):5576-80.
20. Watt FM, Kubler MD, Hotchin NA, Nicholson LJ, Adams JC. Regulation of keratinocyte terminal differentiation by integrin-extracellular matrix interactions. *J Cell Sci* 1993;106 ( Pt 1):175-82.
21. Adams JC, Watt FM. Fibronectin inhibits the terminal differentiation of human keratinocytes. *Nature* 1989;340(6231):307-9.
22. Tziampazis E, Kohn J, Moghe PV. PEG-variant biomaterials as selectively adhesive protein templates: model surfaces for controlled cell adhesion and migration. *Biomaterials* 2000;21(5):511-20.
23. Prime KL, Whitesides GM. Self-assembled organic monolayers: model systems for studying adsorption of proteins at surfaces. *Science* 1991;252(5010):1164-7.
24. Mrksich M, Dike LE, Tien J, Ingber DE, Whitesides GM. Using microcontact printing to pattern the attachment of mammalian cells to self-assembled monolayers of alkanethiolates on transparent films of gold and silver. *Exp Cell Res* 1997;235(2):305-13.
25. Wang H, He Y, Ratner BD, Jiang S. Modulating cell adhesion and spreading by control of FnIII7-10 orientation on charged self-assembled monolayers (SAMs) of alkanethiolates. *J Biomed Mater Res A* 2006;77(4):672-8.
26. Bain C, Evall J, Whitesides GM. Formation of monolayers by the coadsorption of thiols on gold: Variation in the head group, tail group and solvent. *J Am Chem Soc* 1989;111:7155-7164.
27. Mrksich M. A surface chemistry approach to studying cell adhesion. *Chem. Soc. Rev.* 2000;29:267-273.
28. Lee MH, Ducheyne P, Lynch L, Boettiger D, Composto RJ. Effect of biomaterial surface properties on fibronectin- $\alpha$ 5 $\beta$ 1 integrin interaction and cellular attachment. *Biomaterials* 2006;27(9):1907-16.
29. Keselowsky BG, Collard DM, Garcia AJ. Surface chemistry modulates fibronectin conformation and directs integrin binding and specificity to control cell adhesion. *J Biomed Mater Res A* 2003;66(2):247-59.
30. Carter WG, Symington BE, Kaur P. Cell adhesion and the basement membrane in early epidermal morphogenesis. In: Fleming TP, editor. *Epithelial Organization and Development*. London: Chapman and Hall; 1992. p 299-327.
31. Pins GD, Toner M, Morgan JR. Microfabrication of an analog of the basal lamina: biocompatible membranes with complex topographies. *Faseb J* 2000;14(3):593-602.
32. Bowditch RD, Halloran CE, Aota S, Obara M, Plow EF, Yamada KM, Ginsberg MH. Integrin  $\alpha$ IIb  $\beta$ 3 (platelet GPIIb-IIIa) recognizes multiple sites in fibronectin. *J Biol Chem* 1991;266(34):23323-8.
33. Elliott JT, Tona A, Plant AL. Comparison of reagents for shape analysis of fixed cells by automated fluorescence microscopy. *Cytometry A* 2003;52(2):90-100.
34. Obedencio GP, Nuccitelli R, Isseroff RR. Involucrin-positive keratinocytes demonstrate decreased migration speed but sustained directional migration in a DC electric field. *J Invest Dermatol* 1999;113(5):851-855.

35. Simon M, Green H. Participation of membrane-associated proteins in the formation of the cross-linked envelope of the keratinocyte. *Cell* 1984;36(4):827-34.
36. Rice RH, Green H. Presence in human epidermal cells of a soluble protein precursor of the cross-linked envelope: activation of the cross-linking by calcium ions. *Cell* 1979;18(3):681-94.
37. Frey MT, Tsai IY, Russell TP, Hanks SK, Wang YL. Cellular responses to substrate topography: role of myosin II and focal adhesion kinase. *Biophys J* 2006;90(10):3774-82.
38. Scotchford CA, Gilmore CP, Cooper E, Leggett GJ, Downes S. Protein adsorption and human osteoblast-like cell attachment and growth on alkylthiol on gold self-assembled monolayers. *J Biomed Mater Res* 2002;59(1):84-99.
39. Bush KA, Driscoll PF, Soto ER, Lambert CR, McGimpsey WG, Pins GD. Designing Tailored Biomaterial Surfaces to Direct Keratinocyte Morphology, Attachment, and Differentiation. *J Biomed Mater Res A* 2008.
40. Pierschbacher MD, Hayman EG, Ruoslahti E. Location of the cell-attachment site in fibronectin with monoclonal antibodies and proteolytic fragments of the molecule. *Cell* 1981;26(2 Pt 2):259-67.
41. Aota S, Nomizu M, Yamada KM. The short amino acid sequence Pro-His-Ser-Arg-Asn in human fibronectin enhances cell-adhesive function. *J Biol Chem* 1994;269(40):24756-61.
42. Hynes RO. Structure of Fibronectins. *Fibronectins*. New York: Springer-Verlag; 1990. p 113-175.
43. Sigal G, Mrksich M, Whitesides GM. Effect of surface wettability on the adsorption of proteins and detergents. *J Am Chem Soc* 1998;120:3464-3473.
44. Cutler SM, Garcia AJ. Engineering cell adhesive surfaces that direct integrin alpha5beta1 binding using a recombinant fragment of fibronectin. *Biomaterials* 2003;24(10):1759-70.
45. Wilson K, Stuart SJ, Garcia A, Latour RA, Jr. A molecular modeling study of the effect of surface chemistry on the adsorption of a fibronectin fragment spanning the 7-10th type III repeats. *J Biomed Mater Res A* 2004;69(4):686-98.
46. Adams JC, Watt FM. Changes in keratinocyte adhesion during terminal differentiation: reduction in fibronectin binding precedes alpha 5 beta 1 integrin loss from the cell surface. *Cell* 1990;63(2):425-35.
47. Grinnell F. Wound repair, keratinocyte activation and integrin modulation. *J Cell Sci* 1992;101 ( Pt 1):1-5.

---

---

## Chapter 5: Carbodiimide Conjugation of Fibronectin on Collagen Basal Lamina Analogs Enhances Cellular Binding Domains & Epithelialization

---

### 5.1 INTRODUCTION

In the development of bioengineered skin substitutes for replacement of skin lost to trauma or disease, the addition of biologically active molecules, that promote key events in non-scarring self-healing wounds, has the potential to guide epithelialization. In the native wound environment, fibronectin (FN) is part of the provisional matrix that interacts with dermal collagens and promotes the migration of keratinocytes through granulation tissue of the wound.<sup>1-3</sup> Fibronectin is also involved in basement membrane synthesis and organization of the wound site, which are critical for the reestablishment of a healthy functional tissue.<sup>4</sup> *In vitro* studies have examined the effect of FN on keratinocyte functions necessary for reepithelialization. When FN was passively adsorbed on bacteriological plastic, an increase in percentage of adherent cells was obtained.<sup>5</sup> Studies where polystyrene was coated with FN showed enhanced migration<sup>6</sup> and inhibition of terminal differentiation on the FN surfaces.<sup>7</sup> Fibronectin also has been passively adsorbed to biomaterials that have the potential for implantation. Studies incorporating FN on the surface of PLGA, through passive adsorption, found limited keratinocyte migration; however, it was found that when FN was passively adsorbed to collagen, migration increased.<sup>8</sup> Research investigating passive adsorption of FN to collagen-glycosaminoglycan (GAG) membranes found an increase in attachment over non-modified collagen surfaces.<sup>9</sup>

In addition to investigating keratinocyte responses to full FN molecules, the modification of biomaterial surfaces with synthetic peptides located in the central cellular binding domain of FN, specifically the arginine-glycine-aspartic acid (RGD) sequence have been examined. Arginine-glycine-aspartic acid peptides have been covalently coupled to collagen-GAG matrices<sup>10</sup> and to a hyaluronate synthetic matrix.<sup>11</sup> Both studies found increased keratinocyte attachment and spreading in comparison to those on unmodified matrices. Although this approach allows for more RGD sites to be expressed on the surface of the biomaterials, these short sequences lack full biological activity when compared with the native protein.<sup>12,13</sup>

During wound healing, as well as in cell culture expansion from healthy skin, keratinocytes express an increase in the integrin receptor  $\alpha_5\beta_1$  which is specific for the central cellular binding domain of FN.<sup>4,6,14</sup> The availability of this FN domain and its full biological activity is highly dependent on the structural orientation of the protein and has been found to be critical in modulating cellular functions.<sup>15-19</sup> When FN adsorbs to a surface, it undergoes a conformation change, which is highly dependent upon the properties of the surface.<sup>20-22</sup> Recently, our laboratory investigated the availability of the central cellular binding domain of FN and its role on keratinocyte morphology, attachment, and differentiation using self-assembled monolayers as model biomaterial surfaces.<sup>23</sup> A direct relationship was found between keratinocyte spreading area and attachment, and an indirect relationship was found between cellular binding domain availability and cell differentiation. When evaluating focal adhesion formation, it was found that the area density of focal adhesions in individual keratinocytes directly corresponded with the availability of the central cellular binding domain of FN, suggesting that the functions evaluated were integrin mediated.

Although much is known regarding the advantages of using FN to enhance re-epithelialization in the wound environment, little work has been performed investigating its presentation on dermal scaffolds. Furthermore, understanding how to strategically modify a

biomaterial surface to increase the availability of the central cellular binding domain, which has been shown to promote attachment and subsequent intracellular signaling events, is of great importance for enhancing epithelialization of bioengineered skin substitutes as well for engineering other functional tissues.

The purpose of this chapter was to evaluate the presence of the central cellular binding domain of FN on collagen membranes and to analyze how the presentation of this binding site effects epithelialization. Using an *in vitro* skin model, keratinocyte and overall graft morphology, epidermal thickness, and proliferation were evaluated on the surface of collagen-GAG membranes. Fibronectin was found to promote epithelial layers on dermal scaffolds that were found to be morphologically similar to that of native skin. When evaluating proliferation in this model system, we found that FN treated surfaces enhanced the number of proliferative cells at 3 days of air/liquid (A/L) interface culture. To correlate these findings with the presentation of FN on the surfaces, we evaluated the availability of the central cellular binding domain on collagen-GAG membranes. In effort to further enhance the presentation of FN on the surfaces of basal lamina analogs, we developed self-assembled collagen membranes, fabricated from soluble type I collagen molecules (CI) and compared their performance to collagen-GAG membranes. In this chapter we also describe a method to covalently modify the surfaces of self-assembled CI membranes with FN using a carbodiimide conjugation strategy, specifically (1-ethyl-3-(3-dimethylaminopropyl) carbodiimide hydrochloride (EDC). Finally, we evaluated the effect of EDC conjugation on the presentation and bioactivity of FN. Overall, we demonstrated that the EDC conjugation strategy greatly enhances the availability of the central cellular binding domain of FN. We also show that this modification strategy has the potential for increasing the rate of epithelialization on the surfaces of basal lamina analogs.

## 5.2 MATERIALS AND METHODS

### 5.2.1 A/L Interface Culture Devices

To evaluate the effect of FN on epithelialization of bioengineered skin substitutes, a custom designed device was developed to analyze membranes which are precisely conjugated with FN and cultured at the A/L interface. This system creates an individual well on the surface of a collagen membrane and allows for a tight seal to be made on the surface of the composite assuring that FN placement is in the center (Figure 5.1<sup>24</sup>).

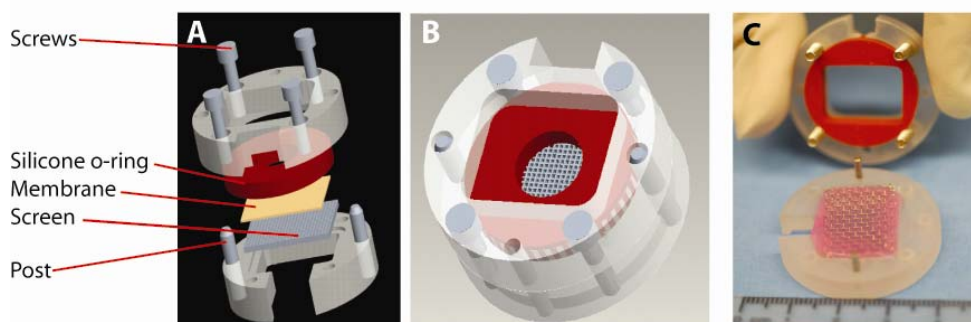


**Figure 5.1. Custom Built A/L Interface Culture Devices.** To culture keratinocytes on basal lamina analogs, a custom developed A/L interface culture device was developed by our laboratory to minimize the use of resources including cells and FN. A) Computer-Aided Design (CAD) drawing of individual parts of the device including the base and top pieces with posts on the base piece to allow for alignment of the two pieces and initial stability. A screen sits on the base piece that the membrane is placed on. This screen facilitates diffusion of cell culture medium from below the membrane and A/L interface culture. A silicone o-ring is fit in the base piece to provide a tight seal that creates a well on the surface of the collagen membrane that allows for protein modification and cell seeding. The complete unit fits in a 6-well plate. B) CAD drawing of device with base and top piece screwed together and C) shows a photograph of one of the devices with a collagen membrane placed on top of the screen during assembly.<sup>24</sup>

### 5.2.2 Basal Lamina Analog Production

#### 5.2.2.1 Collagen-GAG Membranes

A collagen-GAG dispersion containing type I collagen (5 mg/ml) and GAG (0.18 mg/ml) was prepared by placing lyophilized bovine hide derived collagen (Semed-S, Kensey Nash Corp., Exton, PA) in acetic acid (EMD Chemicals, Inc., Gibbstown, NJ) and homogenizing (20,000 rpm) at 4°C for 90 minutes resulting in a bovine-derived collagen suspension.<sup>25</sup>



Shark cartilage chondroitin 6-sulfate (Sigma, St. Louis, MI) was dripped into the blending collagen dispersion and blended for an additional 90 minutes. Once fully blended, the collagen-GAG suspension was degassed by centrifugation. To produce membranes, the suspension was cast onto flat polydimethylsiloxane silicone elastomer (PDMS, Sylgard 184, Dow Corning Corp., Midland, MI) molds 9.62 cm<sup>2</sup> in area, and allowed to air dry in a laminar flow hood at room temperature. The membrane was then gently peeled from the PDMS surface and dehydrothermally (DHT) crosslinked according to previously published methods for 24 hours.<sup>9</sup> Membranes were then stored in a desiccator until use.

#### 5.2.2.2 Self-Assembled Type I Collagen Membranes

Acid-soluble type I collagen (CI) was extracted from rat tail tendons using protocols previously described.<sup>26</sup> Rat tails were received from animals that were euthanized for other protocols, which were approved by Worcester Polytechnic Institute, Worcester, MA, Institutional Animal Care and Use Committee. Briefly, rat tail tendons were extracted from the tails of 13 Sprague Dawley rats, rinsed in dPBS (Hyclone, Logan, UT), and dissolved in 1600 ml of 3% acetic acid at 4°C overnight. The resulting solution was centrifuged at 8590 rpm for 2 hours and 320 ml of a 30% NaCl (Sigma) solution was dripped into the supernatant at 4°C. The resulting solution was allowed to sit for at least 1 hour at 4°C without disruption and then centrifuged at 4690 rpm for 30 minutes to separate precipitated and liquid material. The precipitated material was resuspended in 400 ml of 0.6% acetic acid and dialyzed for 4 hours against 1 mM HCl (JT Baker, Phillipsburg, NJ) and the dialysis solution was changed every 4 hours until a clear collagen solution was obtained. This solution was lyophilized and stored in a sealed container at 4°C, until use. Lyophilized collagen was dissolved in 5 mM HCl to obtain a working solution of 10 mg/ml.<sup>26</sup> To produce self-assembled CI membranes, 800 µl of the soluble CI solution was neutralized using 200 µl of 5x Dulbecco's Modified Eagle's Medium (DMEM, Invitrogen, Carlsbad, CA) with 0.22 M NaHCO<sub>3</sub> and 40 µl of 0.1 M NaOH (Sigma) at 37°C for 18 hours on circular PDMS molds.

### 5.2.3 FN Surface Modification of Collagen Membranes

#### 5.2.3.1 Passive Adsorption of FN to Collagen Membranes

Fibronectin (BD Biosciences, Bedford, MA) was resuspended according to manufacturer's recommendations in 1 ml of dH<sub>2</sub>O and diluted to desired concentrations (30, 100, and 300 µg/ml) using dPBS. For *in vitro* culture on basal lamina analogs, all collagen membranes were placed in A/L culture devices (Fig 5.1<sup>24</sup>) and FN (100 µg/ml) was placed in the well created on the surface of the collagen membrane and allowed to adsorb overnight at room temperature. For FN cellular binding site evaluation of basal lamina analogs, collagen membranes were placed in a custom high throughput screening device<sup>9</sup> and FN was placed into each individual wells at 30, 100, and 300 µg/ml for self-assembled CI membranes, and at 100 µg/ml for collagen-GAG membranes overnight at room temperature.

#### 5.2.3.2 1-ethyl-3-(3-dimethylaminopropyl)carbodiimide hydrochloride (EDC) Conjugation of FN to Collagen Membranes

Using protocols previously described to crosslink collagenous materials,<sup>27,28</sup> the molar ratio of 5:1 (EDC to carboxylic acid groups in collagen) was used to conjugate FN to the surfaces of collagen-GAG and self-assembled CI membranes. The theoretical amount of collagen used for calculations assumed that 1 g of type I collagen contained 1.2 mmol COOH.<sup>27,28</sup> Collagen-GAG membranes contained 12.5 mg of type I collagen and self-assembled CI membranes contained 8 mg of type I collagen, thus receiving 0.075 mmol EDC and 0.048 mmol EDC, respectively. 1-ethyl-3-(3-dimethylaminopropyl)carbodiimide hydrochloride (Sigma) was dissolved in 50 mM MES hydrate (Sigma) dissolved in 40% ethanol (Pharmco Products, Inc., Brookfield, CT) at a pH 5.5 and 1.25 ml of solution was placed on collagen-GAG membranes and 0.8 ml was placed on self-assembled CI membranes for 4 hours. For *in vitro* culture on basal lamina analogs, the membranes were removed from the EDC solution and immediately placed into the A/L culture devices and 100 µg/ml of FN was placed in the well created on the surface of the collagen membrane over night at room

temperature. For FN cellular binding site evaluation, the membranes were immediately placed in a custom high throughput screening device<sup>9</sup> and FN was placed into each individual wells at 30, 100, and 300 µg/ml for self-assembled CI membranes, and at 100 µg/ml for collagen-GAG membranes overnight at room temperature.

#### **5.2.4 Culture of Neonatal Human Keratinocytes**

Neonatal keratinocytes were cultured as previously described.<sup>9,29</sup> Neonatal foreskins were obtained from non-identifiable discarded tissues from UMass Memorial Medical Center, Worcester, MA and were approved with exempt status from the New England Institutional Review Board. Keratinocyte isolations were performed using an enzymatic treatment with a dispase (Gibco, Gaithersburg, MD) solution. The cells were propagated on a feeder layer of 3T3-J2 mouse fibroblasts (generously donated by Dr. Stelios Andreadis, State University of New York at Buffalo, Buffalo, NY) and cultured according to methods previously described<sup>29,30</sup> using keratinocyte media consisting of a 3:1 mixture of DMEM (high glucose) and Ham's F-12 medium (Invitrogen) supplemented with 10% fetal bovine serum (FBS, Hyclone),  $10^{-10}$  M cholera toxin (Vibrio Cholerae, Type Inaba 569 B), 5 µg/ml transferrin, 0.4 µg/ml hydrocortisone (Calbiochem, La Jolla, CA), 0.13 U/ml insulin,  $1.4 \times 10^{-4}$  M adenine,  $2 \times 10^{-9}$  M triiodo-L-thyronine (Sigma), 1% penicillin/streptomycin (Invitrogen), and 0.01 µg/ml epidermal growth factor (EGF, BD Biosciences). After 5 days of culture, cells were detached using 0.05% Trypsin-EDTA (Invitrogen) and then rinsed with serum free and EGF free keratinocyte media. Passage 2 keratinocytes were used in all experiments.

#### **5.2.5 *In vitro* Culture of Keratinocytes on Basal Lamina Analogs**

After FN adsorption or EDC conjugation of FN to membranes, the membranes were sterilized in composite culture devices using 70% ethanol. Membranes and devices were removed from ethanol and rinsed in sterile dPBS, 3 times for 10 minutes each, and left overnight in sterile dPBS. The composite culture devices were placed into individual wells

of a 6-well tissue culture plate and preconditioned for 30 minutes with seeding media consisting of 3:1 mixture of DMEM (high glucose) and Ham's F-12 medium supplemented with  $10^{-10}$  M cholera toxin, 0.2  $\mu\text{g/mL}$  hydrocortisone (Calbiochem), 5  $\mu\text{g/mL}$  insulin, 50  $\mu\text{g/mL}$  ascorbic acid (Sigma), and 1% penicillin/streptomycin (Invitrogen). Keratinocytes were seeded on the surfaces of the membranes at 500,000 cells/cm<sup>2</sup> using this media, and allowed to adhere for 2 hours in 10% CO<sub>2</sub> at 37°C. After 2 hours, seeding media containing 1% FBS was placed in each well, completely submerging the grafts. After 24 h, the keratinocyte seeding medium was removed, and the grafts were submerged for an additional 48 h in a keratinocyte priming medium composed of keratinocyte seeding medium (with FBS) supplemented with 24  $\mu\text{M}$  bovine serum albumin (BSA), 1.0 mM L-serine, 10  $\mu\text{M}$  l-carnitine, and a mixture of fatty acids including 25  $\mu\text{M}$  oleic acid, 15  $\mu\text{M}$  linoleic acid, 7  $\mu\text{M}$  arachidonic acid, and 25  $\mu\text{M}$  palmitic acid (Sigma).<sup>31</sup> After 48 h in priming medium, skin equivalents were cultured for 3 or 7 days with an A/L interface medium composed of serum-free keratinocyte priming medium supplemented with 1.0 ng/mL EGF.

### **5.2.6 Evaluation of Epithelialization**

To assess epithelialization on the basal lamina analogs, epidermal thickness and proliferation were evaluated after 3 or 7 days of A/L interface culture. Grafts were fixed in a 10% buffered formalin solution (EMD Chemicals), dehydrated with increasing concentrations of ethanol, cleared with sec-butyl alcohol (EMD Chemicals), and embedded in Paraplast tissue embedding medium (McCormick Scientific, St. Louis, MO). Sections of skin equivalents, 6  $\mu\text{m}$  in thickness, were cut in a plane perpendicular to the surface of the epithelial layer using a Leica RM 2235 (Leica Microsystems, Inc, Bannockburn, IL). Sections were mounted on poly-L-lysine coated slides (Erie Scientific Company, Portsmouth, NH) for hematoxylin and eosin (H&E) staining and mounted on Superfrost Plus slides (VWR, West Chester, PA) coated with poly-L-lysine (Sigma) to evaluate proliferation. To evaluate thickness of the epithelial layer, the slides were stained with Harris hematoxylin and eosin (Richard-Allan

Scientific, Kalamazoo, MI) and then viewed with a Nikon Eclipse E400 microscope (Nikon, Inc., Melville, NY). Images were captured using an RT Color Spot camera (Spot Diagnostics, Sterling Heights, MI). Thickness measurements were taken in three areas of the image using Image J software (downloaded from <http://rsb.info.nih.gov/ezproxy.umassmed.edu/ij/>) and an average value was reported for each graft. For collagen-GAG membranes with and without passive adsorbed FN, at 3 day or 7 day culture, 7 and 4 cultured basal lamina analogs were evaluated, respectively. For self-assembled CI membranes with no treatment, passive adsorption of FN, and EDC conjugation of FN, 3 grafts were evaluated for each condition.

Keratinocyte proliferation was evaluated by detecting the presence of Ki67, a marker for highly mitotic keratinocytes. The tissue sections were deparaffinized in reverse ethanol-xylene washes, and the antigens were unmasked by placing the slides in boiling Vector Unmasking solution (Vector Laboratories, Inc, Burlingame, CA) in a Mantra pressure cooker (Mantra, Inc., Virginia Beach, VA) for 1 minute after maximum pressure was achieved. Slides were then incubated with blocking solution (10% normal horse serum (Vector Laboratories) in dPBS) for 10 min at room temperature and treated with predilute mouse-antihuman Ki67 (Zymed Laboratories, South San Francisco, CA) overnight in a humidified chamber at room temperature. Slides were incubated with biotinylated anti-mouse IgG (Vector Laboratories) at 1:200 for 30 minutes at RT then washed with dPBS and stained with Vectastain Elite ABC Kit (Vector Laboratories) for 30 minutes at RT. Stained slides were washed with dPBS and developed using a Vector NovaRed Substrate Kit (Vector Laboratories) for approximately 1 min. Slides were rinsed in dPBS, followed by a 5 minute wash with tap water, and counterstained with Harris hematoxylin for 45 seconds. The slides were washed with tap water, rinsed with a series of ethanol-xylene washes and mounted with VectaMount permanent mounting medium (Vector Laboratories). The slides were then viewed with a Nikon Eclipse E400 microscope and images were captured using an RT Color

Spot camera. The number of Ki67 positive cells were counted and divided by the total number of cells in the basal layer to give a percentage of Ki67 positive cells. At 3 days or 7 days of A/L interface culture on collagen-GAG membranes passively adsorbed with FN, 3 different sections of 5 grafts were evaluated.

### **5.2.7 FN Cellular Binding Site Detection**

To measure the availability of the central cellular binding domain of FN, a monoclonal antibody directed towards this domain (HFN 7.1, Developmental Studies Hybridoma Bank, Iowa City, IA) was measured with fluorescence microscopy and image analysis.<sup>23,32</sup> After passive adsorption or EDC conjugation of FN to CI membranes, the scaffolds were sterilized for cellular culture, and then blocked using 1% heat denatured BSA (in dPBS) for 1 hour at room temperature. HFN 7.1 was added to each well for 1 h in 10% CO<sub>2</sub> at 37°C. Each surface was rinsed in blocking buffer (0.05% Tween-20 (Sigma) and 0.25% BSA in dPBS) and incubated with 546 Alexa Fluor conjugated goat anti-mouse IgG (1:200 in blocking buffer, Molecular Probes, Eugene, OR) for 1 h in 10% CO<sub>2</sub> at 37°C. Slides were then rinsed with dPBS, and images were captured using an RT Color Spot camera. Image J Analysis software was used to determine the relative amount of cellular binding sites in each well. The relative fluorescence intensity was calculated over a region of interest and normalized against fluorescence intensity of non-FN modified membranes. Eight samples were evaluated for collagen-GAG and self-assembled CI membranes that were treated with 100 µg/ml of FN using EDC conjugation or passive adsorption strategy. For self-assembled CI membranes treated with 30 or 300 µg/ml of FN, 4 samples were evaluated. Results are reported as averages and standard deviations and each experiment was repeated twice.

### **5.2.8 Statistical Analyses**

Sigma Stat Version 3.10 (Systat Software Inc., Richmond, CA) was used to determine statistical differences among the means of experimental groups. To determine if the means

of two different samples were significantly different, a Student's t-test was performed when the samples were drawn from a normally distributed population with equal variance. Sigma Stat uses the Kolmogorov-Smirnov test to test for a normally distributed population and a P value  $> 0.05$  indicates normality. For all parametric tests, Sigma Stat assumes equal variance. When the data was not drawn from a normally distributed population (P value  $< 0.05$ ), a Mann-Whitney Rank Sum Test was used and a Levene Median test was used to determine equal variance with a P value  $> 0.05$  indicating equal variance. For both the Student's t-test and the Mann-Whitney Rank Sum Test, a p value  $< 0.05$  indicated a significant difference between the means of experimental groups.

To determine statistical differences among the means of three or more experimental groups a One Way Analysis of Variance (ANOVA) was used when the samples were drawn from a normally distributed population with equal variance (Kolmogorov-Smirnov test for normal distribution and equal variance was assumed). When the data was not normally distributed, a Kruskal-Wallis One way ANOVA on ranks was performed (Levene Median test to determine equal variance with a P  $> 0.05$  indicating equal variance). When a statistical difference was detected among the group means, a Tukey post-hoc analysis was performed for both the One Way ANOVA and Kruskal-Wallis One Way ANOVA on ranks. A p value  $< 0.05$ , for both variance tests, indicated a significant difference between the groups.

## **5.3 RESULTS**

### **5.3.1 FN Enhances Epithelialization of Keratinocytes on Basal Lamina Analogs**

#### *5.3.1.1 Graft Morphology and Epidermal Layer Thickness on Collagen-GAG Basal Lamina Analogs*

The effect of passively adsorbed FN on graft morphology and epithelial layer thickness of keratinocytes was evaluated using custom built A/L interface culture devices (Figure 5.1<sup>24</sup>). Fibronectin (100  $\mu\text{g/ml}$ ) was passively adsorbed to the surfaces of collagen-GAG membranes

and keratinocytes were cultured on these basal lamina analogs for 3 or 7 days at the A/L interface. Figure 5.2<sup>24</sup> shows histological results of control grafts compared with grafts that were passively adsorbed with FN, cultured for 3 or 7 days and stained with H&E. A thicker epidermal layer formed on membranes modified with FN when compared with control membranes at 3 or 7 days of culture at the A/L interface. At 3 days, 17.7±0.9 and 52.4±6.3 μm were found for control and FN treated membranes, respectively and at 7 days, 59.6±7.4 and 89.6±4.2 μm were found for control and FN treated membranes, respectively. These differences in epithelial thickness between control and FN treated surfaces were statistically different at both time points (Figure 5.3<sup>24</sup>).

### 5.3.1.2 Keratinocyte Proliferation on Collagen-GAG Basal Lamina Analogs

To analyze keratinocyte proliferation, the presence of Ki67 in basal keratinocytes was measured on the surfaces of cultured basal lamina analogs. This protein is present during active phases of the cell cycle and absent from

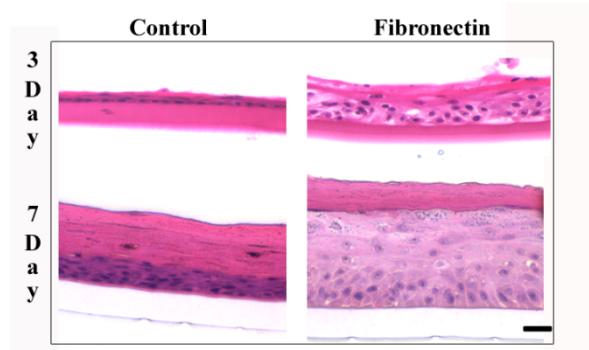


**Figure 5.2. Histological Representations of the Thicknesses of Epidermal Layers on Collagen-GAG Membranes.** Keratinocytes were cultured for 3 or 7 days at the A/L interface on collagen-GAG control (non-modified) membranes or collagen-GAG membranes that were modified by passively adsorbing FN to the surfaces of the scaffolds. At 3 or 7 days of A/L interface culture the thickness of the epithelial layer on collagen-GAG membranes treated with FN was greater than that on untreated collagen-GAG membranes. Scale bar represents 30 μm.<sup>24</sup>

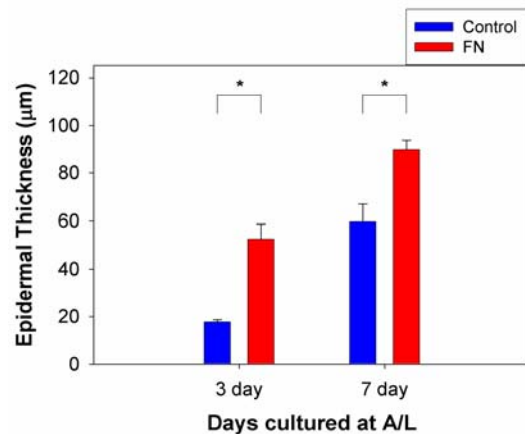


**Figure 5.3. Quantitative Evaluation of Epidermal Thickness on Collagen-GAG Membranes.** The thicknesses of the epithelial layers at 3 or 7 days of A/L interface culture were measured on control (non-modified) collagen-GAG membranes or collagen-GAG membranes that were modified by passively adsorbing FN to the surfaces. At both 3 and 7 days there was a significant difference between untreated and FN treated surfaces. (\* indicates p<0.05 Student's t-test) Samples for 3 day culture are n = 7 and for 7 day culture n = 4.<sup>24</sup>



resting cells.<sup>33</sup> Figure 5.4<sup>24</sup> shows histological images of control collagen-GAG membranes and membranes that were passively adsorbed with FN, cultured for 3 or 7 days at the A/L interface and immunoassayed for Ki67. Quantitative analyses of these images are depicted in Figure 5.5<sup>24</sup>. At 3 days of culture, positive Ki67 basal keratinocytes were counted and control surfaces and FN treated surfaces had 24.3±2.5% and 37±3.9% Ki67 positive basal cells, respectively and at 7 days control surfaces and FN treated surfaces had 23±2.7% and 21.9±2.1% Ki67 positive basal cells, respectively. The percentage of basal keratinocytes expressing Ki67 on FN modified membranes was statistically different than on control membranes at 3 days of culture, however at 7 days of culture no differences were detected.

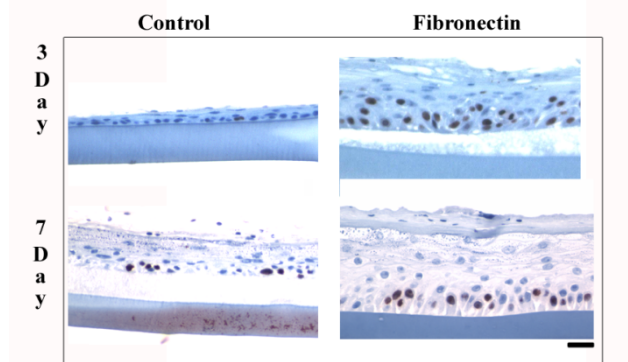


**Figure 5.4. Histological Representations of Ki67 Positive Keratinocytes on Collagen-GAG Membranes.** Keratinocytes were cultured on collagen-GAG membranes for 3 or 7 days at the A/L interface on control (non-modified) collagen-GAG membranes or collagen-GAG membranes modified by passively adsorbing FN to the surfaces. At 3 or 7 days of A/L interface culture Ki67 immunostaining (brown stained nuclei) was used to evaluate proliferation of basal keratinocytes. Scale bar represents 30  $\mu\text{m}$ .<sup>24</sup>

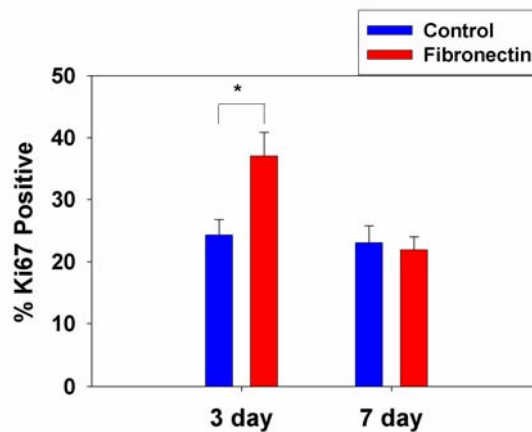


**Figure 5.5. Quantitative Analyses of Ki67 Positive Basal Keratinocytes on Collagen-GAG Membranes.** The percentage of positive Ki67 basal keratinocytes at 3 or 7 days of A/L interface culture was measured on control (non-modified) collagen-GAG membranes or collagen-GAG membranes modified by passively adsorbing FN to the surfaces. At 3 days statistical differences were found between keratinocytes cultured on control surface and FN treated surfaces (\* indicates  $p < 0.05$  Student's t-test). For all experimental conditions,  $n = 5$  samples were measured at both 3 and 7 days of culture.<sup>24</sup>

### 5.3.2 Availability of Cellular Binding Domain of FN Corresponds to Keratinocyte Attachment on Collagen-GAG Basal Lamina Analogs

The availability of the cellular binding domain of FN, specifically the domain that encompasses both the RGD and PHSRN binding sequences, was analyzed on the surfaces of collagen-GAG basal lamina analogs using an antibody directed towards this site. Relative fluorescence intensity (RFI) measurements were made on several regions of interest and an average value was reported. When FN was passively adsorbed to collagen-GAG membranes at 30, 100, or 300  $\mu\text{g/ml}$ , cellular binding sites plateaued at a concentration of 100  $\mu\text{g/ml}$  (Figure 5.6<sup>24</sup>). The fluorescence intensity values obtained at 100  $\mu\text{g/ml}$  and 300  $\mu\text{g/ml}$  were statistically greater than those at 30  $\mu\text{g/ml}$  of F. This data directly corresponds with keratinocyte attachment measurements made on FN treated collagen-GAG membranes in a previously published study.<sup>23</sup>

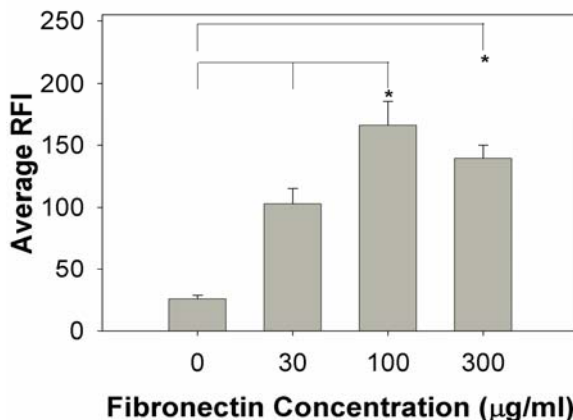


**Figure 5.6. Availability of Cellular Binding Domains for FN Passively Adsorbed on Collagen-GAG Basal Lamina Analogs.** The availability of the cellular binding domain of FN on collagen-GAG basal lamina analogs was evaluated using a quantitative immunofluorescent assay. Fibronectin concentrations of 0, 30, 100, and 300  $\mu\text{g/ml}$  were evaluated and it was determined that at a concentration of 100  $\mu\text{g/ml}$  the average RFI was statistically different from 0, and 300  $\mu\text{g/ml}$ , but did not statistically differ from 300  $\mu\text{g/ml}$  indicating that a saturation plateau was achieved. Data is reported as averages and error bars indicate standard error mean with  $n = 3$ . (\*Indicates statistical difference, one way ANOVA with Tukey post hoc analysis  $p < 0.05$ .)<sup>24</sup>

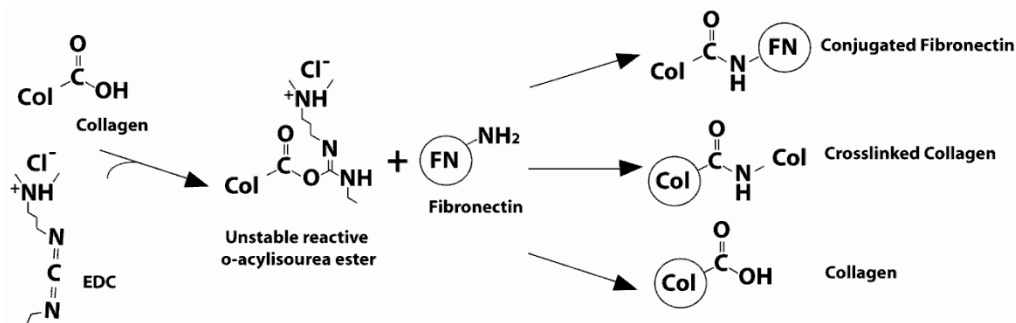


**Figure 5.7. Schematic Representation of EDC-Mediated Conjugation of FN to Collagen.** The carbodiimide 1-ethyl-3-(3-dimethylaminopropyl)carbodiimide hydrochloride (EDC) was added to basal lamina analogs at a 5:1 molar ratio (EDC molecules to carboxylic acids in collagen). The EDC reacts with a carboxylic acid from the collagen molecule to form an unstable reactive o-acylisourea ester that can either couple with an amine group in collagen from the basal lamina analog or an amide group in FN that is added to the collagen membrane. If the unstable reactive o-acylisourea ester does not interact with an amine, it hydrolyzes and the carboxyl group is regenerated, thus returning back to its native state.<sup>24</sup>

### 5.3.3 EDC Conjugation of FN on Self-Assembled CI Basal Lamina Analogs Promotes Increased Cellular Binding Site Availability

To determine whether we could increase the presentation of FN cellular binding sites on the surfaces of collagen-GAG basal lamina analogs, we analyzed the effects of covalently binding FN to the surface using an EDC conjugation strategy (Figure 5.7<sup>24</sup>). Since it was found that 100 µg/ml of FN saturated the surfaces of the collagen-GAG membranes, we chose to evaluate this concentration using both adsorption and EDC modification strategies. When analyzing collagen-GAG membranes, the difference between passive adsorption and EDC conjugation of 100 µg/ml of FN, was that EDC conjugation statistically increased the average RFI on the surfaces of FN treated membranes, suggesting that these membranes have a greater capacity for cellular binding (Figure 5.8<sup>24</sup>).

The availability of cellular binding domains on the surfaces of self-assembled CI basal lamina analogs was evaluated for both passive adsorption of FN and EDC conjugation of FN. These findings were compared with both passive adsorption and EDC conjugation of FN on collagen-GAG collagen basal lamina analogs (Figure 5.8<sup>24</sup>). When we compared the passive adsorption of 100  $\mu\text{g/ml}$  of FN on collagen-GAG and self-

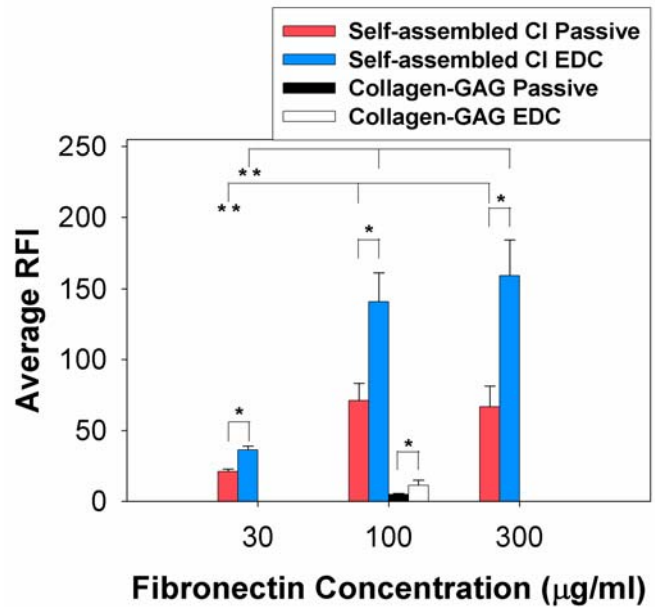


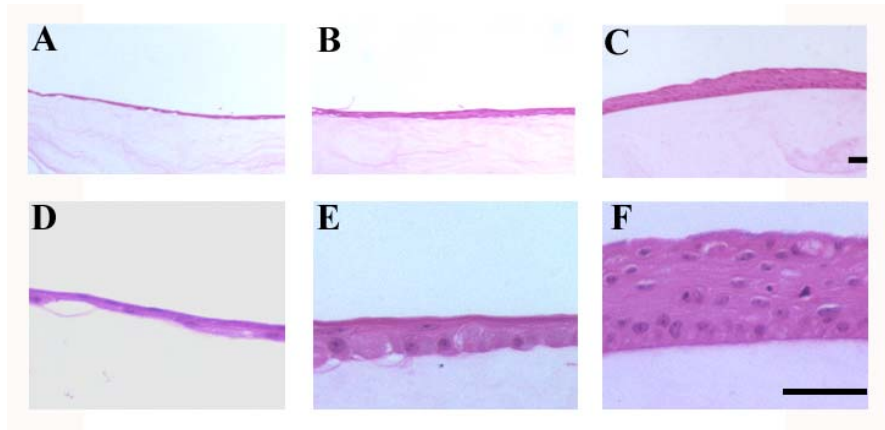
**Figure 5.8. Availability of Cellular Binding Domain of FN on collagen-GAG and Self-Assembled CI Basal Lamina Analogs.** A quantitative immunofluorescent assay was used to measure the availability of the cellular binding domain of FN on the surfaces of modified collagen membranes. \* indicates  $p < 0.05$ , Student's t-test and \*\* indicates  $p < 0.05$ , One Way ANOVA with Tukey post hoc analysis. For collagen-GAG membranes,  $n = 8$  for passive adsorption and EDC conjugation. For self-assembled CI membranes  $n = 4$  for 30 and 300  $\mu\text{g/ml}$  for both passive and EDC and  $n = 8$  for 100  $\mu\text{g/ml}$  for both passive and EDC. Experiments were repeated and similar trends were found.<sup>24</sup>

assembled CI membranes, a significant increase in average RFI was observed on the self-assembled CI membranes. Similarly, when we compared the binding efficiency of FN using an EDC conjugation strategy at a concentration of 100  $\mu\text{g/ml}$  of FN on collagen-GAG and self-assembled CI membranes, a significant increase was found in average RFI on the self-assembled CI membranes. Additional concentrations were analyzed, for both passive adsorption and EDC conjugation of FN on self-assembled CI membranes, to evaluate whether saturation levels of RFI were obtained. When evaluating lower and higher concentrations of FN (30 and 300  $\mu\text{g/ml}$ , respectively), we found that there were no statistical differences between FN concentrations of 100  $\mu\text{g/ml}$  and 300  $\mu\text{g/ml}$  and that the 100  $\mu\text{g/ml}$  concentration had statistically increased values over the 30  $\mu\text{g/ml}$  concentration, regardless of the conjugation strategy that was used. This data indicates that the presentation

of cellular binding domains on the surfaces of self-assembled CI membranes saturated at a FN concentration of 100  $\mu\text{g/ml}$ , similar to the results obtained for collagen-GAG membranes.

### 5.3.4 EDC Conjugation of FN on Self-Assembled CI Basal Lamina Analogs Enhances Epidermal Layer Thickness

Fibronectin was covalently bound to the surface of self-assembled CI membranes using EDC and keratinocytes were



cultured on the surface of basal lamina analog for 3 days at the A/L interface to determine whether

**Figure 5.9. Low and High Magnification Histological Images of Self-Assembled CI Basal Lamina Analogs Treated with FN.** The surfaces of self-assembled CI basal lamina analogs were treated with dPBS (controls) (A and D), passive adsorption of FN (B and E), or EDC conjugation of FN (C and F) and keratinocytes were cultured on the membranes at the A/L interface for 3 days. Conjugation of FN to the surfaces of the self-assembled CI basal lamina analogs using EDC caused an increase in epidermal thickness in comparison to control surfaces and surfaces treated by passively adsorbing FN to the scaffolds. Scale bars represent 50  $\mu\text{m}$ .<sup>24</sup>

increased cellular binding sites on our new model system promoted an increase in epithelial layer thickness. Figure 5.9<sup>24</sup> shows a typical image of a cultured epithelial layer on an untreated self-assembled CI membrane (5.9A and 5.9D), a basal lamina analog with FN passively adsorbed to the surface (5.9B and 5.9E), and a basal lamina analog with FN that was EDC conjugated to the surface (5.9C and 5.9F). These images suggest that the thickness of the epidermal layer on the scaffold corresponds to the presentation and availability of FN central cellular binding domains. Morphometric analyses of these epidermal layers (Figure 5.10<sup>24</sup>) showed that there were statistical differences between all surfaces analyzed.

## 5.4 DISCUSSION

To improve the regenerative capacity of biomaterials scaffolds, biomolecules have been incorporated to present biochemical cues that direct cellular functions. This approach requires that the biomolecules are precisely tailored to the surface of the biomaterial to ensure that the appropriate cellular binding domains are presented for maximum

bioactivity. To improve the compatibility and regenerative potential of biomaterials scaffolds, FN is a protein of interest to adsorb to the surfaces, based on its role in cell adhesions, migration, and differentiation.<sup>5,7-9,21</sup> However, several studies indicate that when FN is passively adsorbed to the surface of

biomaterials, its conformation is effected by surface properties, which modulate cellular binding site presentation as well as biological activity.<sup>21,22,34,35</sup> In this work we evaluated the effect of passive adsorption of FN on epithelialization of a basal lamina analog. Additionally we investigated the presentation sites of the central cellular binding domain of FN based on the preparation technique of the basal lamina analog and the conjugation strategy. Overall we determined that EDC conjugation of FN to the surface of self-assembled CI membranes improved binding site availability.

Fibronectin enhanced epithelial thickness and keratinocyte proliferation on the surfaces of

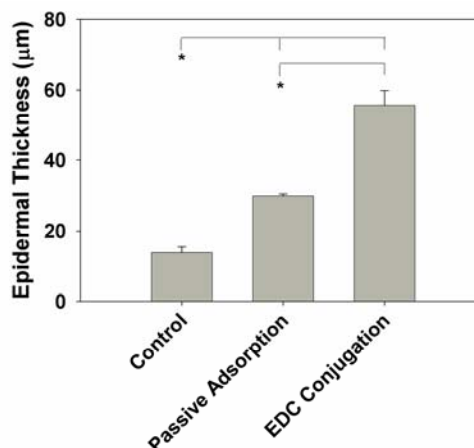


**Figure 5.10. EDC Conjugation of FN on Self-Assembled CI Basal Lamina Analogs Enhances Epidermal Thickness.** Self-assembled CI basal lamina analogs were prepared and the surfaces were treated with dPBS (Control), passive adsorption of FN (Passive Adsorption), EDC conjugation of FN (EDC Conjugation) and keratinocytes were cultured at the A/L interface for 3 days. All surfaces were statistically different from each other. Surfaces treated with EDC conjugation of FN exhibited the greatest epidermal thickness values (\* indicates  $p < 0.05$ , One-Way ANOVA with Tukey post-hoc analysis). Bars indicate mean values and error bars are standard error and sample numbers are  $n = 3$  for control and passive adsorption and  $n = 5$  for EDC conjugation.<sup>24</sup>

collagen-GAG basal lamina analogs. When FN was passively adsorbed at a saturation density previously determined on the surface,<sup>9</sup> epithelial thickness was enhanced in comparison to untreated membranes at both 3 and 7 days of A/L interface culture. The morphology of basal keratinocytes on the FN grafts exhibited a more native columnar morphology than those on the scaffolds without FN. When keratinocyte proliferation was examined using Ki67, a nuclear marker for proliferation, it was found that the percentage of Ki67 positive cells at 3 days of A/L interface culture on FN treated membranes was greater than on untreated membranes, ~35% to ~20% of total basal cells, respectively. At 7 days of A/L interface culture, no differences were found between percentages of Ki67 positive basal keratinocytes, with both membranes having ~20% of total basal cells.

In unwounded epidermis, between 10 and 20% of basal keratinocytes are proliferative, based on the location of the skin.<sup>36-38</sup> In an acute wound environment, keratinocyte proliferation is increased. Within hours after injury, keratinocytes at the wound edge become activated and undergo a phenotypic change which facilitates migration over the wound bed<sup>6,16</sup> A proliferative burst occurs 24 to 72 hours post injury and after wound closure, the proliferative capacity of the basal layer returns to normal status.<sup>39</sup> Our results suggest that FN treated scaffolds closely mimic the wound environment, and provide the appropriate signals for proliferation to occur. Once the cells sense that a monolayer is formed, proliferation returns to normal and the cells begin to undergo differentiation and migrate upward to create a stratum corneum that provides protection from the environment.

After evaluating the effects of FN on graft morphology and proliferation, we investigated the presentation of the cellular binding domain of FN that was passively adsorbed on the collagen-GAG basal lamina analogs. We determined that our FN cellular binding site presentation directly corresponded with previously published values for keratinocyte attachment to collagen-GAG membranes.<sup>9</sup> We concluded that we were saturating our

collagen-GAG membrane surfaces using passive adsorption since there were no differences between membranes that were treated with 100  $\mu\text{g/ml}$  or 300  $\mu\text{g/ml}$  of FN. To increase the number of FN presentation sites, we evaluated different sources of collagen to fabricate membranes as well as conjugation strategies to covalently link FN to the surfaces.

In this study, we analyzed the presentation of FN cellular binding domains on collagen-GAG basal lamina analogs and compared it with the FN cellular binding domains on self-assembled CI basal lamina analogs. Our initial studies focused on the use of collagen-GAG membranes fabricated from an FDA approved, commercially available product, to facilitate a rapid translation from benchtop to bedside.<sup>40</sup> Although this product has many advantageous properties; the starting collagen material is considered “insoluble” when placed in an acidic environment and does not completely dissolve into individual collagen fibrils. When a suspension of these collagen fibrils is air-dried, the aggregates of fibrils come together and form a membrane with random orientation. In contrast, the self-assembled CI membranes developed for this study are fabricated from a solution of acid solution type I collagen molecules. When neutralized, these collagen molecules self-assemble into individual fibrils, and aggregate laterally and linearly to form collagen fibers with structural morphology comparable to native tissue constructs.<sup>41</sup> Our studies indicate that when 100  $\mu\text{g/ml}$  of FN is passively adsorbed to the surfaces of the different collagen membranes, the self-assembled CI basal lamina analog has significantly more FN cellular binding site availability than the collagen-GAG basal lamina analog. With CI, the FN binding site is found on the  $\alpha 1(1)$  chain between amino acid residues 757-791.<sup>42</sup> When the soluble collagen self-assembles it exposes the FN binding site, similar to that in native tissue, unlike the collagen-GAG fibers that do not have all FN binding sites exposed, because of the random packing of the fibrillar aggregates. Additional analysis was performed evaluating the cellular binding site availability of FN on self-assembled CI basal lamina analogs at varying concentrations of FN to determine the saturation limit. We found that the availability of FN on the surfaces of the



self-assembled CI membranes at 100 µg/ml of FN was the optimal concentration for binding site availability, similar to the evaluation of binding site availability on collagen-GAG membranes.

Various investigations have evaluated covalent conjugation strategies to improve the presentation and bioactivity of FN over passive adsorption on various surfaces.<sup>43-45</sup> The use of a carbodiimide conjugation strategy was evaluated to crosslink our membranes as well as to covalently bind FN. This crosslinking agent has been highly successful in crosslinking collagen and improving its degradation resistance and mechanical properties,<sup>46,47</sup> as well as coupling chondroitin sulfate, heparin sulfate, and heparin to the surface of collagen scaffolds.<sup>48-50</sup> We investigated its use as a potential method to covalently conjugate FN to the surface of both collagen based scaffolds and found a significant increase in cellular binding site availability of FN when compared to that of using passive adsorption. When keratinocytes were cultured at 3 days at the A/L interface on self-assembled basal lamina analogs with no FN, passively adsorbed FN, and EDC conjugated FN, an increase in epithelial thickness was found between all surfaces. This data also corresponds with the data from the FN cellular binding domain availability analysis. Future studies will evaluate EDC conjugation of FN on epithelialization of a basal lamina analog laminated to a dermal scaffold to determine the effects of this conjugation strategy on proliferation and differentiation in a composite model of bioengineered skin substitute.

Overall the results from these studies indicate that the cellular binding domain of FN can be enhanced on collagen-based biomaterials and directly influences functions important for epithelialization. The information gained from this study can be applied to other model systems where the enhancement of cellular binding sites of FN on collagenous biomaterials would enhance tissue functionality. Additionally this information can be used in the design of engineered tissues where the incorporation of a basal lamina analog is necessary to direct

epithelial polarity and functions as well as to separate cell types and act as a selectively permeable barrier, such as in the glomerulus of the kidney or the small intestine.

## 5.5 ACKNOWLEDGEMENTS

This research was funded by the NIH (EB-005645) and the U.S. Army Medical Research and Material Command (USAMRC); grant W81XWH-08-01-0422. The views, opinions, and/or findings and information contained in this manuscript are those of the authors and should not be construed as an official Department of Defense position or policy, unless so designated by other documentation. No official endorsement should be made. The HFN 7.1 hybridoma supernatant was obtained from the Developmental Studies Hybridoma Bank developed under the auspices of the NICHD and maintained by the University of Iowa, Department of Biological Sciences, Iowa City, Iowa: R.J. contributor. I would like to thank the Department of Obstetrics and Gynecology at UMMS (Worcester, MA) for providing us with neonatal foreskins for keratinocyte isolations and Russell Kronengold at Kensey Nash Corporation (Exton, PA) for his generous donations of SEMED-S collagen. I would also like to thank the co-author, my advisor George Pins for his scientific contribution to the work as well as Jeannine Coburn, Donna Davidson, Christina Mezzone, and Kevin Cornwell for their technical assistance. Also, Brett Downing and Stuart Howes should be acknowledged for their assistance in the development of the A/L interface culture device.

## 5.6 REFERENCES

1. Clark RA, Folkvord JM, Wertz RL. Fibronectin, as well as other extracellular matrix proteins, mediate human keratinocyte adherence. *J Invest Dermatol* 1985;84(5):378-83.
2. Woodley D. Reepithelialization. In: Clark RA, editor. *The Molecular and Cellular Biology of Wound Repair*. New York: Plenum Press; 1996. p 339-354.
3. Martin P. Wound healing-aiming for perfect skin regeneration. *Science* 1997;276(5309):75-81.
4. Grinnell F. Fibronectin and wound healing. *J Cell Biochem* 1984;26(2):107-16.
5. Adams JC, Watt FM. Expression of beta 1, beta 3, beta 4, and beta 5 integrins by human epidermal keratinocytes and non-differentiating keratinocytes. *J Cell Biol* 1991;115(3):829-41.

6. Guo M, Toda K, Grinnell F. Activation of human keratinocyte migration on type I collagen and fibronectin. *J Cell Sci* 1990;96 ( Pt 2):197-205.
7. Adams JC, Watt FM. Fibronectin inhibits the terminal differentiation of human keratinocytes. *Nature* 1989;340(6231):307-9.
8. Tjia JS, Aneskievich BJ, Moghe PV. Substrate-adsorbed collagen and cell secreted fibronectin concertedly induce cell migration on poly(lactide-glycolide) substrates. *Biomaterials* 1999;20(23-24):2223-33.
9. Bush KA, Downing BR, Walsh SE, Pins GD. Conjugation of extracellular matrix proteins to basal lamina analogs enhances keratinocyte attachment. *J Biomed Mater Res A* 2007;80(2):444-52.
10. Grzesiak JJ, Pierschbacher MD, Amodeo MF, Malaney TI, Glass JR. Enhancement of cell interactions with collagen/glycosaminoglycan matrices by RGD derivatization. *Biomaterials* 1997;18(24):1625-32.
11. Cooper ML, Hansbrough JF, Polarek JW. The effect of an arginine-glycine-aspartic acid peptide and hyaluronate synthetic matrix on epithelialization of meshed skin graft interstices. *J Burn Care Rehabil* 1996;17(2):108-16.
12. Garcia AJ, Schwarzbauer JE, Boettiger D. Distinct activation states of alpha5beta1 integrin show differential binding to RGD and synergy domains of fibronectin. *Biochemistry* 2002;41(29):9063-9.
13. Pierschbacher MD, Ruoslahti E. Cell attachment activity of fibronectin can be duplicated by small synthetic fragments of the molecule. *Nature* 1984;309(5963):30-3.
14. Grinnell F. Wound repair, keratinocyte activation and integrin modulation. *J Cell Sci* 1992;101 ( Pt 1):1-5.
15. Pettit DK, Hoffman AS, Horbett TA. Correlation between corneal epithelial cell outgrowth and monoclonal antibody binding to the cell binding domain of adsorbed fibronectin. *J Biomed Mater Res* 1994;28(6):685-91.
16. Grinnell F, Feld MK. Adsorption characteristics of plasma fibronectin in relationship to biological activity. *J Biomed Mater Res* 1981;15(3):363-81.
17. Iuliano DJ, Saavedra SS, Truskey GA. Effect of the conformation and orientation of adsorbed fibronectin on endothelial cell spreading and the strength of adhesion. *J Biomed Mater Res* 1993;27(8):1103-13.
18. Garcia AJ, Ducheyne P, Boettiger D. Effect of surface reaction stage on fibronectin-mediated adhesion of osteoblast-like cells to bioactive glass. *J Biomed Mater Res* 1998;40(1):48-56.
19. Underwood PA, Steele JG, Dalton BA. Effects of polystyrene surface chemistry on the biological activity of solid phase fibronectin and vitronectin, analysed with monoclonal antibodies. *J Cell Sci* 1993;104 ( Pt 3):793-803.
20. Garcia AJ, Boettiger D. Integrin-fibronectin interactions at the cell-material interface: initial integrin binding and signaling. *Biomaterials* 1999;20(23-24):2427-33.
21. Garcia AJ, Vega MD, Boettiger D. Modulation of cell proliferation and differentiation through substrate-dependent changes in fibronectin conformation. *Mol Biol Cell* 1999;10(3):785-98.
22. Keselowsky BG, Collard DM, Garcia AJ. Surface chemistry modulates fibronectin conformation and directs integrin binding and specificity to control cell adhesion. *J Biomed Mater Res A* 2003;66(2):247-59.
23. Bush KA, Driscoll PF, Soto ER, Lambert CR, McGimpsey WG, Pins GD. Designing Tailored Biomaterial Surfaces to Direct Keratinocyte Morphology, Attachment, and Differentiation. *J Biomed Mater Res A* 2008.
24. Bush KA, Pins GD. Carbodiimide Conjugation of Fibronectin on Collagen Basal Lamina Analogs Enhances Cellular Binding Domains and Epithelialization. In preparation 2009.
25. Chamberlain L, Yannas I. Preparation of collagen-glycosaminoglycan copolymers for tissue regeneration. In: Morgan J, Yarmush M, editors. *Tissue engineering methods and protocols*. Totowa, NJ: Humana Press; 1998. p 3-17.

26. Elsdale T, Bard J. Collagen substrata for studies on cell behavior. *J Cell Biol* 1972;54(3):626-37.
27. Olde Damink LH, Dijkstra PJ, van Luyn MJ, van Wachem PB, Nieuwenhuis P, Feijen J. Cross-linking of dermal sheep collagen using a water-soluble carbodiimide. *Biomaterials* 1996;17(8):765-73.
28. Olde Damink LH, Dijkstra PJ, van Luyn MJ, van Wachem PB, Nieuwenhuis P, Feijen J. In vitro degradation of dermal sheep collagen cross-linked using a water-soluble carbodiimide. *Biomaterials* 1996;17(7):679-84.
29. Pins GD, Toner M, Morgan JR. Microfabrication of an analog of the basal lamina: biocompatible membranes with complex topographies. *Faseb J* 2000;14(3):593-602.
30. Carter WG, Symington BE, Kaur P. Cell adhesion and the basement membrane in early epidermal morphogenesis. In: Fleming TP, editor. *Epithelial Organization and Development*. London: Chapman and Hall; 1992. p 299-327.
31. Boyce ST, Williams ML. Lipid supplemented medium induces lamellar bodies and precursors of barrier lipids in cultured analogues of human skin. *J Invest Dermatol* 1993;101(2):180-4.
32. Bowditch RD, Halloran CE, Aota S, Obara M, Plow EF, Yamada KM, Ginsberg MH. Integrin alpha IIb beta 3 (platelet GPIIb-IIIa) recognizes multiple sites in fibronectin. *J Biol Chem* 1991;266(34):23323-8.
33. Scholzen T, Gerdes J. The Ki-67 protein: from the known and the unknown. *J Cell Physiol* 2000;182(3):311-22.
34. Allen LT, Tosetto M, Miller IS, O'Connor DP, Penney SC, Lynch I, Keenan AK, Pennington SR, Dawson KA, Gallagher WM. Surface-induced changes in protein adsorption and implications for cellular phenotypic responses to surface interaction. *Biomaterials* 2006;27(16):3096-108.
35. Kowalczyńska HM, Nowak-Wyrzykowska M, Dobkowski J, Kolos R, Kaminski J, Makowska-Cynka A, Marciniak E. Adsorption characteristics of human plasma fibronectin in relationship to cell adhesion. *J Biomed Mater Res* 2002;61(2):260-9.
36. Heenen M, Thiriar S, Noel JC, Galand P. Ki-67 immunostaining of normal human epidermis: comparison with 3H-thymidine labelling and PCNA immunostaining. *Dermatology* 1998;197(2):123-6.
37. Caldwell CJ, Hobbs C, McKee PH. The relationship of Ki67 and involucrin expression in proliferative, pre-neoplastic and neoplastic skin. *Clin Exp Dermatol* 1997;22(1):11-6.
38. Usui ML, Mansbridge JN, Carter WG, Fujita M, Olerud JE. Keratinocyte migration, proliferation, and differentiation in chronic ulcers from patients with diabetes and normal wounds. *J Histochem Cytochem* 2008;56(7):687-96.
39. Usui ML, Underwood RA, Mansbridge JN, Muffley LA, Carter WG, Olerud JE. Morphological evidence for the role of suprabasal keratinocytes in wound reepithelialization. *Wound Repair Regen* 2005;13(5):468-79.
40. PMA Approval for Integra Dermal Regeneration Template United States Food and Drug Administration; 1996.
41. Pins GD, Christiansen DL, Patel R, Silver FH. Self-assembly of collagen fibers. Influence of fibrillar alignment and decorin on mechanical properties. *Biophys J* 1997;73(4):2164-72.
42. Kleinman HK, McGoodwin EB, Martin GR, Klebe RJ, Fietzek PP, Woolley DE. Localization of the binding site for cell attachment in the alpha1(I) chain of collagen. *J Biol Chem* 1978;253(16):5642-6.
43. Vallieres K, Chevallier P, Sarra-Bournet C, Turgeon S, Laroche G. AFM imaging of immobilized fibronectin: does the surface conjugation scheme affect the protein orientation/conformation? *Langmuir* 2007;23(19):9745-51.
44. Vallieres K, Petitclerc E, Laroche G. Covalent grafting of fibronectin onto plasma-treated PTFE: influence of the conjugation strategy on fibronectin biological activity. *Macromol Biosci* 2007;7(5):738-45.

45. Zhang Y, Chai C, Jiang S, Teoh S, Leong K. Fibronectin immobilized by covalent conjugation or physical adsorption shows different bioactivity on aminated-PET. *Materials Science and Engineering C* 2007;27:213-219.
46. Powell HM, Boyce ST. EDC cross-linking improves skin substitute strength and stability. *Biomaterials* 2006;27(34):5821-7.
47. Powell HM, Boyce ST. Wound closure with EDC cross-linked cultured skin substitutes grafted to athymic mice. *Biomaterials* 2007;28(6):1084-92.
48. Pieper JS, Hafmans T, Veerkamp JH, van Kuppevelt TH. Development of tailor-made collagen-glycosaminoglycan matrices: EDC/NHS crosslinking, and ultrastructural aspects. *Biomaterials* 2000;21(6):581-93.
49. Pieper JS, van Wachem PB, van Luyn MJA, Brouwer LA, Hafmans T, Veerkamp JH, van Kuppevelt TH. Attachment of glycosaminoglycans to collagenous matrices modulates the tissue response in rats. *Biomaterials* 2000;21(16):1689-99.
50. Pieper JS, Oosterhof A, Dijkstra PJ, Veerkamp JH, van Kuppevelt TH. Preparation and characterization of porous crosslinked collagenous matrices containing bioavailable chondroitin sulphate. *Biomaterials* 1999;20(9):847-58.

---

---

## **Chapter 6: Microenvironments of Basal Lamina Analogues Influence Epithelialization and Epidermal Stem Cell Localization on Bioengineered Skin Substitutes**

---

### **6.1 INTRODUCTION**

Bioengineered skin substitutes offer a promising approach in the treatment of severe burns or chronic wounds when autografts are not an option for the patient. Clinically, these substitutes provide a barrier to prevent infection and water loss as well as therapeutic effects that induce dermal tissue repair and stimulate healing of chronic wounds. Although there has been clinical success with these grafts, limitations still exist including prolonged healing times, mechanically induced graft failure, poor graft take, and residual scarring. Additionally, current bioengineered skin substitutes only restore a subset of anatomical structures that play key roles in normal physiological functions of skin.<sup>1-3</sup>

One design feature common to current bioengineered skin substitutes is a flat interface between the dermal and epidermal components. At the dermal-epidermal junction (DEJ) of native skin there is a basal lamina which contributes critical cues involved in regulating keratinocyte functions necessary for the maintenance of the tissue architecture, as well as skin's overall homeostasis with the surrounding environment.<sup>4</sup> The basal lamina is a thin membranous sheet composed of both collagenous and non-collagenous extracellular matrix (ECM) proteins including type IV collagen (CIV), laminin (LN), fibronectin (FN), and heparin sulfate proteoglycans. The basal lamina is not flat, but rather conforms to a series of three dimensional ridges and invaginations formed by papillae located in the upper region of

the dermis that range from 50-400  $\mu\text{m}$  in width and 50-200  $\mu\text{m}$  in depth.<sup>5</sup> It has been determined that in different regions of the body, the number and dimensions of dermal papillae and rete ridges differ. In areas of skin exposed to excessive friction, such as the palms and soles, the basal lamina conforms to a series of longer and more numerous dermal papillae and deeper rete ridges, suggesting that the increased surface area provided by the topographical features also aids in enhancing mechanical stability.<sup>6</sup>

Keratinocytes in direct contact with the basal lamina are the only population of cells in the epidermis with the capacity to proliferate. The epidermis is in constant renewal, thus proliferation is necessary in order to provide proper barrier function. The population of proliferating basal keratinocytes is heterogeneous and contains epidermal stem cells (ESCs) and transit amplifying (TA) cells that have different regenerative and differentiation capabilities. Epidermal stem cells are non-differentiated cells that are responsible for the assembly and maintenance of the epidermis as well as the rapid regeneration of damaged tissue. They are capable of self-renewal and give rise to TA cells, which divide a finite number of times to amplify the basal layer and then undergo terminal differentiation.<sup>7</sup>

Epidermal stem cells exhibit a high degree of spatial organization and clustering along the complex topography of the basal lamina. Epidermal stem cells can be further classified based on their localization into bulge ESCs, found in the bulge region of the hair follicle and interfollicular ESCs found either in the bottom of rete ridges or tips of papillary projections.<sup>8-</sup>

<sup>10</sup> Several studies have examined the localization of proliferating keratinocytes and interfollicular ESCs in the basal layer of native epidermis using cell cycling or integrin detection techniques. In monkey palm epidermis, DNA label-retaining cells (LRCs) were found in the deep rete ridges;<sup>11</sup> which is indicative of slowly cycling cells, a well accepted characteristic of ESCs.<sup>12</sup> This cell-cycle kinetic analysis has been used to investigate the localization of ESC populations in other species and tissue sites such as hamster epidermis

and oral mucosa,<sup>13</sup> the bulge region in hair follicles,<sup>7</sup> and human embryonic and fetal epidermis.<sup>14</sup> In addition to label retaining cells, research has been conducted evaluating the intensity of  $\beta_1$  integrin receptors and correlating the findings with interfollicular ESC localization. All basal keratinocytes express  $\beta_1$  which mediates adhesion to the ECM of the basal lamina and regulates terminal differentiation.<sup>15-17</sup> Enhanced  $\beta_1$  expression has been found to distinguish ESCs from keratinocytes with lower proliferative potential.<sup>18</sup> The expression of  $\beta_1$  has been found to be distributed differently along the microtopography of the basal lamina, based on body site location. These findings correspond with label-retaining experiments previously mentioned. In human skin,  $\beta_1$ -bright regions are found in deep rete ridges in the palms and soles; whereas in interfollicular epidermis of the scalp, foreskin, and breast,  $\beta_1$ -bright regions were found at the tips of the papillary projections.<sup>12,19</sup>

In addition to studies evaluating microtopographic features of the basal lamina in native tissues and interfollicular ESC localization, other researchers have focused their efforts on investigating the effects of the biochemical composition of the basal lamina that influences keratinocyte attachment and ESC selection, proliferation, and terminal differentiation. Keratinocyte attachment was investigated on CI, CIV, LN, and FN at varying concentrations and amounts of time. It was determined that the percentage of keratinocytes that adhered to each surface was time dependent as well as ECM protein and concentration dependent with adhesion to FN giving the highest percentage of adherent cells.<sup>17</sup> Studies have also investigated the ability to select for ESCs based on using rapid adhesion assays on ECM proteins. Differences in colony forming efficiency (CFE), a metric that can be used to demonstrate the presence of an ESC population or proliferative potential of the population, have been detected based on this selection technique.<sup>8,18,20</sup> Additionally, flow cytometry has been used to sort keratinocytes based on  $\beta_1$  integrin expression. When evaluating the CFE of keratinocytes separated using this technique, a linear relationship was found between log fluorescence and CFE, which implies a log linear relationship between  $\beta_1$  integrin density on



the cell surface and proliferative potential.<sup>18</sup> Studies have further examined the effects of ECM proteins of the basal lamina, specifically FN, on differentiation of keratinocytes. It has been shown that when cells are induced to undergo differentiation in culture, they become less adhesive to FN, and no longer express the  $\beta_1$  integrin.<sup>16</sup>

Understanding how the microenvironment found at the DEJ influences ESC localization and promotes the development of a functional tissue is critical in the development of the next generation of bioengineered skin grafts as well as for longevity of the tissue. We hypothesize that by incorporating microfabricated basal lamina analog, containing biochemical and microtopographic features mimicking those found at the DEJ, we will promote enhanced epithelialization and epidermal stem cell clustering on the surface of novel dermal scaffolds. Previously, our laboratory has created basal lamina analogs on the surface of collagen-glycosaminoglycan (GAG) dermal scaffolds that recapitulate the native topographical features found at the DEJ utilizing photolithography and material processing techniques. It was determined that topographical features with the greatest aspect ratios enhanced keratinocyte stratification, proliferation, and differentiation.<sup>21,22</sup> Additionally, we found that passively adsorbing the ECM protein FN, on the surface of flat collagen-GAG membranes increased keratinocyte attachment over non-modified control collagen-GAG surfaces by 22%.<sup>23</sup> When further investigating FN binding domains and conjugation strategies, we determined that through carbodiimide conjugation, we could enhance the presentation of the cellular binding site domain of FN on the surfaces of self-assembled CI membranes.<sup>24</sup> In this chapter, we have developed a novel system that incorporates both microtopographic and biochemical features that have been previously defined by our laboratory to enhance epithelialization. Using histological stains and immunohistochemistry coupled with quantitative morphometric analyses of microscopic images, we have determined the effect of this combined microenvironment on epithelial thickness, morphology, proliferation, and ESC localization. Furthermore we have compared our bioengineered skin substitutes that contain

microfabricated basal lamina analogs with both native adult and neonatal tissues as well as de-epithelialized acellular dermis (DED) cultured under the same conditions as our experimental system. Overall, we have developed a bioengineered skin substitute with a microfabricated basal lamina analog that imparts the ability to direct ESC localization, as well as a model system to further investigate advanced ESC markers and the mechanisms by which ESC localization occurs.

## **6.2 MATERIALS and METHODS**

### **6.2.1 Production of Dermal Scaffold Containing a Microfabricated Basal Lamina Analog**

#### *6.2.1.1 Photolithography of a Master Pattern and Negative Replicates*

To mimic the microtopography found at the DEJ, photolithography was used. Master patterns consisting of parallel, three-dimensional channels with widths of 50-400  $\mu\text{m}$  and depth of 200  $\mu\text{m}$  were designed using Pro/Engineer software (PTC, Needham, MA). The two dimensional drawing was then printed onto acetate film (CAD/Art Service Inc, Poway, CA) with a high resolution laser photoplotter (7008MF: 20,000 dots/inch, Orbotech, Billerica, MA). The transparency masks were then aligned on the surface of silicon wafers coated with 200  $\mu\text{m}$  thickness of SU-8 photoresist (Microchem Co., Newton, MA) and exposed to a collimated beam of UV light. The wafer was immersed in propylene glycol methyl ether acetate (PGMEA; SU-8 Developer, Microchem Co.) and the unexposed regions were dissolved, leaving a three-dimensional pattern on the silicon wafer (Figure 6.1A<sup>25</sup>). To create negative replicate molds, polydimethylsiloxane silicone elastomer (PDMS, Sylgard 184, Dow Corning Corp., Midland, MI) was poured onto the surface of the wafer (10:1 base to curing agent), degassed to remove trapped air bubbles, and allowed to polymerize for 2 hours at 65°C. The PDMS was then carefully separated from the silicon wafer (Figure 6.1B<sup>25</sup>).

### 6.2.1.2 Purification of CI

Acid-soluble type I collagen (CI) was extracted from rat tail tendons using protocols previously described.<sup>26</sup> Rat tails were received from animals that were euthanized for other protocols, which were approved by Worcester Polytechnic Institute, Worcester, MA, Institutional Animal Care and Use Committee. Briefly, rat tail tendons were extracted from the tails of 13 Sprague Dawley rats, rinsed in dPBS (Hyclone, Logan, UT), and dissolved in 1600 ml of 3% acetic acid (EMD Chemicals, Inc., Gibbstown, NJ) at 4°C overnight. The resulting solution was centrifuged at 8590 rpm for 2 hours and 320 ml of a 30% NaCl (Sigma, St. Louis, MI) solution was dripped into the supernatant at 4°C. The resulting solution was allowed to sit for at least 1 hour at 4°C without disruption and then centrifuged at 4690 rpm for 30 minutes to separate precipitated and liquid material. The precipitated material was resuspended in 400 ml of 0.6% acetic acid and dialyzed for 4 hours against 1 mM HCl (JT Baker, Phillipsburg, NJ) and the dialysis solution was changed every 4 hours until a clear collagen solution was obtained. This solution was lyophilized and stored in a sealed container at 4°C, until use. Lyophilized collagen was dissolved in 5 mM HCl to obtain a working solution of 10 mg/ml.<sup>26</sup> To produce self-assembled CI membranes, 800 µl of the soluble CI solution was neutralized using 200 µl of 5x Dulbecco's Modified Eagle's Medium (DMEM, Invitrogen, Carlsbad, CA) with 0.22 M NaHCO<sub>3</sub> and 40 µl of 0.1 M NaOH (Sigma) at 37°C for 18 hours on circular PDMS molds (Figure 6.1C<sup>24</sup>).

### 6.2.1.3 Dermal Scaffold Production

To create dermal scaffolds, a collagen-GAG coprecipitate containing collagen (5 mg/ml) and GAG (0.18 mg/ml) was prepared by placing lyophilized bovine hide derived collagen (Semed-S, Kensey Nash Corp., Exton, PA) in acetic acid and homogenizing (20,000 rpm) at 4°C for 90 minutes resulting in a bovine derived collagen suspension.<sup>27</sup> Shark cartilage chondroitin 6-sulfate (Sigma) was dripped into the blending collagen dispersion and blended

for an additional 90 minutes. Once fully blended, the collagen-GAG coprecipitate was degassed by centrifugation. Dermal scaffolds were created by placing 20 ml of the collagen-GAG suspension in 70 mm diameter aluminum weigh boats (VWR, West Chester, PA) and freezing at  $-80^{\circ}\text{C}$  for 1 hour. Following the initial freezing, the tins were placed in a freeze dryer (Virtis Advantage, Virtis, Inc., Gardner, NY) pre-frozen to  $-45^{\circ}\text{C}$  then lyophilized overnight at a vacuum of 100 mtorr. Following lyophilization, the scaffolds were covalently crosslinked by thermal dehydration (DHT) at  $105^{\circ}\text{C}$  in a vacuum of less than 200 mtorr for 48 hours. Scaffolds were cut into rectangles approximately  $7\text{ cm}^2$  (2.5 cm width x 3 cm height) in area and placed in desiccator until use.

#### *6.2.1.4 Production of Dermal Scaffolds with Microfabricated Basal Lamina Analogs*

The production of dermal scaffolds with microfabricated basal lamina analogs began with the fabrication of a self-assembled CI membrane. Initially, a microfabricated self-assembled CI membrane was made by neutralizing 800  $\mu\text{l}$  of 10 mg/ml CI using 200  $\mu\text{l}$  of 5x DMEM containing 0.22 M  $\text{NaHCO}_3$  and 40  $\mu\text{l}$  of 0.1 M NaOH (Sigma) at  $37^{\circ}\text{C}$  for 18 hours on PDMS molds containing the negative replicate of the desired channel topography (molds  $9.85\text{ cm}^2$ ) (Figure 6.1C<sup>25</sup>). After incubation, 400  $\mu\text{l}$  of 10 mg/ml of CI was neutralized using 100  $\mu\text{l}$  of 5x DMEM containing 0.22 M  $\text{NaHCO}_3$  and placed directly on the self-assembled CI membrane, and gently spread to cover the entire surface area. Immediately following this step, a pre-cut lyophilized dermal scaffold was placed on top of the neutralizing CI and then incubated at  $37^{\circ}\text{C}$  for 2 hours to facilitate complete self-assembly of the CI and lamination of the dermal scaffold to the basal lamina analog (Figure 6.1D<sup>25</sup>).

#### *6.2.1.5 FN Conjugation to Microfabricated Basal Lamina Analogs Laminated to Dermal Scaffolds*

Carbodiimide 1-ethyl-3-(3-dimethylaminopropyl)carbodiimide hydrochloride (EDC, Sigma) was used to covalently conjugate FN to the surface of the microfabricated basal lamina

analog as well as chemically crosslink the basal lamina analog and dermal scaffold. Previously we have reported that this method increases cellular binding site availability of FN.<sup>24</sup> Using protocols described previously, the mole ratio of 5:1 of EDC to carboxylic acid groups in CI was used.<sup>28</sup> Theoretical calculations which estimated the amount of COOH in 1000 amino acids of collagen were used to make the assumption that 1 g of CI contains 1.2 mmol COOH based on amino acid composition of CI.<sup>28,29</sup> Each dermal scaffold containing a microfabricated basal lamina contains 30 mg of CI for a total of 0.036 mmol COOH, thus requiring 0.18 mmol of EDC. This amount of EDC was dissolved in 50 mM MES (Sigma), prepared in 40% ethanol (Pharmco Products, Inc., Brookfield, CT) at a pH of 5.5, and 3 mls of the solution was placed on the dermal scaffold containing a microfabricated basal lamina analog for 4 hours at room temperature (Figure 6.1E<sup>25</sup>). Dermal scaffolds containing microfabricated basal lamina analogs were then removed from the EDC solution and immediately placed into air/liquid (A/L) interface culture devices<sup>24</sup> and FN (BD Biosciences, Bedford, MA) at 100 µg/ml was placed in the well created on the surface of the collagen membrane over night at room temperature (Figure 6.1F<sup>25</sup>). Control dermal scaffolds containing microfabricated basal lamina analogs without FN conjugation were also prepared. These controls received EDC and dPBS instead of FN.

### **6.2.2 Preparation of De-Epithelialized Acellular Dermis**

Following methods previously described by Hamoen et al.,<sup>30</sup> De-epithelialized acellular dermis (DED) was prepared to use as a control tissue scaffold. Cadaver skin was obtained from New England Eye and Tissue Transplant Bank and washed 3 times in sterile dPBS. From this point on, sterile conditions were maintained. The cadaver skin was placed in an antibiotic cocktail containing 1x DMEM with 10 µg/ml Ciprofloxacin (Sigma), 2.5 µg/ml Amphotericin B, 100 U/ml Penicillin, 100 µg/ml Streptomycin, and 100 µg/ml Gentamycin (Invitrogen) and kept at 4°C for 1 day. The following day, the skin was transferred to a cryopreservation solution composed of 1x DMEM with 15% glycerol (J.T. Baker) and placed

at 4°C for 2 hours. Following this step, skin was placed in sterile mesh gauze soaked in cryopreservation solution and wrapped in sterile aluminum pouches and plastic. Wrapped packages of skin were transferred to -20°C for 24 hours, and then moved to -80°C for long term storage.

To prepare the skin for tissue culture, pouches containing cryopreserved tissue were immersed in a tub of water at 15-20°C until skin was pliable, then refrozen rapidly in liquid nitrogen. This freeze-thaw cycle was repeated 3 times to devitalize the cells. Skin was removed from pouches and washed 3 times in DMEM then placed in antibiotic cocktail for 1 week at 4°C. After 1 week, the skin was transferred into new antibiotic cocktail and incubated for 1 week at 37°C. At the end of the incubation, the epidermis was separated from the dermis, and the dermis was placed into fresh antibiotic cocktail for 4 weeks at 4°C. After 4 weeks, the DED was ready for tissue culture.

### **6.2.3 *In vitro* Culture of Dermal Scaffolds Containing Microfabricated Basal Lamina Analogs**

#### *6.2.3.1 Sterilization of Dermal Scaffolds Containing Microfabricated Basal Lamina Analogs*

Air/liquid culture devices containing dermal scaffolds with microfabricated basal lamina analogs were placed in sterile containers in 60 ml of 70% ethanol for 1 hour in a laminar flow hood. After 1 hour, devices were transferred to new sterile containers and were rinsed 3 times for 10 minutes each in sterile dPBS and then left overnight in dPBS under sterile conditions.

#### *6.2.3.2 Culture of Neonatal Human Keratinocytes*

Neonatal keratinocytes were cultured as previously described.<sup>22,23</sup> Neonatal foreskins were obtained from non-identifiable discarded tissues from UMass Memorial Medical Center, Worcester, MA and were approved with exempt status from the New England Institutional

Review Board. Keratinocyte isolations were performed using an enzymatic treatment with a dispase (Gibco, Gaithersburg, MD) solution. The cells were propagated on a feeder layer of 3T3-J2 mouse fibroblasts (generously donated by Dr. Stelios Andreadis, State University of New York at Buffalo, Buffalo, NY) and cultured according to methods previously described<sup>22,31</sup> using keratinocyte media consisting of a 3:1 mixture of DMEM (high glucose) and Ham's F-12 medium (Invitrogen) supplemented with 10% fetal bovine serum (FBS, Hyclone),  $10^{-10}$  M cholera toxin (Vibrio Cholerae, Type Inaba 569 B), 5 µg/ml transferrin, 0.4 µg/ml hydrocortisone (Calbiochem, La Jolla, CA), 0.13 U/ml insulin,  $1.4 \times 10^{-4}$  M adenine,  $2 \times 10^{-9}$  M triiodo-L-thyronine (Sigma), 1% Penicillin/Streptomycin (Invitrogen), and 0.01 µg/ml epidermal growth factor (EGF, BD Biosciences). After 5 days of culture, keratinocytes were detached using 0.05% Trypsin-EDTA (Invitrogen) and passage 2-3 keratinocytes, from multiple donors were used in all experiments.

#### *6.2.3.3 Culture of Dermal Scaffolds Containing Microfabricated Basal Lamina Analogs*

After sterilization of dermal scaffolds with microfabricated basal lamina analogs, A/L interface culture devices were transferred to sterile 6 well plates for immediate cell culture. Dermal scaffolds with microfabricated basal lamina analogs were preconditioned with seeding media consisting of 3:1 mixture of 1x DMEM (high glucose) and Ham's F-12 medium supplemented with  $10^{-10}$  M cholera toxin, 0.2 µg/mL hydrocortisone (Calbiochem), 5 µg/mL insulin, 50 µg/mL ascorbic acid (Sigma), and 100 IU/mL and 100 µg/mL penicillin–streptomycin. Keratinocytes were seeded using this media at 500,000 cells/cm<sup>2</sup> and allowed to adhere for 2 hours in 10% CO<sub>2</sub> at 37°C. After 2 hours, seeding media containing 1% FBS was placed in each well, completely submerging the bioengineered skin substitutes. After 24 h, the keratinocyte seeding medium was removed, and the bioengineered skin substitutes were submerged for an additional 48 h in a keratinocyte priming medium composed of keratinocyte seeding medium (with FBS) supplemented with 24 µM bovine serum albumin (BSA), 1.0 mM L-serine, 10 µM L-carnitine, and a mixture of

fatty acids including 25  $\mu\text{M}$  oleic acid, 15  $\mu\text{M}$  linoleic acid, 7  $\mu\text{M}$  arachidonic acid, and 25  $\mu\text{M}$  palmitic acid (Sigma).<sup>32</sup> After 48 h in priming medium, the bioengineered skin substitutes were cultured for 3 or 7 days with an air liquid interface medium composed of serum-free keratinocyte priming medium supplemented with 1.0 ng/mL EGF (Figure 6.1G<sup>25</sup>). As controls, composites without FN treatment and DED were cultured in parallel using the same process; however, DED was not sterilized, but placed directly into sterile A/L interface culture devices and keratinocytes were seeded on the papillary surface.

### **6.3.3 Quantitative Morphometric Analysis of Microfabricated Features of Basal Lamina Analogs**

The morphology of the microtopographical features of the surfaces of the basal lamina analogs were evaluated using histology coupled with quantitative image analysis. The specified values for the channels were 200  $\mu\text{m}$  depth and 50  $\mu\text{m}$ , 100  $\mu\text{m}$ , 200  $\mu\text{m}$ , and 400  $\mu\text{m}$  widths. To measure the surface features of the basal lamina analogs, a series of unseeded dermal scaffolds containing microfabricated basal lamina analogs were fixed with 10% buffered formalin solution (EMD Chemicals), dehydrated with increasing concentrations of ethanol, cleared with sec-butyl alcohol (EMD Chemicals), and embedded in Paraplast tissue embedding medium (McCormick Scientific, St. Louis, MO). Six micron sections were cut using a Leica RM 2235 (Leica Microsystems, Inc., Bannockburn, IL) in a plane perpendicular to the surface of the basal lamina. Sections were mounted on poly-l-lysine coated slides (Erie Scientific Company, Portsmouth, NH). Tissue sections were deparaffinized in reverse ethanol–xylene (Pharmco Products, Inc. and EMD Chemicals) washes and stained with Harris Hematoxylin (Richard Allen Scientific, Kalamazoo, MI) for 4 minutes. Slides were rinsed with  $\text{dH}_2\text{O}$  and 1% acid alcohol and stained with Eosin (Richard Allen Scientific) for 30 seconds. The slides were then cleared in a series of ethanol and xylene and cover slipped using Permount (Fisher Scientific, Hampton, NH) mounting medium. Brightfield images were captured of each section using a Nikon Eclipse E400



microscope (Nikon, Inc., Melville, NY) coupled to an RT Color Spot camera (Spot Diagnostics, Sterline Heights, MI). For each sample the depths of the channels and the widths of the channels were measured using Image J software (downloaded from <http://rsb.info.nih.gov.ezproxy.umassmed.edu/ij/>). Values are reported as mean +/- SEM.

### **6.3.4 Analyses of Epithelialization and Regenerative Capacity of Bioengineered Skin Substitutes Containing Microfabricated Basal Lamina Analogs**

#### *6.3.4.1 Epidermal Thickness and Graft Morphology*

Epidermal thickness and graft morphology on the surfaces of the basal lamina analogs laminated to dermal scaffolds were evaluated after 3 or 7 days of A/L interface culture. Samples were embedded in paraffin wax, sectioned, and mounted as described previously in the Quantitative Morphometric Analyses of Microfabricated Features of Basal Lamina Analogs Laminated to Dermal Scaffolds (Section 6.3.3). Paraffin sections were deparaffinized in reverse ethanol–xylene washes and stained with Hematoxylin and Eosin. Brightfield images were captured and using Image J measurements of channel depth, channel widths, and epithelial thickness in each channel. Additionally the epidermal thickness of the flat region adjacent to the channels (papillary plateau) was measured (Figure 6.2A<sup>25</sup> insert). Multiple measurements were made for each sample since each sample contained multiple channels. For epithelialized DED and native tissues, the thickness of the epidermal layer was measured in the rete ridges and on the papillary plateaus. The dimensions of the rete ridges were also measured.

To characterize the effect of channel dimensions on epidermal thickness, the epidermal thicknesses were measured in channels with widths that were within +/- 2 SEM of the topography validation width measurements, for each specified channel width. Data points were excluded from all other channels from this analysis. These data points were then individually normalized to the depth of their channel. The normalized data from each

specified channel width was then averaged and reported as a mean value +/- SEM. Sample values for the 50, 100, 200, and 400  $\mu\text{m}$  width channels were  $n = 5, 5, 6, 11$  at 3 days, respectively and  $n = 5, 6, 15, \text{ and } 13$  at 7 days, respectively. At both 3 and 7 days  $n = 4$  for DED and  $n = 4$  for foreskin tissue.

#### 6.3.4.2 *Keratinocyte Proliferation*

Keratinocyte proliferation was evaluated after 3 or 7 days of A/L interface culture by measuring the presence of Ki67, a cell cycle associated antigen. Samples were embedded in paraffin, sectioned, and mounted on Superfrost Plus slides (VWR, West Chester, PA) coated with poly-L-lysine (Sigma). The paraffin sections were deparaffinized in reverse ethanol-xylene washes, and the antigens were unmasked by placing the slides in boiling Vector UnMasking solution (Vector Laboratories, Inc, Burlingame, CA) in a Mantra pressure cooker (Mantra, Inc., Virginia Beach, VA) for 1 minute after maximum pressure was achieved. Slides were then incubated with blocking solution (10% normal horse serum (Vector Laboratories) in dPBS) for 10 min at room temperature and then treated with predilute mouse-antihuman Ki67 antibody (Zymed Laboratories, South San Francisco, CA) overnight in a humidified chamber (Sigma) at room temperature. Slides were incubated with biotinylated anti-mouse IgG (Vector Laboratories) at 1:200 for 30 minutes at RT. The slides were washed with dPBS and stained with Vectastain Elite ABC Kit (Vector Laboratories) for 30 minutes at room temperature. Slides were washed with dPBS and developed using a Vector NovaRed Substrate Kit (Vector Laboratories) for approximately 1 min for bioengineered skin substitutes and epithelialized DED, and 5 min for native tissues. Slides were with rinsed in dPBS, followed by a 5 minute wash with tap water, and counterstained with Harris hematoxylin for 45 s. The slides were washed with tap water and then went through ethanol-xylene washes and mounted with VectaMount permanent mounting medium (Vector Laboratories). The slides were viewed with a Nikon Eclipse E400 microscope and images were captured using an RT Color Spot camera. The number of Ki67 positive basal

cells and total basal cell number were counted over the length of the basal lamina in each channel and for control tissues, over the entire image. The data from each specified channel width was averaged and reported as the mean value +/- SEM. Samples for 50, 100, 200, and 400  $\mu\text{m}$  width channels were  $n = 5, 6, 7,$  and  $10$  at 3 days, respectively and  $n = 5, 6, 10,$  and  $11$  at 7 days, respectively. At both 3 and 7 days of A/L interface culture  $n = 4$  for epithelialized DED. Samples for foreskin tissue were  $n = 5$ . Only one sample of breast control tissue was obtained and 3 images of the sample were evaluated and averaged reported as the mean +/- standard deviations. Breast tissue was not included in statistical analyses.

#### *6.4.3.3 Beta-1 Analysis of Keratinocyte Colonies*

To evaluate keratinocyte expression of  $\beta_1$  integrins in routine keratinocyte co-culture, we utilized quantitative immunofluorescence staining on tissue culture substrates. For the tissue culture substrates, keratinocytes were cultured in 6 well culture plates, using methods previously described. After 5 days of culture, each well was rinsed with dPBS and treated for 10 minutes with a fixing and permeabilizing solution containing dPBS, 4% formaldehyde (Ted Pella, Redding, CA), and 0.2% of Triton X-100 (Sigma). Wells were then rinsed to remove fixative and permeabilizing solution and blocked with a 1% BSA solution in dPBS for 10 minutes. Silicone gaskets made from PDMS with inner diameter of  $\sim 2 \text{ cm}^2$  were secured in the center of each well using silicone vacuum grease (Dow corning, Midland, MI). A primary antibody directed against  $\beta_1$  (Anti-CD29, BioGenex, San Ramon, CA) at a concentration of 1:100 in blocking solution was applied for 2 hours at  $37^\circ \text{C}$ . Following incubation, each sample was washed with dPBS twice, 5 minutes each time. Goat anti-mouse (Alexa Fluor 546, Invitrogen) secondary antibody at a dilution of 1:100 in blocking solution was placed in each well and incubated for 1 hour at  $37^\circ \text{C}$ . After incubation, the wells were rinsed and Hoeschst nuclear reagent (Invitrogen) was added at 0.06 mM (in  $\text{dH}_2\text{O}$ ) for 5 minutes at  $37^\circ \text{C}$ . The wells were rinsed with dPBS, the gaskets removed, and the wells were cover slipped using an aqueous mounting medium containing anti-fading

agents (Biomedica Corp, Foster City, CA). Each image was captured using the same exposure time. Using Image J software, the histogram function was used to determine the greatest fluorescence intensity. Following previously published methods, the greatest fluorescence intensity recorded was subdivided into three regions, the duller (bottom 1/3), the brightest (top 1/3) and the remaining (middle 1/3). Cells that had intensity values in the top 1/3 around their perimeter were considered integrin-bright.<sup>19,33,34</sup> The number of cells that were integrin bright were counted as well as the total number of cells in the colony. The average percent of integrin-bright keratinocytes for 4 separate wells was reported as a mean value +/- SEM since multiple images were captured and analyzed for each well.

#### *6.3.3.4 Beta-1 Expression in Bioengineered Skin Substitutes, Epithelialized DEDs, and Human Tissue*

The expression of  $\beta_1$  for basal keratinocytes in bioengineered skin substitutes, epithelialized DED, and human tissues, was analyzed using immunohistochemistry and quantitative analyses of fluorescent microscope images. Tissue samples, 6  $\mu\text{m}$  thick, were mounted on Superfrost Plus slides coated with poly-L-lysine. Following the same procedure as for Ki67 detection, all samples were deparaffinized and the antigens were unmasked. The same procedure was then followed as for the analysis of  $\beta_1$  of keratinocyte colonies on tissue culture plastic, except samples were cover slipped with Vectashield Mounting Medium with DAPI (Vector Laboratories) to visualize nuclei. Human foreskins and breast tissue were obtained from non-identifiable discarded tissues from UMass Memorial Medical Center, Worcester, MA and were exempt from New England Institutional Review Board review. The human tissues were processed the same way as the bioengineered skin substitutes and epithelialized DED.

Using Image J software, the average relative fluorescence intensity (RFI) value of cell borders was mapped for basal keratinocytes for all tissues evaluated. Previously, it has been determined that  $\beta_1$  intensities correspond with ESC populations and integrin-bright patches

have been used as an indicator of ESC localization areas.<sup>19,34</sup> Once measured, the average RFI was plotted to evaluate integrin-bright and integrin-dull regions of the basal lamina. Similar to  $\beta_1$  expression in the colonies, cells that had intensity values in the top 1/3 were considered integrin-bright.<sup>19,33,34</sup>

### 6.3.5 Statistical Analyses

Sigma Stat Version 3.10 (Systat Software Inc., Richmond, CA) was used to determine statistical differences among the means of experimental groups. To determine if the means of two different samples were significantly different, a Student's t-test was performed when the samples were drawn from a normally distributed population with equal variance. Sigma Stat uses the Kolmogorov-Smirnov test to test for a normally distributed population and a P value  $> 0.05$  indicates normality. For all parametric tests, Sigma Stat assumes equal variance. When the data was not drawn from a normally distributed population (P value  $< 0.05$ ), a Mann-Whitney Rank Sum Test was used and a Levene Median test was used to determine equal variance with a P value  $> 0.05$  indicating equal variance. For both the Student's t-test and the Mann-Whitney Rank Sum Test, a p value  $< 0.05$  indicated a significant difference between the means of experimental groups.

To determine statistical differences among the means of three or more experimental groups a One Way Analysis of Variance (ANOVA) was used when the samples were drawn from a normally distributed population with equal variance (Kolmogorov-Smirnov test for normal distribution and equal variance was assumed). When the data was not normally distributed, a Kruskal-Wallis One way ANOVA on ranks was performed (Levene Median test to determine equal variance with a P  $> 0.05$  indicating equal variance). When a statistical difference was detected among the group means, a Tukey post-hoc analysis was performed for both the One Way ANOVA and Kruskal-Wallis One Way ANOVA on ranks. A p value  $< 0.05$ , for both variance tests, indicated a significant difference between the groups.

## 6.4 RESULTS

### 6.4.1 Development of Bioengineered Skin Substitutes Containing Microfabricated Basal Lamina Analogs

In native skin, the DEJ is not flat, but rather has a microtopography that conforms to a series of ridges and invaginations that, in combination with the biochemical composition, provides a microenvironment to direct basal keratinocyte functions. To investigate the role of this microenvironment on epithelialization and the regenerative capacity of bioengineered skin substitutes, we developed a process to create a dermal scaffold containing microfabricated basal lamina analogs composed of a defined starting collagen material EDC conjugated with FN (Figure 6.1<sup>25</sup>).

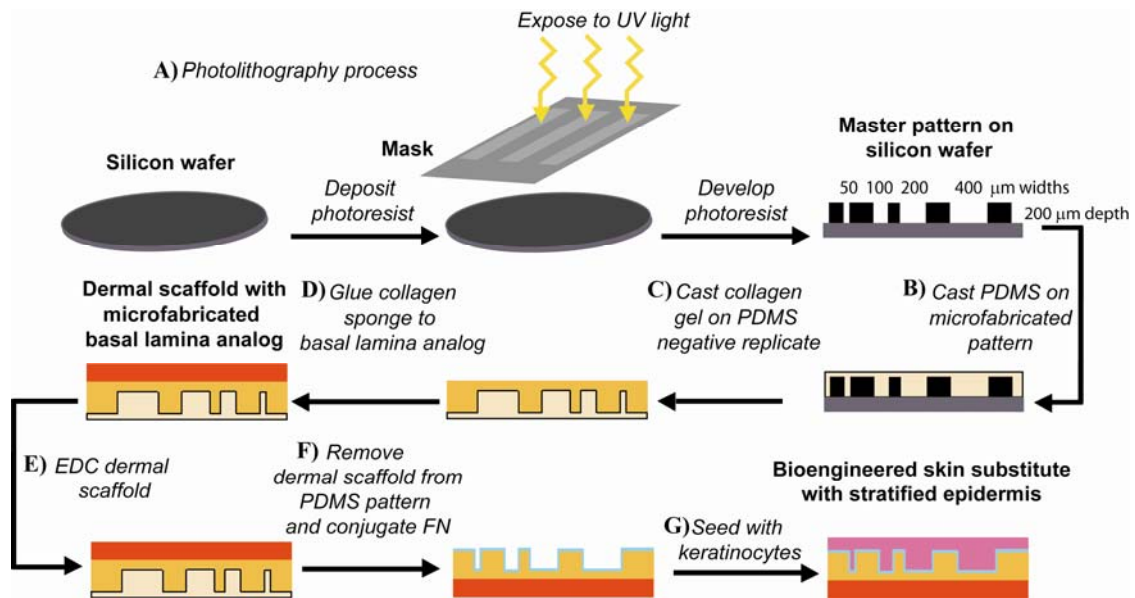
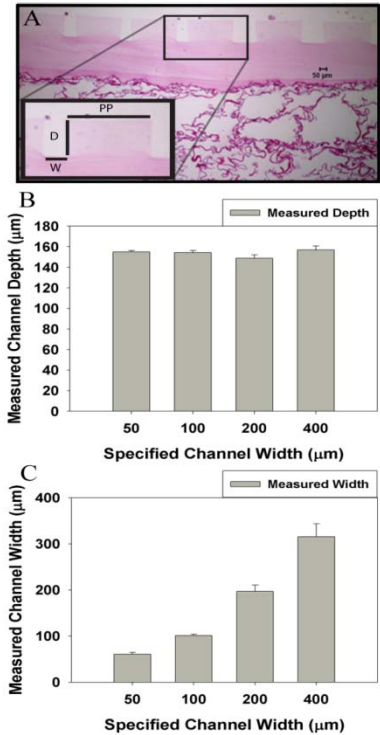


**Figure 6.1. Production of Bioengineered Skin Substitute Containing Microfabricated Basal Lamina Analogs.** Photolithography (A) was used to create a master pattern on a silicon wafer containing channels with a depth of 200 μm and widths of 50, 100, 200, and 400 μm. Polydimethylsiloxane (PDMS) was cast on the microfabricated silicon wafer (B) and allowed to polymerize. The PDMS pattern was inverted and a collagen gel was cast onto the surface containing the negative replicate of the original pattern (C). Once polymerized, another collagen gel was cast onto the back surface of the original collagen gel which acts as a glue to laminate a collagen-GAG sponge (D). This composite was EDC crosslinked (E). The composite was removed from the PDMS and FN was conjugated to the surface (F). The composite was sterilized, seeded with keratinocytes (G), and cultured to create an engineered graft with a stratified epidermis.<sup>25</sup>

Photolithography was utilized to create a master pattern containing channels with specified depths of 200  $\mu\text{m}$  and widths of 50, 100, 200, and 400  $\mu\text{m}$ . Type I collagen was cast onto a PDMS negative replicate of the master pattern and allowed to polymerize. A collagen-GAG sponge was then adhered to the back of the microfabricated self-assembled type I collagen



membrane and the composite was EDC crosslinked to provide mechanical and degradation stability,<sup>35,36</sup> as well as to provide sites for chemical conjugation of FN to the topographical features.<sup>37</sup>

The topographical features provided on the surface of the basal lamina analog were analyzed through histological techniques before cellular seeding. Depths and widths of the channels were measured using Image J (Figure 6.2<sup>25</sup>). It was found that the depths for each channel were approximately 150  $\mu\text{m}$  (Figure 6.2B<sup>25</sup> and Table 6.1<sup>25</sup>) and widths for 50  $\mu\text{m}$  were 60.8 $\pm$ 3.8, 100  $\mu\text{m}$  were 101.2  $\pm$  2.4, 197.1  $\pm$ 13.5, and for 400  $\mu\text{m}$  315.7 $\pm$  27.9 (Figure 6.2C<sup>25</sup> and Table 6.1<sup>25</sup>).

**Figure 6.2. Topographical Measurements of the Surfaces of Bioengineered Basal Lamina Analogs.** To determine the dimensions of basal lamina analogs created using photolithography, histological sections were analyzed. A) represents a section stained with eosin. The insert illustrates the measurements made for depths (D) and widths (W) of the channels as well as the papillary plateau (PP) which will be discussed in later sections. All channels in the bioengineered skin substitutes were measured. These values were averaged and plotted in B (width) and in C (depth) against specified channel widths. Values are reported as averages  $\pm$  SEM. Sample numbers for the 50  $\mu\text{m}$  width channels are  $n = 4$  and for the 100, 200, and 400  $\mu\text{m}$  width channels  $n = 5$ .<sup>25</sup>

**Table 6.1. Specified and Measured Topographical Features of Basal Lamina Analog<sup>25</sup>**

Specified Values		Measured Values		Analyzed Channels
Width ( $\mu\text{m}$ )	Depth ( $\mu\text{m}$ )	Width ( $\mu\text{m}$ )	Depth ( $\mu\text{m}$ )	Width ( $\mu\text{m}$ )
50	200	60.8 $\pm$ 3.8 (4)	154.9 $\pm$ 1.4 (4)	53 - 68
100	200	101.2 $\pm$ 2.4 (5)	154.3 $\pm$ 2.1 (5)	96 - 106
200	200	197.1 $\pm$ 13.5 (5)	148.8 $\pm$ 3.4 (5)	170 - 224
400	200	315.7 $\pm$ 27.9 (5)	156.9 $\pm$ 3.9 (5)	260 - 371

#### 6.4.2 Microenvironments Provided By a Microfabricated Basal Lamina Analog Influence Epidermal Thickness and Morphology of the Epidermal Layer of Bioengineered Skin Substitutes

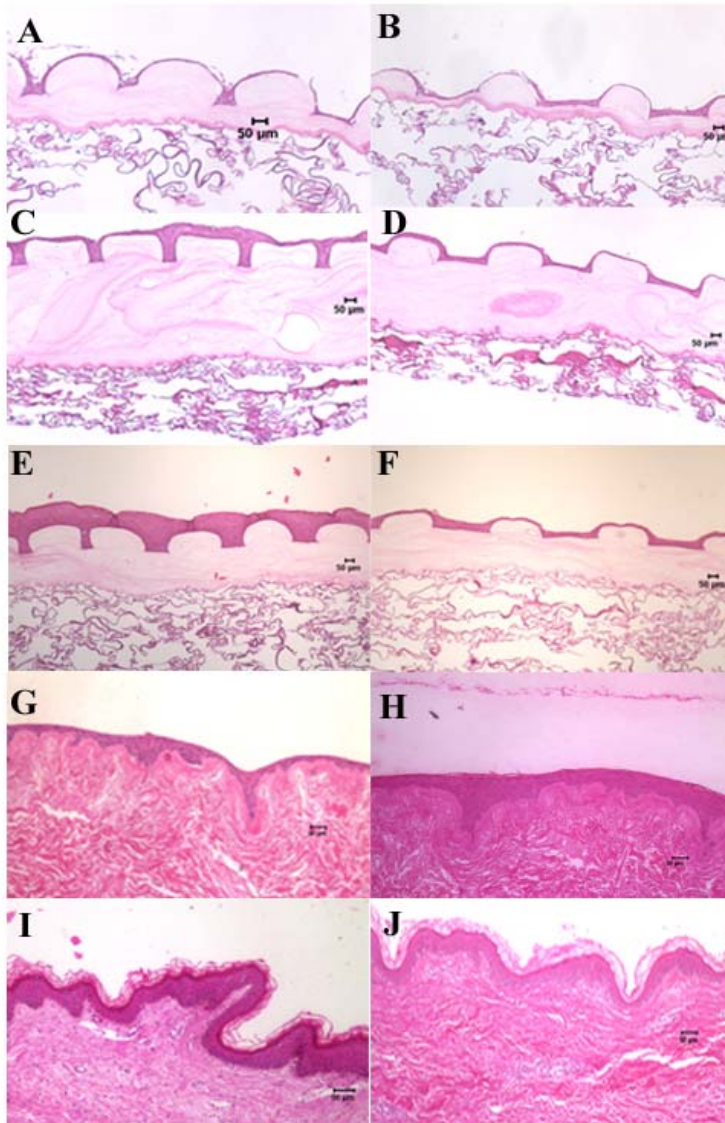


**Figure 6.3. Histological Representation of Hematoxylin and Eosin Stained Bioengineered Skin Substitutes.** To evaluate the effects of FN and topography on epithelialization, the epidermal thickness of the composite was measured without FN cultured for 3 days at the A/L interface (A and B), on composites with FN cultured for 3 or 7 days at the A/L interface (C and D, and E and F, respectively) and compared to keratinocytes cultured on DED cultured for 3 or 7 days at the A/L interface (G and H, respectively) and foreskin and breast control tissues (I and J, respectively). Composites without FN lacked a continuous layer of keratinocytes in all regions and only contained 1 to 3 cellular layers as well as cellular debris. Cells cultured on scaffolds containing FN had a continuous monolayer and comparable epidermal thicknesses and morphology to epithelial layers on DED and in native tissues. Scale bars = 50 µm.<sup>25</sup>

The effect of the microenvironment on epidermal thickness was analyzed at 3 or 7 days of A/L interface culture on a bioengineered skin substitute containing a microfabricated basal lamina. Epidermal thickness was evaluated using histological techniques and quantitative morphometric analyses of microscopy images. Figure 6.3<sup>25</sup> displays representative hematoxylin and eosin stained channels that were evaluated. Previously our laboratory has shown that the presence of FN conjugated to the surface of a self-assembled CI basal



lamina analog enhances epithelialization.<sup>24</sup> When comparing basal lamina analog surfaces

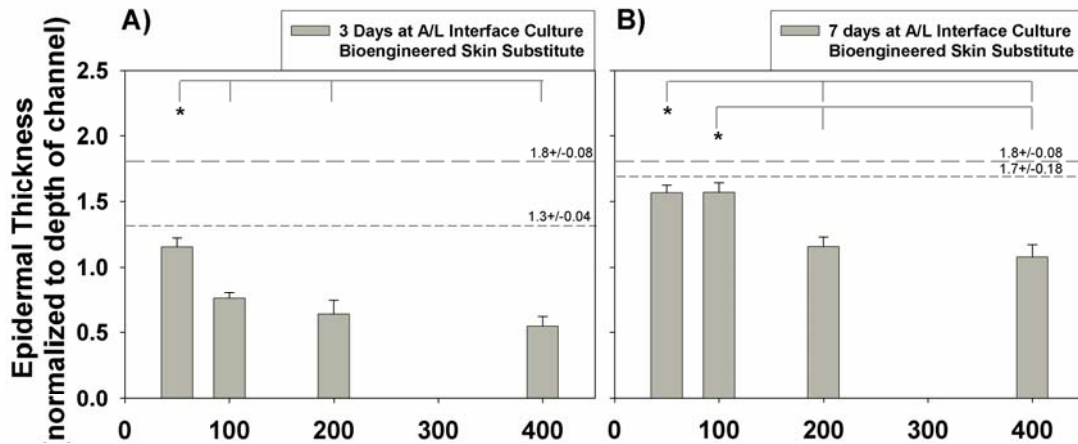


**Figure 6.4. Epidermal Thickness of Bioengineered Skin Substitutes Normalized to Depth of Channel.** Epidermal thickness was measured in each channel of each composite and normalized to the depth of the channel. A) At 3 days of A/L interface culture, epidermal thicknesses measured in 50 µm channels were statistically increased over that of all other channels measured (\* indicates  $p < 0.05$ , One-Way ANOVA, Tukey post-hoc analysis). B) When evaluating epidermal thicknesses at 7 days of A/L interface culture the 50 µm width channels and the 100 µm width channels were statistically different than the 200 and 400 µm channels (\* indicates  $p < 0.05$ , One-Way ANOVA, Tukey post-hoc analysis). Large dashed lines represent epidermal thickness of foreskin tissue and smaller dashed lines represent epidermal thickness on DED. Values represent means +/- SEM. Samples for 50 µm and 100 µm widths at 3 and 7 days are  $n = 5$  and for the 200 µm widths  $n = 6$  and 15 at 3 and 7 days, respectively, and  $n = 11$  and 13 for 400 µm channels at 3 and 7 days, respectively.<sup>25</sup>

without FN conjugation (Figure 6.3A<sup>25</sup> and 6.3B<sup>25</sup>) with basal lamina analog surface with FN conjugation (Figure 6.3C<sup>25</sup> and 6.3D<sup>25</sup>), it can be seen that the FN surfaces have a continuous multi-layer of cells, regardless of topographical geometry (Figure 6.3A-6.3D<sup>25</sup>) in comparison with the non-continuous multi-layers of cells found cultured on the surfaces without FN.

When comparing grafts cultured with FN at various time points, it can be seen that the geometrical features play a role in epidermal thickness. At 3 days of A/L interface culture, channels with widths of 50 µm have a noticeably thicker epidermis than channels with

widths of 200  $\mu\text{m}$  (Figures 6.3C<sup>25</sup> and 6.3D<sup>25</sup>, respectively). Epidermal thickness normalized to the depth of the channel at 3 days of A/L interface culture for the 50  $\mu\text{m}$  channels, was statistically greater than the thickness measured for the 100  $\mu\text{m}$  width, 200  $\mu\text{m}$  width, and 400  $\mu\text{m}$  width channels (Figure 6.4A<sup>25</sup>)

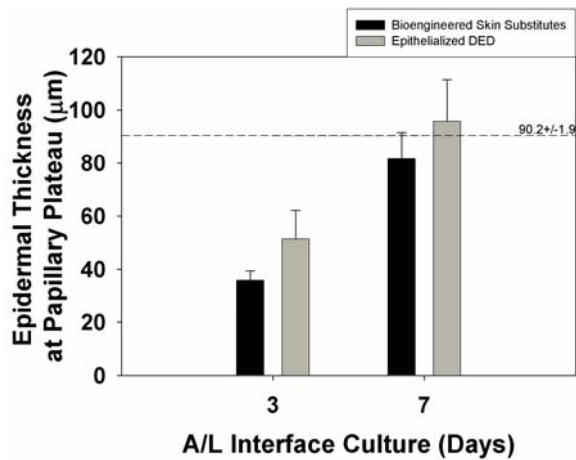


**Figure 6.5. Epidermal Thickness at Papillary Plateau.**

The thicknesses of the epidermal layers at the papillary plateau of bioengineered skin substitutes, epithelialized DED, and in native foreskin were measured. The dashed line represents the epithelial thickness of foreskin tissue. No statistical differences were detected between the thicknesses of bioengineered skin substitutes and epithelialized decellularized dermis at 3 or 7 days of A/L interface culture (One-Way ANOVA with Tukey post-hoc analysis). At 7 days there were no statistical differences between foreskin tissue (dashed line) and either the bioengineered skin substitutes or epithelialized decellularized dermis (Kruskal-Wallis One-Way ANOVA on Ranks). Values represent mean  $\pm$  SEM. For bioengineered skin grafts  $n = 14$  and  $15$  at 3 and 7 days, respectively,  $n = 4$  and  $7$  for epithelialized DED at 3 and 7 days, respectively, and  $n = 4$  for foreskin tissues.<sup>25</sup>

The epidermal layer on the bioengineered skin substitutes cultured in the 50  $\mu\text{m}$  width channels was similar in thickness and morphology to the epidermal layer cultured on DED for 3 days at the A/L interface (Figure 6.3G<sup>25</sup>). When quantifying the epidermal thickness, no statistical differences were found between the decellularized dermis and the 50  $\mu\text{m}$  width

channels at 3 days (Figure 6.4A<sup>25</sup>). At the 7 day A/L interface culture time point for bioengineered skin substitutes, the 50  $\mu\text{m}$  width and 100  $\mu\text{m}$  width (Figure 6.3E<sup>25</sup>) channels have similar morphologies and epidermal thicknesses and when compared to the 200  $\mu\text{m}$  width channels (Figure 6.3F<sup>25</sup>) are much thicker.

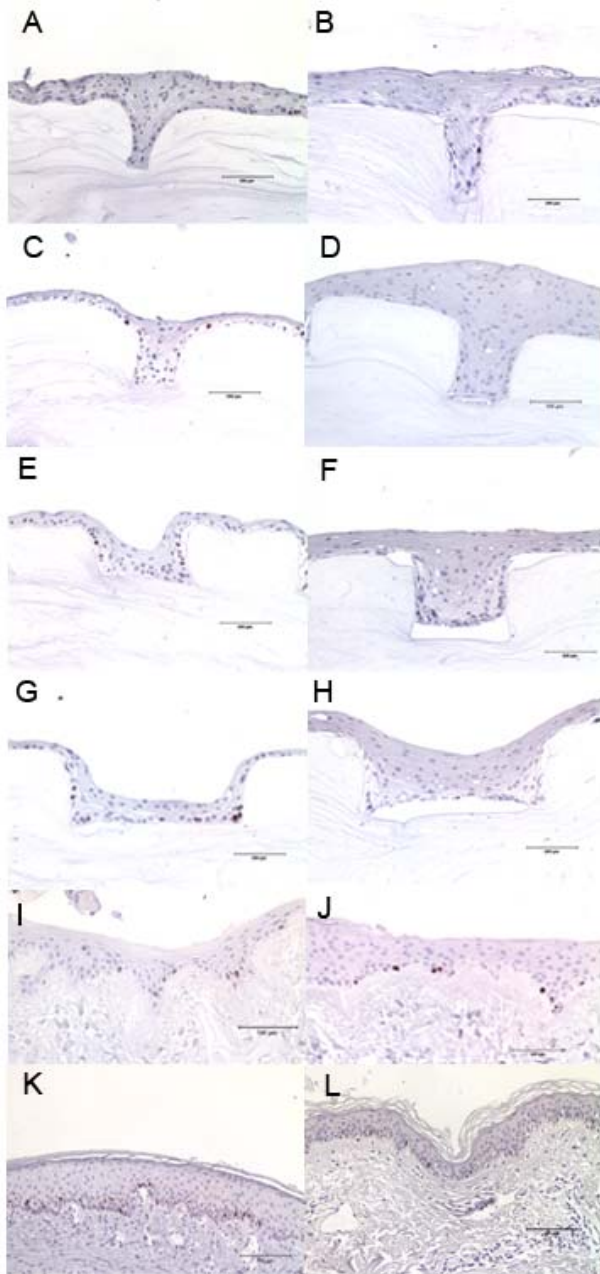


**Figure 6.6. Histological Representation of Ki67 Expression of Basal Keratinocytes Present in Bioengineered Skin Substitutes.** To evaluate the effects of topography on the presence of proliferating basal keratinocytes, Ki67, a marker for highly mitotic cells was used. The presence of Ki67 positive basal keratinocytes was evaluated on bioengineered skin substitutes. A and B represent channels with 50  $\mu\text{m}$  widths at 3 and 7 days, respectively. C and D represent channels with 100  $\mu\text{m}$  widths at 3 and 7 days, respectively. E and F represent channels with 200  $\mu\text{m}$  widths at 3 and 7 days, respectively. G and H represent channels with 400  $\mu\text{m}$  widths at 3 and 7 days respectively. I and J represent epithelialized DED at 3 and 7 days. K and L are foreskin and breast tissue. Scale bars in all images = 100  $\mu\text{m}$ .<sup>25</sup>

Epidermal thickness for the 50  $\mu\text{m}$  width and 100  $\mu\text{m}$  width channels had similar values, and were both statistically different from the 200  $\mu\text{m}$  width and 400  $\mu\text{m}$  width channels (Figure 6.4B<sup>25</sup>). When comparing the bioengineered skin substitutes at 7 days of A/L interface culture to the epidermal layer on DED (Figure 6.3H<sup>25</sup>) and native skin (Figure 6.3I<sup>25</sup> and 6.3J<sup>25</sup>), it can be seen that the 50  $\mu\text{m}$  width and 100  $\mu\text{m}$  width channels have similar morphologies and thickness. No statistical differences were found in epidermal thickness between 50  $\mu\text{m}$  width and 100  $\mu\text{m}$  width channels. Additionally, no statistical differences were found in epidermal thickness between 50  $\mu\text{m}$  width and 100  $\mu\text{m}$  width channels and the epidermal thickness of cells cultured for 7 days at A/L interface on DED or foreskin tissue (Figure 6.4B<sup>25</sup>).

To compare the thicknesses achieved regardless of depth of channels or depths of rete ridges, we measured the epidermal thicknesses at the papillary plateaus for the bioengineered skin substitutes. (Figure 6.5<sup>25</sup> see Figure 6.2A<sup>25</sup> for papillary plateau measurement clarification if necessary). The papillary plateaus between all channels were then averaged and compared to the epidermal thicknesses on the papillary projections for epithelialized DED and foreskin tissue. At 3 days of A/L interface culture, bioengineered skin substitutes and epithelialized DED were not statistically different from each other but different from native foreskin. At 7 days of A/L interface culture, the epidermal thicknesses at the papillary plateau were not statistically different between any measured tissues.

### 6.4.3 Proliferation Capacity of Bioengineered Skin Substitutes is Affected by the Microenvironment Provided by a Microfabricated Basal Lamina Analog

To determine the effects of microtopography on cell proliferation bioengineered skin substitutes and epithelialized DED were evaluated after 3 or 7 days of A/L interface culture. The samples were stained for the nuclear proliferation antigen Ki67 and counterstained with hematoxylin (Figure 6.6<sup>25</sup>).

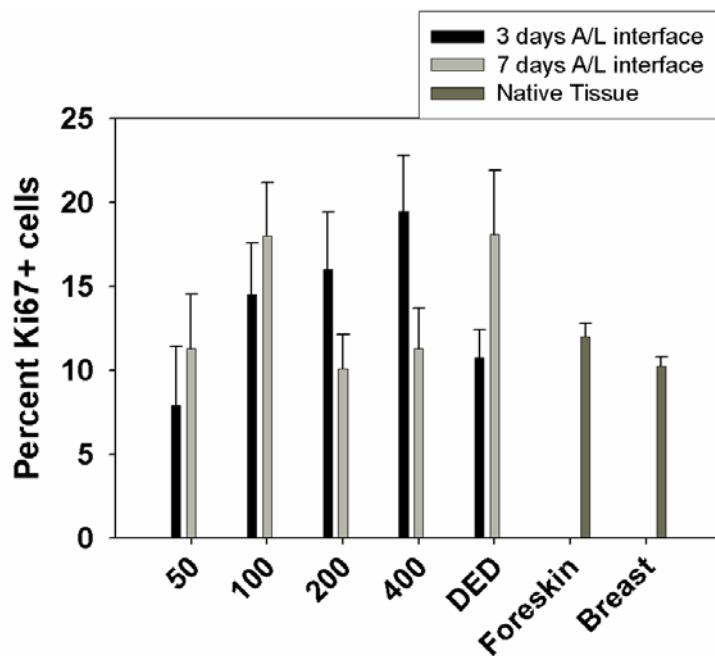


**Figure 6.7. Percentage of Ki67 Positive Basal Keratinocytes in Bioengineered Skin Substitutes.** The number basal keratinocytes that were Ki67 positive cells were counted in each channel as well as total number of basal keratinocytes and the percentage positive was determined. For native tissues, basal keratinocytes that were Ki67 positive as well as total basal keratinocytes were counted over a length ranging from 650  $\mu\text{m}$  to 950  $\mu\text{m}$  based on topographical features. Values are reported as averages  $\pm$  SEM. For 50  $\mu\text{m}$ , 100  $\mu\text{m}$ , 200  $\mu\text{m}$ , 400  $\mu\text{m}$  widths, and epithelialized DED at 3 days, n = 5, 6, 7, 11, and 4, respectively. For 50  $\mu\text{m}$ , 100  $\mu\text{m}$ , 200  $\mu\text{m}$ , 400  $\mu\text{m}$ , and epithelialized DED at 7 days, n = 4, 5, 11, 10, and 4, respectively. Samples for foreskin tissues are n = 5. For breast tissue 3 separate sections of the same tissue were evaluated.<sup>25</sup>

Foreskin and breast tissues were also evaluated as native skin controls (Figure 6.6K<sup>25</sup> and L<sup>25</sup>). The percentage of Ki67 positive cells was quantified in each channel, or over the entire basal lamina for epithelialized DED or native tissues (Figure 6.7<sup>25</sup>).

At 3 days of A/L interface culture, the 50  $\mu\text{m}$  width channels had the lowest average percentage of Ki67 positive cells (approximately 7.5% Figure 6.7<sup>25</sup>), and 40% of these channels had zero positive cells. At 7 days of A/L interface culture, the 50  $\mu\text{m}$  width

channels had a slightly higher average percentage of Ki67 positive cells than at 3 days, and 20% of the channels analyzed had zero positive cells (Figure 6.7<sup>25</sup>). When analyzing the 100  $\mu\text{m}$  width channels after 3 days of A/L interface culture, it was found that all channels contained positive cells and an average of approximately 15% Ki67 positive cells was found. At 7 days of A/L interface culture, the percentage of Ki67 positive cells was approximately the same as at 3 days and all 100  $\mu\text{m}$  width channels analyzed contained positive cells (Figure 6.7<sup>25</sup>).

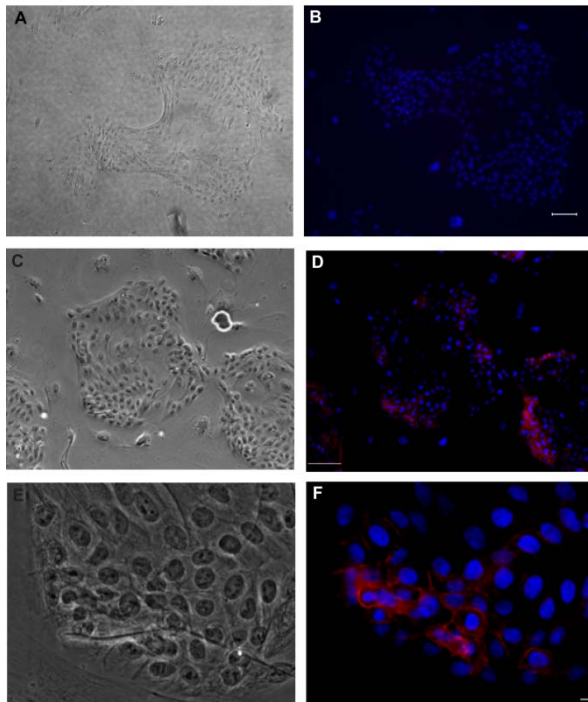


**Figure 6.8. Keratinocyte Colonies with  $\beta_1$  and Nuclear Expression.** Keratinocytes after 4 days of co-culture were immunostained for  $\beta_1$  (red) and nuclei (blue) expression. Images A and B represent phase contrast and merged fluorescent images obtained in control wells, respectively. Scale bar = 100  $\mu\text{m}$ . Images C and D represent phase contrast and merged fluorescent images, respectively captured at 10x to evaluate cells and expression in total colonies. Scale bar = 100  $\mu\text{m}$ . Images E and F represent phase contrast and merged fluorescent images captured at 40x to demonstrate perinuclear expression of  $\beta_1$ . Scale bar = 5  $\mu\text{m}$ .<sup>25</sup>

The 200  $\mu\text{m}$  width and 400  $\mu\text{m}$  width channels had similar values and trends at both 3 and 7 days of A/L interface culture. At 3 days of A/L interface culture the 200  $\mu\text{m}$  width channels had approximately 15%

Ki67 positive cells and the 400  $\mu\text{m}$  width channels had approximately 18% Ki67 positive cells. At 7 days, both channels decreased in percentage Ki67 positive cells to approximately 10% (Figure 6.7<sup>25</sup>). Epithelialized DED exhibited approximately 10% Ki67 positive cells at 3 days of A/L interface culture and approximately 18% Ki67 positive cells at 7 days of A/L interface culture. When analyzing native tissues, it was found that the basal keratinocytes of neonatal foreskin were approximately 12% Ki67 positive and basal keratinocytes in breast tissue were approximately 10% Ki67 positive. Overall our Ki67 data suggests that no significant differences exist among any sample evaluated at either 3 days or 7 days of A/L interface culture (Figure 6.7<sup>25</sup>) When performing a power analysis, it was found that  $P < 0.8$  for both the 3 and 7 day data, therefore to further support these findings, sample sizes need to be increased.

#### **6.4.4 *Beta-1* Expression in Keratinocyte Colonies Detected in Edge Keratinocytes**

The expression of  $\beta_1$  in colonies of keratinocytes was evaluated after 4 days of co-culture with a feeder layer of J2s. It was found that for all colonies in each culture well,  $\beta_1$  expression was found in the periphery of keratinocytes on the perimeter of each colony. To analyze the localization of  $\beta_1$  bright regions, the maximal fluorescence intensity was determined so that no saturation occurred in the image. This value was then divided into three equal regions, thus giving three regions of integrin expression values (bright, medium, and dull). Any value in the top third was considered  $\beta_1$ -bright similar to previously reported literature.<sup>19,33,34</sup> When analyzing the percentage of cells were  $\beta_1$ -bright it was determined that 25% +/- 0.1 of the colony were  $\beta_1$ -bright. Figure 6.8A<sup>25</sup> and 6.8C<sup>25</sup> are phase contrast images that display a representative colony at 10 and 40x and 6.8B<sup>25</sup> and 6.8D<sup>25</sup> are fluorescent images displaying  $\beta_1$  expression (red) and cell nuclei (blue) at 10 and 40x, respectively.

#### 6.4.5 Microenvironments Control Spatial Localization of $\beta_1$ -Bright Basal Keratinocytes

To determine localization of  $\beta_1$ -bright keratinocytes in bioengineered skin substitutes, epithelialized DEDs, and in native foreskins, we utilized immunohistochemistry coupled with quantitative digital image analyses. Fluorescent intensity values were determined for cell-cell borders similar to previously reported literature for 3 day A/L interface cultures.<sup>19,33,34</sup> Figure 6.9 displays representative images of 100  $\mu\text{m}$  width channels (Figures 6.9A<sup>25</sup> and 6.9B<sup>25</sup>), 400  $\mu\text{m}$  width channels (Figures 6.9D,<sup>25</sup> 6.9E,<sup>25</sup> 6.9G,<sup>25</sup> and 6.9H<sup>25</sup>), flat regions of bioengineered skin substitutes (Figures 6.9J<sup>25</sup> and 6.9K<sup>25</sup>), epithelialized DED (Figures 6.9M<sup>25</sup> and 6.9N<sup>25</sup>), and neonatal foreskin (Figures 6.9P<sup>25</sup> and 6.9Q<sup>25</sup>).

It was found that in the 100  $\mu\text{m}$  width (Figures 6.9A,<sup>25</sup> 6.9B,<sup>25</sup> and 6.9C<sup>25</sup>) and 400  $\mu\text{m}$  width (Figures 6.9D,<sup>25</sup> 6.9E,<sup>25</sup> and 6.9F<sup>25</sup>) channels, there were no  $\beta_1$ -bright cells in the flat sections next to the channels (papillary plateaus), but in the channels 16.7% and 23% of basal keratinocytes were  $\beta_1$ -bright, respectively (dashed lines in 6.9C and 6.9F separate flat regions from channel regions). Figures 6.9G,<sup>25</sup> 6.9H,<sup>25</sup> and 6.9I<sup>25</sup> are another representative image of the 400  $\mu\text{m}$  width channels demonstrating  $\beta_1$ -bright regions localized to the corners of the channels. In the corners of the 400  $\mu\text{m}$  width channels we found that 50% of the total basal keratinocyte population was  $\beta_1$ -bright.

When  $\beta_1$  was evaluated on flat regions of the bioengineered skin substitutes, 30% of the basal keratinocyte population was  $\beta_1$ -bright, however the cells were not localized, but heterogeneously distributed (Figures 6.9J,<sup>25</sup> 6.9K,<sup>25</sup> 6.9L<sup>25</sup>). The expression of  $\beta_1$ -bright basal keratinocytes on epithelialized DED was found to be 15.6% and the  $\beta_1$ -bright cells were localized to the rete ridges. Additionally,  $\beta_1$  expression was evaluated in native foreskin tissue. It was found that the  $\beta_1$ -bright basal keratinocytes localized to the tips of the papillary projections. Overall 6.8% of the total basal keratinocyte population was  $\beta_1$ -bright.

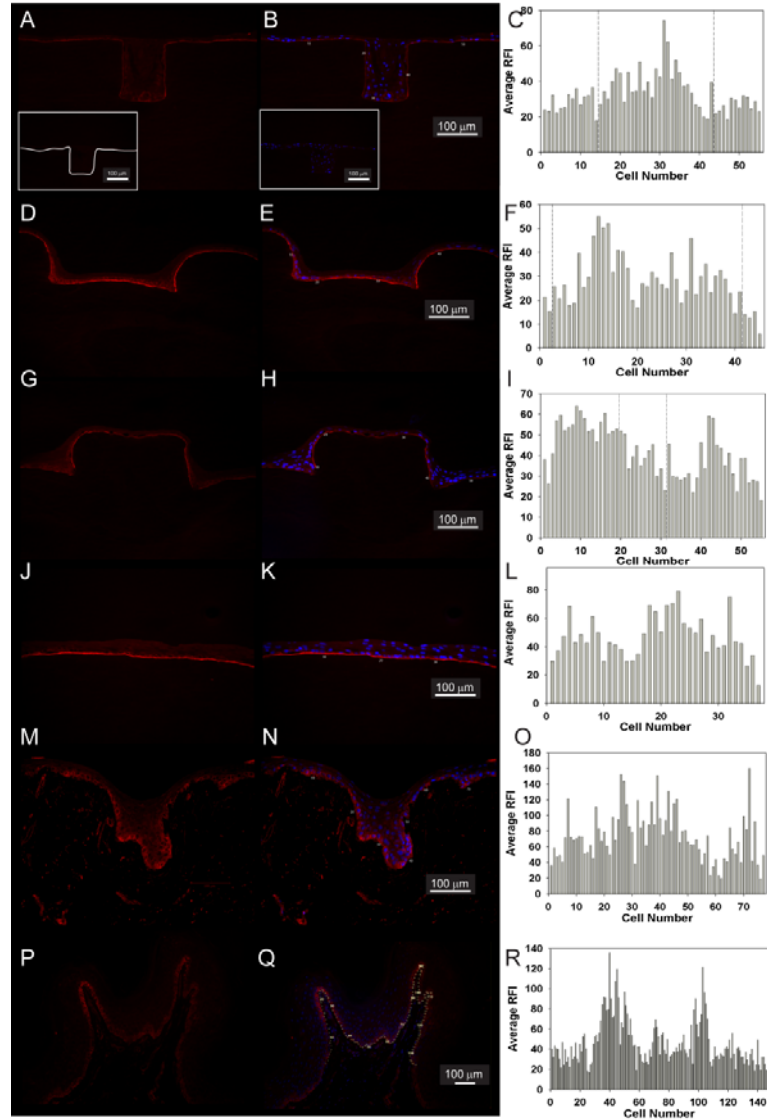


**Figure 6.9. *Beta-1* Expression of Basal Keratinocytes in Bioengineered Skin Substitutes.** To determine the localization of  $\beta_1$  bright basal keratinocytes, immunohistochemistry coupled with digital image analyses was used. Figures 6.9A, 6.9D, 6.9G, 6.9J, 6.9M, and 6.9P are images with  $\beta_1$  expression in red and Figures 6.9B, 6.9E, 6.9H, 6.9N, and 6.9Q are images with  $\beta_1$  expression in red and nuclear expression in blue. Figures 6.9C, 6.9F, 6.9I, 6.9M, and 6.9R are plots of the average relative fluorescence intensities (RFI) of cell-cell borders in the region evaluated. Dashed lines in 6.9C, 6.9F, and 6.9I separate flat regions from the channel. It can be seen that for the 100, 400, and DED samples (Figures 6.9B, 6.9E, 6.9H, and 6.9N)  $\beta_1$  bright cells localized to the rete ridges, whereas in native foreskin  $\beta_1$  bright cells localized to the tips of the dermal papillae. Additionally when evaluating the flat region of the bioengineered skin substitute,  $\beta_1$  cells were heterogeneously distributed. Each cell was measured and the average RFI was reported. Insert in A and B represent controls for  $\beta_1$  and  $\beta_1$  and nuclear staining. Error bars represent 100  $\mu\text{m}$  in all images.<sup>24</sup>



## 6.5 DISCUSSION

Understanding how the biochemical and three-dimensional microenvironment of the basal lamina modulates keratinocyte proliferation and differentiation, as well as contributes to localization of ESCs, is of great importance when designing bioengineered skin substitutes. In native tissues, the basal lamina provides instructive cues that are critical in skin architecture, cellular organization, and the regeneration of the epidermal layer.<sup>4</sup> The regeneration of skin is of great importance, because in order for skin to provide the protective barrier against the surrounding environment, the epidermis must be in constant renewal. In this study we developed a novel dermal scaffold that contains both biochemical and microtopographical cues provided by the native basal lamina and investigated the role of the microenvironment on bioengineered skin substitutes morphology, epidermal thickness, keratinocyte proliferation, and ESC localization. Additionally we compared our findings with epithelialized DED and native foreskin tissues.

To create a microfabricated basal lamina analog produced from self-assembled CI, photolithography was used. A master pattern was created on a silicon wafer to produce channels with specified features of 200  $\mu\text{m}$  depth and 50  $\mu\text{m}$ , 100  $\mu\text{m}$ , 200  $\mu\text{m}$ , and 400  $\mu\text{m}$  widths. A negative replicate was produced using PDMS and acid soluble type I collagen was self-assembled on the surface of the negative replicate PDMS pattern. Previously, our laboratory has used a similar strategy to create basal lamina analogs using a collagen-GAG coprecipitate with different processing techniques to create a basal lamina analog laminated to a dermal scaffold.<sup>21,22</sup> When comparing the two strategies to produce microfabricated basal lamina analogs, we found that the features of the microfabricated basal laminas when composed of collagen-GAG had a greater error associated with both the widths and depths (mean width error varied from 13-30% and mean depth varied from 7.4-16.2%), than the features on the self-assembled CI lamina analogs (mean width errors varied from 2-9% and mean depths varied from 0.9-2.5%). Although the depths and widths of the self-assembled

CI membranes varied from the design specifications, our new method using self-assembled CI demonstrates improved fidelity for recapitulating topographical features as well as a defined starting biochemistry for enhanced FN EDC conjugation.<sup>24</sup>

After analyzing the topography of the channels, we investigated the responses of keratinocytes cultured for 3 or 7 days at the A/L interface on the surfaces of microfabricated basal lamina analogs laminated to dermal scaffold and compared the results to keratinocytes cultured on DED as well as with native neonatal foreskin and adult breast tissue. When evaluating histological images, we determined that the epidermal thickness varied based on the geometry of the channels. We also determined that after culturing keratinocytes on the microfabricated basal lamina analogs, that the topographic features had greater errors associated with their dimensions, than when measured prior to cellular culture. Therefore to account for the change in channel width, we only analyzed channels with widths that deviated from the mean by +/- 2 SEM, and normalized the epidermal thickness values to the depths of the channel based on previous data that suggests depth plays a role in the microenvironment.<sup>21</sup>

The observed changes in topographical features of the epithelialized microfabricated self-assembled CI basal lamina analog can be explained based on *in vivo* analysis of MMPs in normal wound healing. Matrix metalloproteinases (MMPs) are found in the wound environment and are responsible for the degradation and modification of ECM proteins at the wound site.<sup>38</sup> Matrix metalloproteinase-1 (MMP-1), or collagenase-1, is keratinocyte derived and initially found at high levels in the wound to enable keratinocyte migration and monolayer formation. Once a monolayer and basement membrane proteins are formed, this enzyme ceases (as well as other MMPs) to be produced at high levels, and returns to normal levels that contribute to the constant balance of matrix synthesis and breakdown and recycling of the ECM.<sup>39,40</sup> Since the keratinocytes initially seeded on the microfabricated

basal lamina analogs exhibit similar characteristics to wounded keratinocytes, it is hypothesized that there was an upregulation of MMP levels similar to *in vivo* wounds which caused the change in the dimensions of the topographic features.<sup>41-45</sup>

We evaluated the epidermal layer of bioengineered skin substitutes, after 3 days of A/L interface culture, and determined that keratinocytes cultured in 50  $\mu\text{m}$  width channels had statistically similar epidermal thickness values as epithelialized DED. At 7 days of A/L interface culture the 50  $\mu\text{m}$  and 100  $\mu\text{m}$  width channels exhibited the same epidermal thicknesses as keratinocyte cultured on DED and foreskin tissue and these conditions were statistically different from epidermal thickness values in the 200  $\mu\text{m}$  width and 400  $\mu\text{m}$  width channels.

The morphology of the epidermal layer on the FN conjugated basal lamina analog surfaces, suggests well differentiated epidermal layers, based on cellular size and loss of nuclei from the stratum corneum layer. Keratinocytes found in the basal layer are cuboidal in shape and as the cells progress to the stratum corneum, exhibit a more flattened morphology, similar to what is found in native skin. Furthermore, in native skin, these morphological changes are accompanied by changes in the expression of keratin proteins and water proofing lipids, which are both important in functionality of the skin in providing a protective barrier against the environment as well as structural integrity of the epidermis.<sup>46</sup>

Additionally, to demonstrate functionality of our bioengineered skin substitute, we determined the percentage of Ki67 positive basal keratinocytes. Native skin is under constant renewal, thus having a bioengineered skin substitute with similar regenerative capacity is necessary in order to maintain a healthy tissue. Ki67 positive basal keratinocytes were measured at the 3 and 7 day time points. At 3 days of A/L interface culture, the 50  $\mu\text{m}$  width channels contained a lower percentage of Ki67 positive basal cells than any other

channels and was similar to the percentage of Ki67 basal keratinocytes on DED. At 7 days of A/L interface culture, the 200  $\mu\text{m}$  width and 400  $\mu\text{m}$  width channels had displayed a decrease in percentage of Ki67 positive basal keratinocytes, whereas the 50  $\mu\text{m}$  width and 100  $\mu\text{m}$  width channels stayed relatively consistent.

The data obtained from our Ki67 study helps to elucidate the trends from the epithelial thickness experiments and suggests that a space filling mechanism can be used to explain the data. Our data suggests that after initial seeding, a monolayer of cells was present and that a proliferative burst occurred, similar to results seen during *in vitro* cultures of low-density to high-density keratinocytes<sup>47-50</sup> as well as in the *in vivo* wound healing environment once a monolayer of keratinocytes is formed and contact inhibition occurs.<sup>41</sup> This burst can be characterized by the basal cells undergoing two to four mitotic divisions and committing to terminal differentiation that leads to epithelialization.<sup>49-51</sup> Since the 50  $\mu\text{m}$  width channels have much smaller dimensions, they require a fewer number of cells to fill the topographic feature, followed by the 100, 200, and 400  $\mu\text{m}$  width channels. At 3 days of A/L interface culture (6 days of culture); the 50  $\mu\text{m}$  width channels had a complete epithelial layer; however the 100, 200, and 400  $\mu\text{m}$  width channels did not. Our Ki67 data suggests that a proliferative burst occurred before the 3 days time point and this channel was in a steady state of proliferation between 3 and 7 day time points, whereas the other channels were still undergoing a proliferative burst to fill the channel. At 7 days of A/L interface culture (10 days of culture); the 100  $\mu\text{m}$  width channels had the same epithelial thickness as the 50  $\mu\text{m}$  width channels and native skin; however the 200  $\mu\text{m}$  and 400  $\mu\text{m}$  width channels contained a less thick epidermis. The percentage of Ki67 positive cells for the 200  $\mu\text{m}$  and 400  $\mu\text{m}$  width channels both decreased at the 7 day time point but were not statistically different from the 3 days, which could indicate that the epithelial thickness in these channels was as thick as it would form. To further support the proposed mechanism, as well as to further explain the trends observed, future studies should focus on collecting data at the initial seeding time to

verify a monolayer as well as data at later time points to evaluate whether the epithelial thickness of the wider channels reaches similar thickness values as the 50  $\mu\text{m}$  width and 100  $\mu\text{m}$  width channels, epithelialized DED, and native tissue.

Although we evaluated the presence of Ki67 a marker for proliferative cells, this marker does not distinguish between the two types of proliferating cells, ESCs and TAs, found in the basal layer of the epidermis. In order to create a bioengineered skin substitute that has the capacity for continuous renewal, it is necessary for ESCs to be present on the surface of the bioengineered skin substitute. In the basal layer of the epidermis, keratinocytes express receptors of the integrin family that mediate adhesion to the basal lamina<sup>17,52,53</sup> and also regulate the onset of terminal differentiation.<sup>52-54</sup> Adhesion to ECM proteins and fluorescence activated cell sorting (FACS) have both been used to separate basal keratinocytes based on their integrin expression levels. When plating the separated fractions of keratinocytes and examining CFE, the cells expressing a two- to threefold increase in  $\beta_1$  levels were determined to have greater proliferative potential. Additionally when using fluorescence microscopy, the location of  $\beta_1$ -bright regions in native tissues was compared with the location of LRCs from previous studies, and it was found that they both resided in the same location, which was based upon tissue site.

We first investigated the presence of  $\beta_1$  in colonies of cultured keratinocytes and determined that 25% of cells in the colony were  $\beta_1$ -bright and these cells were located at the colony border. This data corresponds with previously published literature that selected for keratinocytes using rapid adhesion to CIV. In this study the keratinocytes that adhered were 28% of the total starting population and had a higher modal  $\alpha_2\beta_1$  fluorescence than the total (unselected) basal population.<sup>19</sup> Our finding of our keratinocyte population is important because this is the starting population of cells to be cultured on the surface of a dermal scaffold with a microfabricated basal lamina analog.

To evaluate the location of these  $\beta_1$ -bright cells on bioengineered skin substitutes, we utilized immunofluorescent microscopy and image analysis of sections of the grafts. For our bioengineered skin substitutes, we found that the  $\beta_1$ -bright regions were located in the channels and not on the papillary plateaus. Analyses indicated that for the 100  $\mu\text{m}$  width channel, 16.7% of the total basal keratinocyte population in the channel was  $\beta_1$ -bright. Similar analysis for the 400  $\mu\text{m}$  width channel indicated that 23% of the total basal keratinocyte population in the channel was  $\beta_1$  bright. Additionally it was found that the  $\beta_1$ -bright regions in the 400  $\mu\text{m}$  width channels localized to the corners of the channels as seen in Figures 6.9G<sup>25</sup> and 6.9H.<sup>25</sup> When just evaluating the “corner” regions of the 400  $\mu\text{m}$  width channels it was found that 50% of the basal keratinocytes in this region were  $\beta_1$ -bright. When evaluating the papillary plateaus, it was found that there were no  $\beta_1$  bright cells (0%). When flat regions of the bioengineered skin substitutes were evaluated, we found that the  $\beta_1$ -bright cells were heterogeneously dispersed and that 30% of the total basal keratinocyte population was  $\beta_1$  bright. For epithelialized DED we found that 15.6% of the total basal keratinocyte population was  $\beta_1$ -bright and these cells were localized to the rete ridges. In native foreskin tissue, we found that 7% of the total population of basal keratinocytes was  $\beta_1$ -bright and these cells were localized to the tips of the dermal papillae. This localization finding is consistent with literature; although our percentage of integrin bright cells was much lower.<sup>19,33</sup> This could be caused by the variation of fluorescence intensities that the samples were exposed to. In our study, care was taken to not overexpose the regions, thus lower values could be caused by this factor.

In addition to identifying ESCs in bioengineered skin substitutes, an interesting finding is that the  $\beta_1$ -bright cells were found primarily in the channels as well as in the rete ridges of epithelialized DED. Also our analysis of  $\beta_1$  in foreskin tissue is consistent with previous studies indicating that  $\beta_1$ -bright regions are localized to the tips of the papillary projections.<sup>12,19</sup> In native skin the localization of integrin bright regions varies with location

in the body. It has been thought that this localization is a mechanism to protect the cells that contribute to the maintenance of population of cells responsible for the continuous regeneration of the skin. The question of what are the cells being protected from has been addressed by previous investigators.<sup>11,55</sup> There are many insults that can occur from the outside environment such as ultraviolet light or chemicals, which would make the deep rete ridges a more protective microenvironment for the ESCs, however insults can also occur from the dermal tissue as well. Inflammation or a burst of oxidative stress could damage the cells in the bottom of the rete ridges and therefore the safer place would be in the tips of the papillary projects. Neither of these groups of insults explains why in one location of the body, the ESCs in skin would be in the bottom of the rete ridges or in the tips since all insults mentioned can occur in all locations of the body. Another possible explanation for the localization of ESCs is based on the occurrence of mechanical friction in different regions of the body. The palms and soles of the human body are areas of skin that are exposed to excessive friction and contain more numerous dermal papillae and deep rete ridges.<sup>6,12</sup> When investigating  $\beta_1$  expression in these tissues, it was found that the bright regions are in the deep rete ridges, unlike other areas of the body that experience less friction and have  $\beta_1$ -bright expression on the tips of the papillary projections.<sup>12,19</sup>

In our study, we demonstrated a similar range of percentages of  $\beta_1$ -bright basal keratinocytes that correspond with previous literature in suggesting that 25-50% of basal keratinocyte are  $\beta_1$ -bright.<sup>19</sup> However, other analyses suggest that only 10% of basal keratinocytes are ESCs<sup>56</sup> and another report suggest a much lower percentage (1%) of the basal cells are actually ESCs.<sup>57</sup> It has been agreed that quantitative differences in the expression of one particular cell surface marker is not sufficient to uniquely define the stem cell population, since  $\beta_1$  is not unique to ESCs. Consequently, our analysis of the effect of the microenvironment on ESC localization, necessitates that future studies investigate additional means of interfollicular ESC detection.<sup>19</sup> A major caveat to these future studies is that there

is no universally accepted criterion to define interfollicular ESCs and that surface markers used to isolate a population may not isolate a distinct population, but one that has overlapping population of cells. Until a detection technique is discovered, it will be necessary to compile evidence of “stemness” combining many techniques<sup>57</sup> such as the evaluation of the expression of  $\beta_1$ ,<sup>18</sup> transferrin receptors,<sup>58,59</sup> connexin 43,<sup>60</sup> isoform of CD133,<sup>61</sup> desmosomal proteins,<sup>62</sup> and proteins mediating intercellular adhesions,<sup>34</sup> as well as label retaining studies.<sup>7,11,13,14</sup> Additionally, studies evaluating the transcriptional profiles of cells isolated using surface markers will have an impact on identifying a true interfollicular ESC population.<sup>63</sup>

Overall this study has focused on developing a bioengineered skin substitute that recapitulates biochemical and microtopographical features found at the DEJ to enhance epithelialization and interfollicular ESC localization. We have found that 50 and 100  $\mu\text{m}$  width channels with approximate depths of 150  $\mu\text{m}$  contain a full epithelial layer after 7 days at A/L interface culture. When comparing these values to epithelialized DED or native skin, it was found that the epithelial thicknesses were not statistically different from one another and also contain similar values of proliferating basal keratinocytes. The information gained from this study will help with design features of the next generation of bioengineered skin substitutes that will overcome limitations such as prolonged culture times and healing times. In the future we will also evaluate if the increased surface area provided by the microfabricated basal lamina analog with the smaller width features will increase mechanical stability, thus helping to overcome mechanical induced graft failures. Additionally, our bioengineered skin substitute containing a microtopographical basal lamina analog provides an excellent model system to evaluate the proper ESC niche through both surface markers and label-retaining studies in order to enhance the regenerative capacity of bioengineered skin substitutes.



## 6.6 ACKNOWLEDGEMENTS

This research was funded by the NIH (EB-005645). Microfabrication was performed at the BioElectroMechanical Systems (BioMEMS) Resource Center, Massachusetts General Hospital, Boston, MA (NIH Grant: P41 EB02503 (MT)). I would like to thank the Department of Obstetrics and Gynecology at UMMS (Worcester, MA) for providing us with neonatal foreskins for keratinocyte isolations and Russell Kronengold, PhD at Kensey Nash Corporation (Exton, PA) for his generous donations of SEMED-S collagen. I would also like to thank my advisor George Pins for his scientific contribution to the work as well as Donna Davidson, Christina Mezzone, Stacy Gutowski, Sahil Bhagat, and Kevin Cornwell for their technical assistance.

## 6.6 REFERENCES

1. Boyce ST, Goretsky MJ, Greenhalgh DG, Kagan RJ, Rieman MT, Warden GD. Comparative assessment of cultured skin substitutes and native skin autograft for treatment of full-thickness burns. *Ann Surg* 1995;222(6):743-52.
2. Sheridan RL, Tompkins RG. Skin substitutes in burns. *Burns* 1999;25(2):97-103.
3. Parenteau N, Sabolinski M, Prosky S, Nolte C, Oleson M, Kriwet K, Bilbo P. Biological and physical factors influencing the successful engraftment of a cultured skin substitute. *Biotech. Bioeng.* 1996;52:3-14.
4. Vracko R. Basal lamina scaffold-anatomy and significance for maintenance of orderly tissue structure. *Am J Pathol* 1974;77(2):314-46.
5. Young B, Burkitt HG, Heath JW, Wheater PR. Wheater's Functional Histology: Figure 9.2.
6. Odland GF. The morphology of the attachment between the dermis and the epidermis. *Anat Rec* 1950;108(3):399-413.
7. Cotsarelis G, Cheng SZ, Dong G, Sun TT, Lavker RM. Existence of slow-cycling limbal epithelial basal cells that can be preferentially stimulated to proliferate: implications on epithelial stem cells. *Cell* 1989;57(2):201-9.
8. Bickenbach JR, Chism E. Selection and extended growth of murine epidermal stem cells in culture. *Exp Cell Res* 1998;244(1):184-95.
9. Blanpain C, Lowry WE, Geoghegan A, Polak L, Fuchs E. Self-Renewal, Multipotency, and the Existence of Two Cell Populations within an Epithelial Stem Cell Niche. *Cell* 2004;118:635-648.
10. Cotsarelis G, Sun TT, Lavker RM. Label-retaining cells reside in the bulge area of pilosebaceous unit: implications for follicular stem cells, hair cycle, and skin carcinogenesis. *Cell* 1990;61(7):1329-37.
11. Lavker RM, Sun TT. Heterogeneity in epidermal basal keratinocytes: morphological and functional correlations. *Science* 1982;215(4537):1239-41.
12. Lavker RM, Sun TT. Epidermal stem cells. *J Invest Dermatol* 1983;81(1 Suppl):121s-7s.
13. Bickenbach JR, Mackenzie IC. Identification and localization of label-retaining cells in hamster epithelia. *J Invest Dermatol* 1984;82(6):618-22.
14. Bickenbach JR, Holbrook KA. Label-retaining cells in human embryonic and fetal epidermis. *J Invest Dermatol* 1987;88(1):42-6.

15. Adams JC, Watt FM. Fibronectin inhibits the terminal differentiation of human keratinocytes. *Nature* 1989;340(6231):307-9.
16. Adams JC, Watt FM. Changes in keratinocyte adhesion during terminal differentiation: reduction in fibronectin binding precedes alpha 5 beta 1 integrin loss from the cell surface. *Cell* 1990;63(2):425-35.
17. Adams JC, Watt FM. Expression of beta 1, beta 3, beta 4, and beta 5 integrins by human epidermal keratinocytes and non-differentiating keratinocytes. *J Cell Biol* 1991;115(3):829-41.
18. Jones PH, Watt FM. Separation of human epidermal stem cells from transit amplifying cells on the basis of differences in integrin function and expression. *Cell* 1993;73(4):713-24.
19. Jones PH, Harper S, Watt FM. Stem cell patterning and fate in human epidermis. *Cell* 1995;80(1):83-93.
20. Bajaj BG, Lei P, Andreadis ST. Efficient gene transfer to human epidermal keratinocytes on fibronectin: in vitro evidence for transduction of epidermal stem cells. *Mol Ther* 2005;11(6):969-79.
21. Downing BR, Cornwell K, Toner M, Pins GD. The influence of microtextured basal lamina analog topography on keratinocyte function and epidermal organization. *J Biomed Mater Res A* 2005;72(1):47-56.
22. Pins GD, Toner M, Morgan JR. Microfabrication of an analog of the basal lamina: biocompatible membranes with complex topographies. *Faseb J* 2000;14(3):593-602.
23. Bush KA, Downing BR, Walsh SE, Pins GD. Conjugation of extracellular matrix proteins to basal lamina analogs enhances keratinocyte attachment. *J Biomed Mater Res A* 2007;80(2):444-52.
24. Bush KA, Pins GD. Carbodiimide Conjugation of Fibronectin on Collagen Basal Lamina Analogs Enhances Cellular Binding Domains and Epithelialization. In preparation 2009.
25. Bush KA, Toner M, Pins GD. Microenvironments of Basal Lamina Analogs Influence Epithelialization and Stem Cell Localization on Bioengineered Skin Substitutes. In preparation 2009.
26. Elsdale T, Bard J. Collagen substrata for studies on cell behavior. *J Cell Biol* 1972;54(3):626-37.
27. Chamberlain L, Yannas I. Preparation of collagen-glycosaminoglycan copolymers for tissue regeneration. In: Morgan J, Yarmush M, editors. *Tissue engineering methods and protocols*. Totowa, NJ: Humana Press; 1998. p 3-17.
28. Olde Damink LH, Dijkstra PJ, van Luyn MJ, van Wachem PB, Nieuwenhuis P, Feijen J. Cross-linking of dermal sheep collagen using a water-soluble carbodiimide. *Biomaterials* 1996;17(8):765-73.
29. Olde Damink LH, Dijkstra PJ, van Luyn MJ, van Wachem PB, Nieuwenhuis P, Feijen J. In vitro degradation of dermal sheep collagen cross-linked using a water-soluble carbodiimide. *Biomaterials* 1996;17(7):679-84.
30. Hamoen KE, Erdag G, Cusick JL, Rakhorst HA, Morgan JR. Genetically Modified Skin Substitutes: Preparation and Use. In: Morgan JR, editor. *Methods in Molecular Medicine: Gene Therapy Protocols*. Totowa, NJ: Humana Press Inc.; 1997.
31. Carter WG, Symington BE, Kaur P. Cell adhesion and the basement membrane in early epidermal morphogenesis. In: Fleming TP, editor. *Epithelial Organization and Development*. London: Chapman and Hall; 1992. p 299-327.
32. Boyce ST, Williams ML. Lipid supplemented medium induces lamellar bodies and precursors of barrier lipids in cultured analogues of human skin. *J Invest Dermatol* 1993;101(2):180-4.
33. Jensen UB, Lowell S, Watt FM. The spatial relationship between stem cells and their progeny in the basal layer of human epidermis: a new view based on whole-mount labelling and lineage analysis. *Development* 1999;126(11):2409-18.
34. Moles JP, Watt FM. The epidermal stem cell compartment: variation in expression levels of E-cadherin and catenins within the basal layer of human epidermis. *J Histochem Cytochem* 1997;45(6):867-74.
35. Powell HM, Boyce ST. EDC cross-linking improves skin substitute strength and stability. *Biomaterials* 2006;27(34):5821-7.

36. Powell HM, Boyce ST. Wound closure with EDC cross-linked cultured skin substitutes grafted to athymic mice. *Biomaterials* 2007;28(6):1084-92.
37. Bush KA, Pins GD. Carbodiimide Conjugation of FN on Collagen Basal Lamina Analogs Enhances Cellular Binding Domains and Epithelialization of Collagen Basal Lamina Analogs. In Preparation 2008.
38. Pilcher BK, Dumin J, Schwartz MJ, Mast BA, Schultz GS, Parks WC, Welgus HG. Keratinocyte collagenase-1 expression requires an epidermal growth factor receptor autocrine mechanism. *J Biol Chem* 1999;274(15):10372-81.
39. Pilcher BK, Wang M, Qin XJ, Parks WC, Senior RM, Welgus HG. Role of matrix metalloproteinases and their inhibition in cutaneous wound healing and allergic contact hypersensitivity. *Ann N Y Acad Sci* 1999;878:12-24.
40. Sudbeck BD, Pilcher BK, Welgus HG, Parks WC. Induction and repression of collagenase-1 by keratinocytes is controlled by distinct components of different extracellular matrix compartments. *J Biol Chem* 1997;272(35):22103-10.
41. Clark R. Wound Repair, Overview and General Considerations. In: Clark R, editor. *The Molecular and Cellular Biology of Wound Repair (Second Edition)*. New York: Plenum Press; 1995. p 3-44.
42. Guo M, Toda K, Grinnell F. Activation of human keratinocyte migration on type I collagen and fibronectin. *J Cell Sci* 1990;96 ( Pt 2):197-205.
43. Larjava H, Koivisto, L., Hakkinen, L. Keratinocyte Interactions with Fibronectin During Wound Healing. In: Heino J, Kaharia, V.M., editor. *Cell Invasion: Landes Bioscience*; 2002.
44. Larjava H, Salo T, Haapasalmi K, Kramer RH, Heino J. Expression of integrins and basement membrane components by wound keratinocytes. *J Clin Invest* 1993;92(3):1425-35.
45. Takashima A, Grinnell F. Fibronectin-mediated keratinocyte migration and initiation of fibronectin receptor function in vitro. *J Invest Dermatol* 1985;85(4):304-8.
46. Holbrook KA. Ultrastructure of the epidermis. In: Leigh I, Lane B, Watt FM, editors. *The Keratinocyte Handbook*. New York: Cambridge University Press; 1994. p 3-39.
47. Yuspa SH, Kilkenny AE, Steinert PM, Roop DR. Expression of murine epidermal differentiation markers is tightly regulated by restricted extracellular calcium concentrations in vitro. *J Cell Biol* 1989;109(3):1207-17.
48. Pillai S, Bikle DD, Mancianti ML, Cline P, Hincenbergs M. Calcium regulation of growth and differentiation of normal human keratinocytes: modulation of differentiation competence by stages of growth and extracellular calcium. *J Cell Physiol* 1990;143(2):294-302.
49. Poumay Y, Pittelkow MR. Cell density and culture factors regulate keratinocyte commitment to differentiation and expression of suprabasal K1/K10 keratins. *J Invest Dermatol* 1995;104(2):271-6.
50. Kolly C, Suter MM, Muller EJ. Proliferation, cell cycle exit, and onset of terminal differentiation in cultured keratinocytes: pre-programmed pathways in control of C-Myc and Notch1 prevail over extracellular calcium signals. *J Invest Dermatol* 2005;124(5):1014-25.
51. Watt FM, Lo Celso C, Silva-Vargas V. Epidermal stem cells: an update. *Curr Opin Genet Dev* 2006;16(5):518-24.
52. Watt FM, Hertle, M.D. Keratinocyte integrins. In: Leigh I, Birgitte, L, and Watt, F., editor. *The Keratinocyte Handbook*. New York, New York: Press Syndicate of the University of Cambridge; 1994.
53. Watt FM. Role of integrins in regulating epidermal adhesion, growth and differentiation. *Embo J* 2002;21(15):3919-26.
54. Adams JC, Watt FM. Regulation of development and differentiation by the extracellular matrix. *Development* 1993;117(4):1183-98.
55. Muffler S, Stark HJ, Amoros M, Falkowska-Hansen B, Boehnke K, Buhring HJ, Marme A, Bickenbach JR, Boukamp P. A stable niche supports long-term maintenance of human epidermal stem cells in organotypic cultures. *Stem Cells* 2008;26(10):2506-15.
56. Potten CS, Morris RJ. Epithelial stem cells in vivo. *J Cell Sci Suppl* 1988;10:45-62.

57. Kaur P. Interfollicular epidermal stem cells: identification, challenges, potential. *J Invest Dermatol* 2006;126(7):1450-8.
58. Li A, Simmons PJ, Kaur P. Identification and isolation of candidate human keratinocyte stem cells based on cell surface phenotype. *Proc Natl Acad Sci U S A* 1998;95(7):3902-7.
59. Webb A, Li A, Kaur P. Location and phenotype of human adult keratinocyte stem cells of the skin. *Differentiation* 2004;72(8):387-95.
60. Matic M, Evans WH, Brink PR, Simon M. Epidermal stem cells do not communicate through gap junctions. *J Invest Dermatol* 2002;118(1):110-6.
61. Yu Y, Flint A, Dvorin E, Bischoff J. AC133-2, a novel isoform of human AC133 stem cell antigen. *J Biol Chem* 2004;277:20711-20716.
62. Wan H, Stone MG, Simpson C, Reynolds LE, Marshall JF, Hart IR, Hodivala-Dilke KM, Eady RA. Desmosomal proteins, including desmoglein 3, serve as novel negative markers for epidermal stem cell-containing population of keratinocytes. *J Cell Sci* 2003;116(Pt 20):4239-48.
63. Kocer SS, Djuric PM, Bugallo MF, Simon SR, Matic M. Transcriptional profiling of putative human epithelial stem cells. *BMC Genomics* 2008;9:359.

---

---

## Chapter 7: Conclusions and Future Work

---

### 7.1 OVERVIEW

The work in this thesis describes the development of a bioengineered skin substitute that recapitulates features found in native skin critical for maintaining tissue integrity. Unlike other current bioengineered skin substitutes, our system contains a basal lamina analog, containing biochemical and microtopographic features. Similar to native tissue, our microfabricated basal lamina analog separates the dermal and epidermal layers of our bioengineered skin substitute and provides cellular microenvironments that direct epithelialization and epidermal stem cell (ESC) localization.

### 7.2 RESULTS AND CONCLUSIONS

#### 7.2.1 PART I: EVALUATION OF ECM IN THE REGULATION OF KERATINOCYTE FUNCTION

We began to develop our bioengineered skin substitute by investigating the biochemical composition of the extracellular matrix (ECM) that enhances keratinocyte attachment and subsequent cellular functions including proliferation and differentiation. Proteins present in native basal lamina, such as type IV collagen (CIV) and laminin (LN), as well as ECM proteins found in the wound healing environment, such as fibronectin (FN) and type I collagen (CI) from the underlying dermis, were passively adsorbed at various concentrations to collagen-glycosaminoglycan (GAG) membranes and keratinocyte attachment was assessed. We found that a greater percentage of keratinocytes adhered to FN than on all other proteins investigated, similar to other *in vitro* studies investigating keratinocyte adhesion to ECM coated bacteriological plastic.<sup>1</sup> When keratinocytes are cultured *in vitro*,

they express a similar phenotype to keratinocytes located at the margins of a wound. These keratinocytes are considered “activated” in both scenarios. This activated phenotype is characterized by morphological changes, reorganization of cytoskeletal and junctional complexes, and changes in integrin expression, most notably an increase in  $\alpha_5\beta_1$  the integrin for fibronectin.<sup>2-7</sup> Therefore, we hypothesize that the increased levels of  $\alpha_5\beta_1$  played a role in the increased keratinocyte attachment to FN in our study.

After identifying that FN enhanced the percentage of keratinocytes attached to the collagen-GAG membranes, we cultured keratinocytes on collagen-GAG membranes for 3 or 7 days at the air/liquid (A/L) interface with passively adsorbed FN to investigate epithelialization parameters. An increase in epidermal thickness and an increase in the percentage of Ki67 positive basal keratinocytes were found at 3 days of A/L interface culture compared to membranes without FN modified surfaces. At 7 days of A/L interface culture, the FN modified surfaces still had a thicker epidermis, although Ki67 values between FN-treated and non-treated membranes were similar. Our results suggest that FN-treated scaffolds closely mimic the wound environment; providing the appropriate signals for proliferation and epithelialization to occur. In an acute wound environment *in vivo*, keratinocyte proliferation is increased. Within hours after injury, activated keratinocytes migrate over the wound bed,<sup>8,9</sup> and approximately 24 to 72 hours post injury a proliferative burst occurs. This burst is responsible for the reepithelialization of the wound bed,<sup>10</sup> and after closure of the wound, the basal layer returns to normal status with 10 to 20% of basal keratinocytes proliferating.<sup>11-</sup>

13

Although significant research has elucidated the roles of FN on epithelialization in the native wound environment, little work has been performed investigating its presentation on dermal scaffolds and the resulting effect on keratinocyte functionality. Furthermore, characterizing strategies to modify a biomaterial surface to increase the availability of the central cellular binding domain of FN, which has been shown to promote keratinocyte attachment and

subsequent intracellular signaling events, is of great importance for enhancing epithelialization as well as for engineering other tissue functions on the surfaces of bioengineered scaffolds.

To investigate methods to strategically modify dermal scaffolds, we initially evaluated the cellular binding domain of FN passively adsorbed to collagen-GAG surfaces and determined that the binding sites were saturated and a plateau occurred at a FN concentration of 0.1 mg/ml. In the native wound environment, FN interactions with CI are mediated by specific domains on the surfaces of collagen molecules that produce oriented FN binding and presents FN binding sites for cellular interactions.<sup>14</sup> Based on results from a previous study comparing the effects of adsorbed FN conformation on tissue culture polystyrene and collagen coated polystyrene, it was shown that the saturation density of FN on collagen was approximately half the amount of that on tissue culture polystyrene.<sup>15</sup> Additionally, when the surfaces were immunoprobed for quantities of cell binding domains at saturation densities, FN treated tissue culture polystyrene exhibited an increase in fluorescence intensity for HFN 7.1 binding relative to the values observed on FN treated collagen surfaces. Furthermore, when equal surface densities of FN were adsorbed to tissue culture polystyrene and collagen surfaces, minimal cellular differentiation was found on the tissue culture polystyrene surface in comparison with the collagen surface. These findings suggest that passively adsorbing FN to collagen surfaces and collagen membranes represents a promising, but suboptimal approach to directing keratinocyte functions on engineered biomaterials. Therefore we began to investigate how the properties of a biomaterial surface affect FN adsorption, and furthermore the affects of the FN conformation on keratinocyte functions.

To investigate the effect of surface chemistries on FN conformations that could be translated to the surfaces of collagen membranes to enhance FN cellular binding site presentation, we used self-assembled monolayers (SAMs) of alkanethiols on gold surfaces as a model biomaterial surface. We chose this model system since the hydrophobicity and charge of the

surface can be modified by changing the functional end groups of the alkanethiols without changing any other surface property.<sup>16,17</sup> It was determined that when uniform quantities of FN were adsorbed to each surface, the OH terminated SAMs demonstrated the greatest increase in the presentation of the cellular binding domains relative to the other SAMs surfaces as well as tissue culture plastic. When saturation densities of FN were evaluated on each surface, we found that increased FN densities did not always correspond with increased presentation of cellular binding domains, suggesting that surface chemistries modulated FN conformation. When keratinocyte functions were measured on FN treated SAMs at low or saturated densities we found that the availability of the synergy binding sites correlated with keratinocyte spreading, attachment, and differentiation. We also found that the density of focal adhesion complexes significantly increased on surfaces with increased presentation of FN cell binding domains. Additionally, the density of focal adhesion complexes corresponded with keratinocyte attachment and spreading in a direct fashion, and the density of focal adhesion complexes corresponded with cell differentiation in an indirect fashion. These findings suggest that keratinocyte attachment, spreading, and differentiation were integrin mediated processes. This data suggests that tailoring the surface chemistries of implantable biomaterials scaffolds, to enhance FN conformations which expose the cellular binding domains, will lead to improved control of cellular functions and enhance the rate of tissue regeneration on bioengineered skin substitutes.

To begin to translate our findings from the SAMs model of a biomaterials surface to implantable scaffolds, we investigated the use of a new starting collagen material, and we compared the availability of FN cellular binding sites with collagen-GAG membranes using passive adsorption techniques. We found that self-assembled CI membranes increased the presentation of FN cellular binding sites suggesting that the self-assembled CI membranes facilitate a more favorable binding interaction with FN. Additionally we chose to investigate covalent conjugation strategies to improve the presentation and overall bioactivity of FN on the surfaces of collagen membranes.<sup>18-20</sup> We chose a carbodiimide conjugation strategy,



specifically 1-ethyl-3-(3-dimethylaminopropyl)carbodiimide hydrochloride (EDC) because of previously successful outcomes. This strategy has been used to crosslink collagenous biomaterials and improves their degradation resistance and mechanical properties.<sup>21,22</sup> Additionally EDC has been used to couple chondroitin sulfate, heparin sulfate, and heparin to the surface of collagen scaffolds.<sup>23-25</sup> When FN was covalently conjugated to either type of collagen membrane using EDC, we found a significant increase in the presentation of cellular binding domains, however when comparing self-assembled CI membranes with collagen-GAG membranes, a significant increase in the availability of cellular binding domains was observed on the surface of the self-assembled CI membranes.

*In conclusion of Part I: Evaluation of ECM in the Regulation of Keratinocyte Function of this thesis, we determined i) FN enhances keratinocyte attachment to collagen-GAG membranes more than CI, CIV, as well as LN, and ii) the presence of FN in an in vitro model enhances epidermal thickness and proliferation. Additionally we conclude iii) when FN is covalently conjugated to collagen membranes through use of EDC enhanced FN cellular binding site availability is detected over passive adsorption, and iv) when FN is covalently conjugated through use of EDC to self-assembled CI membranes increased FN binding site presentation occurs over that on collagen-GAG membranes. In conjunction with data obtained from the SAMs studies we conclude that v) providing a surface with increased presentation of the cellular binding domain of FN will enhance keratinocyte functions necessary for epithelialization.*

## **7.2.2 PART II: ROLE OF SCAFFOLD MICROARCHITECTURE IN THE REGULATION OF KERATINOCYTE FUNCTION**

In this section of this thesis, we incorporated the findings from PART I: EVALUATION OF ECM IN THE REGULATION OF KERATINOCYTE, onto the surface of a microfabricated basal lamina analog laminated to a dermal sponge. This microfabricated basal lamina analog contains microtopographical features that mimic the native microenvironment found at the

DEJ. We evaluated the effects of both surface biochemistry and topography on epithelialization as well as epidermal stem cell (ESC) localization and compared our results with keratinocytes cultured on de-epithelialized acellular dermis (DED) and native tissue.

In order to recapitulate the topographical features found at the DEJ, we used photolithography to create a silicon wafer containing channels with features of 200  $\mu\text{m}$  depths and widths ranging from 50-400  $\mu\text{m}$ . A negative replicate of the pattern was formed using polydimethylsiloxane (PDMS) and CI was self-assembled on the surface of the PDMS negative replicate. A dermal sponge was laminated to the back surface of the self-assembled CI basal lamina analog. Fibronectin was then covalently conjugated, through the use of EDC, to the surface of the self-assembled CI membrane containing the microtopography. Using this novel composite, we evaluated the epidermal layer of bioengineered skin substitutes, after 3 days or 7 days of A/L interface culture. After 3 days, we determined that keratinocytes cultured in 50  $\mu\text{m}$  width channels had similar epidermal thickness values as epithelialized DED. At 7 days of A/L interface culture the 50  $\mu\text{m}$  and 100  $\mu\text{m}$  width channels exhibited similar epidermal thicknesses as keratinocytes cultured on DED and foreskin tissue. These conditions were statistically different from epidermal thickness values in 200  $\mu\text{m}$  width and 400  $\mu\text{m}$  width channels. The percentage of Ki67 positive basal keratinocytes was also measured at the 3 and 7 day time points. At 3 days of A/L interface culture, the 50  $\mu\text{m}$  width channels contained a lower percentage of Ki67 positive basal cells than any other channels and were similar to the percentage of Ki67 basal keratinocytes on DED. At 7 days of A/L interface culture, the 200  $\mu\text{m}$  width and 400  $\mu\text{m}$  width channels had displayed a decrease in percentage of Ki67 positive basal keratinocytes, whereas the 50  $\mu\text{m}$  width and 100  $\mu\text{m}$  width channels stayed relatively consistent.

The data obtained from the Ki67 study helps to elucidate the trends observed from the epithelial thickness experiments on the surfaces of the microfabricated basal lamina analogs and it suggests that a space filling mechanism can be used to explain the trends. Our data suggests that a proliferative burst occurred before the 3 day time point for the 50  $\mu\text{m}$  width

channels due to contact inhibition, similar to events that occur during *in vivo* wound healing after a monolayer of cells covers the wound bed.<sup>7</sup> This proliferative burst can be characterized by the basal cells undergoing two to four mitotic divisions and committing to terminal differentiation to reepithelialize the wound surface.<sup>26-28</sup> Since the 50  $\mu\text{m}$  width channels have smaller dimensions; the cells in these channels likely experience contact inhibition before the cells in channels with the larger dimensions. Additionally, the smaller width channels have smaller overall dimensions, thus it takes a less number of cells to fill these channels. By the 7 day A/L interface culture time point, the 100  $\mu\text{m}$  width channels had approximately the same epithelial thickness as the 50  $\mu\text{m}$  width channels and native skin; however the 200 and 400  $\mu\text{m}$  width channels contained a less thick epidermis. The percentage of Ki67 positive cells for the 200 and 400  $\mu\text{m}$  width channels decreased at the 7 day time point but were not statistically different from the 3 days, which could indicate that the epithelial thickness in these channels had reached a steady state. To further support the proposed model of a space filling mechanism, as well as to further explain the trends observed in this study, future studies should evaluate the microenvironments of the basal lamina analogs after initial seeding time as well as 14 days at the A/L interface. These experiments will provide information regarding the initial distribution of cells, and if the epithelial thickness of the wider channels reaches similar thickness values as the 50  $\mu\text{m}$  width, 100  $\mu\text{m}$  width, epithelialized DED, and foreskin tissue.

Additionally, we investigated the localization of epidermal stem cells (ESCs) on the surfaces of our bioengineered skin substitutes as well as in epithelialized DED and in native foreskin tissue. Previous studies have demonstrated that the  $\beta_1$  integrin is a preliminary marker for ESCs using cellular separation techniques based on integrin levels in combination with colony forming efficiency studies.<sup>29</sup> When investigating  $\beta_1$  expression in native human tissues, these studies found that  $\beta_1$ -bright and dull regions of the basal layer have a non-random distribution. Patches of integrin-bright cells were found at the tips of the papillary projections or tips of the rete ridges depending on location of the skin.<sup>29</sup> When we evaluated

the presence of  $\beta_1$ -bright regions on the surfaces of our microfabricated basal lamina analogs as well as on epithelialized DED, and we found that integrin-bright regions were localized in the channels, and in the bottom in the rete ridges. In native foreskin tissue, the  $\beta_1$ -bright regions were localized to the tips of the dermal papillae, similar to previously reported data.<sup>29,30</sup> We also evaluated the localization of ESCs on flat regions of the basal lamina analog, and found a heterogeneously distributed population of  $\beta_1$ -bright cells.

Our data suggests that the microtopographical features of the basal lamina analog enhance ESC localization over that found on a flat basal lamina analog. In native skin, ESCs in the epidermis, defined by integrin-bright analysis, are located in clusters of 9-14 cells.<sup>29</sup> Based on our data, we have created a cellular microenvironment or ESC “niche” that promotes the localization of integrin-bright cells similar to that found in native skin. Creating an environment that mimics the native ESC “niche” is critical for continual regeneration of a bioengineered skin substitute. Although the exact mechanism of localization *in vivo* as well as in our *in vitro* model is unknown, it is hypothesized that the cellular microenvironment or “niche” provides the conditions necessary for maintenance of ESC phenotype including the proper combinations of growth factors, ECM proteins, and neighboring cells.

*In conclusion of Part II: Roles of Scaffold Microarchitecture in the Regulation of Keratinocyte Function in this thesis, we developed i) a novel bioengineered skin substitute that contains FN covalently conjugated to the surface of a basal lamina analog that contains microtopographical features similar to the native DEJ. Additionally we determined ii) after 7 days of A/L interface culture that smaller width topographical features (50 and 100  $\mu\text{m}$  widths with 200  $\mu\text{m}$  depths) contain a morphologically and physiologically similar epithelial layer as epithelialized DED or native tissue and iii) provide microtopographic cues that facilitate enhanced ESC clustering in comparison with a flat basal lamina analog.*

## 7.3 FUTURE WORK

### 7.3.1 *The Next Generation of Bioengineered Skin Substitutes*

The ultimate goal for bioengineered skin substitutes is to provide complete restoration and physiology of uninjured skin after the treatment and healing of wound sites.<sup>31</sup> Researchers have agreed that in order to achieve optimal function and appearance of the treated wound, it is necessary to create a bioengineered skin substitute that consists of both dermal and epidermal components.<sup>32</sup> *In vivo* the morphogenesis and homeostasis of human skin are maintained by cells interacting with specialized structures and biochemical cues provided by components found in the dermal and epidermal layers of the skin. In this thesis, we investigated the role of ECM proteins and topographical features of the basal lamina on keratinocyte functions; however we did not examine the role of epithelial-mesenchymal interactions known to influence epithelialization and basement membrane synthesis through paracrine signaling.<sup>33-35</sup>

In skin, the basal lamina acts as a barrier that prevents fibroblasts located in the dermis from directly contacting epidermal keratinocytes, but it does not prevent the diffusion of macromolecules into or out of the epidermis.<sup>36</sup> This is an extremely important characteristic of the basal lamina and these diffusible molecules, specifically growth factors and cytokines have been found to play an important role in regulating tissue homeostasis of the epidermal layer.<sup>33,35,37</sup> In co-culture systems containing keratinocytes and mesenchymal cells, as well as in skin, IL-1, IL-6, IL-8, granulocyte macrophage colony stimulating factor (GMC-SF), TGF  $\alpha$  and  $\beta$ , NGF, PDGF, FGF, and KGF are present in the environment, and have been identified as potential mediators of keratinocyte growth and stimuli of wound repair.<sup>38-40</sup> It has also been shown that keratinocyte growth is stimulated by factors produced by keratinocytes/fibroblast co-cultures, and that keratinocytes actively induce the expression of these factors. Thus, it has been determined that epithelial maintenance is modulated by a two-way paracrine signaling mechanism.<sup>41,42</sup>

*In vitro* studies investigating the role of epithelial-mesenchymal interaction, by incorporating fibroblasts into the dermal component of cultured composite bioengineered skin substitutes, found enhanced performance of the grafts over culture systems without fibroblasts. In the presence of fibroblasts, it was found that keratinocyte proliferation was stimulated, cell differentiation was shifted toward the granulosum layer, and epidermal morphology was improved.<sup>43-47</sup> A study utilizing keratinocytes seeded on a collagen with fibroblasts cultured at the A/L interface in serum free conditions, found that when the number of fibroblasts seeded into the dermal component was increased, the proliferation index of the epithelial layer also increased after 1 week of culture. After 3 weeks of culture all conditions, ranging from 2-20\*10<sup>4</sup> fibroblasts/cm<sup>2</sup>, contained the same percentage of positive Mb67 basal keratinocytes (10-13%) which is similar to native epidermis. This study also investigated the proliferation index of keratinocytes seeded on collagen matrices without fibroblasts and found at 1 and 2 weeks a small percentage of basal keratinocytes were positive and by the 3 week time point, no cells were positive for the proliferation marker.<sup>48</sup> Although there were no significant differences in proliferation among grafts with varying number of fibroblasts at the 3 week time point, it was found that at the high fibroblast density, differentiation markers were not properly expressed in the epidermis. Additionally, a murine implant study using keratinocytes cultured on DED with fibroblasts also showed that the addition of fibroblasts improved epidermal formation as well as enhanced dermal regeneration including vascularization and reduced graft contraction.<sup>49</sup> These data suggests that fibroblasts are necessary for long term maintenance of bioengineered skin substitutes and that an optimal fibroblast density is required for proper epidermal morphogenesis.

In addition to improving keratinocyte growth and proper morphogenesis of the epidermal layer, epithelial-mesenchymal interactions are important in mediating the synthesis of ECM proteins that contribute to the formation of the basal lamina. Interactions between keratinocytes and proteins of the basal lamina are important in maintaining tissue integrity and modulating adhesion,<sup>1,29</sup> differentiation,<sup>50</sup> proliferation,<sup>37</sup> migration,<sup>9,51</sup> and gene

expression.<sup>37</sup> Thus, the formation of a native basal lamina at the DEJ in bioengineered skin substitutes is important in providing the proper cues to enhance the longevity of the tissue.

From *in vivo* studies, the deposition and assembly of the basal lamina proteins occurs concurrently with epithelial growth and differentiation<sup>52,53</sup> and keratinocytes and fibroblasts both contribute proteins which include CIV, and types V and VII collagens, LN, FN, nidogen, and hemidesmosomal plaque proteins.<sup>54</sup> During wound healing *in vivo*, studies have found FN present under the tip of a migrating epithelial layer and an absence of both LN and CIV. Once the wound surface has been covered with a monolayer of keratinocytes by migration, LN and CIV reappear in a very ordered sequence from the margin of the wound inward, and keratinocytes return to the standard proliferation and differentiation program of the cell.<sup>55-57</sup>

Additionally, *in vitro* culture systems have investigated the role of epithelial-mesenchymal interactions on the synthesis and organization of ECM proteins of the basal lamina. Studies have used three-dimensional skin models such as collagen gels or DED with incorporated fibroblasts, and cultured keratinocytes on the surface at the A/L interface to evaluate the origin of basal lamina proteins and hemidesmosomal plaque protein formation. It has been found in serum free conditions, by El Ghalbzouri et al., that cultured keratinocytes on the surface of fibroblast populated collagen gels constitutively produce hemidesmosomal proteins (plectin, BP230, BP180) and that laminins are expressed by keratinocytes only when fibroblasts or exogenous growth factors are present. It was also found that the expression of CIV and type VII collagen are regulated by fibroblasts.<sup>58</sup> Although multiple studies have been conducted, the information gained regarding which cell type, keratinocyte or fibroblast, synthesizes particular basal lamina proteins is still controversial because of the different model systems used, as well as if serum proteins or exogenous growth factors are present in the culture media.<sup>42,53,54,59</sup>

*Collectively, the results of these studies strongly suggest that, our future efforts must include the incorporation of fibroblasts in the dermal component of our bioengineered skin substitute to provide the complete biochemical environment necessary to achieve optimal functionality and longevity of our tissue in the wound site.*

### 7.3.2 Model System

After incorporating fibroblasts into the dermal component of our bioengineered skin substitutes, we believe that we will not only have developed a bioengineered skin substitute with improved tissue morphology and functionality, but we will have an excellent *in vitro* model system that provides spatial tissue organization to i) establish the interactive role that the microenvironment of the basal lamina has on ESC selection and localization, ii) investigate markers to distinguish between transit amplifying (TA) and ESCs located in microniches (specifically including label retaining studies) and iii) further investigate the role of ESCs in the wound healing environment by creating a wound in an epithelialized graft. Using this system we can also investigate epithelial-mesenchymal interactions and the origin of iv) growth factors and cytokines and their effects on morphogenesis and epithelialization as well as v) basal lamina protein synthesis, deposition, and organization in a controlled (non-serum) environment. Additionally, this model system can also be used as an *in vitro* model system of skin to vi) study disease pathologies including skin cancer, psoriasis, and chronic wounds vii) further enhance percutaneous implants, and viii) evaluate benefits and harms of cosmetics and chemical products as well as ix) evaluate diffusion properties for transcutaneous drug delivery systems. Furthermore, we could also x) use our model system to study other body systems which contain complex microarchitectures, such as in the glomerulus of the kidney, or the crypts of the small intestine.

## 7.4 FINAL CONCLUSIONS

In this thesis a novel bioengineered skin substitute was developed that recapitulates the topography found at the DEJ and provides a biochemical environment to direct tissue



functionality. We investigated the role that spatial tissue organization had on epidermal thickness and proliferation in our model system by creating a basal lamina analog with microtopographic features. We found that the geometry of cellular microenvironments played a role in the growth of the tissue, with small width features (50 and 100  $\mu\text{m}$  widths) providing statistically similar results to that of cultures on DED as well as native tissues. Also we evaluated the localization of ESCs and determined their presence in the channels, in comparison to their distribution on flat basal lamina analogs. Based on these findings we believe we have created an environment, or stem cell niche that promotes their localization. Future work should be performed investigating these findings as well as the mechanism by which the localization occurs using a variety of ESC markers.

Additionally, we hypothesize that incorporation of fibroblasts into our dermal scaffold will further improve tissue morphology and functionality of our bioengineered skin substitutes through paracrine signaling mechanisms. The addition of fibroblasts to our model system will also enhance the regeneration of a native basal lamina critical for structural and mechanical stability of the tissue and for directing cellular proliferation and differentiation through ECM cues. To evaluate the longevity and functionality of the tissue, longer culture times should be evaluated as well as implantation studies in animal models combined with indicators of epidermal barrier formation through measuring surface electrical capacitance as well as differentiation markers distributed throughout the layers of the epidermis.

## 7.5 REFERENCES

1. Adams JC, Watt FM. Expression of beta 1, beta 3, beta 4, and beta 5 integrins by human epidermal keratinocytes and non-differentiating keratinocytes. *J Cell Biol* 1991;115(3):829-41.
2. Nguyen BP, Ren XD, Schwartz MA, Carter WG. Ligation of integrin alpha 3beta 1 by laminin 5 at the wound edge activates Rho-dependent adhesion of leading keratinocytes on collagen. *J Biol Chem* 2001;276(47):43860-70.
3. Odland G, Ross R. Human wound repair. I. Epidermal regeneration. *J Cell Biol* 1968;39(1):135-51.
4. Stenn KS, and L, Depalma. Re-epithelialization. In: Clark RA, Hensen PM, editors. *The Molecular and Cellular Biology of Wound Repair*, 1st edition. New York: Plenum Press; 1988. p 321-325.
5. Martin P. Wound healing-aiming for perfect skin regeneration. *Science* 1997;276(5309):75-81.
6. Knust E. Control of epithelial cell shape and polarity. *Curr Opin Genet Dev* 2000;10(5):471-5.

7. Clark R. Wound Repair, Overview and General Considerations. In: Clark R, editor. *The Molecular and Cellular Biology of Wound Repair (Second Edition)*. New York: Plenum Press; 1995. p 3-44.
8. Grinnell F, Feld MK. Adsorption characteristics of plasma fibronectin in relationship to biological activity. *J Biomed Mater Res* 1981;15(3):363-81.
9. Guo M, Toda K, Grinnell F. Activation of human keratinocyte migration on type I collagen and fibronectin. *J Cell Sci* 1990;96 ( Pt 2):197-205.
10. Usui ML, Underwood RA, Mansbridge JN, Muffley LA, Carter WG, Olerud JE. Morphological evidence for the role of suprabasal keratinocytes in wound reepithelialization. *Wound Repair Regen* 2005;13(5):468-79.
11. Heenen M, Thiriar S, Noel JC, Galand P. Ki-67 immunostaining of normal human epidermis: comparison with 3H-thymidine labelling and PCNA immunostaining. *Dermatology* 1998;197(2):123-6.
12. Caldwell CJ, Hobbs C, McKee PH. The relationship of Ki67 and involucrin expression in proliferative, pre-neoplastic and neoplastic skin. *Clin Exp Dermatol* 1997;22(1):11-6.
13. Usui ML, Mansbridge JN, Carter WG, Fujita M, Olerud JE. Keratinocyte migration, proliferation, and differentiation in chronic ulcers from patients with diabetes and normal wounds. *J Histochem Cytochem* 2008;56(7):687-96.
14. Kleinman HK, McGoodwin EB, Martin GR, Klebe RJ, Fietzek PP, Woolley DE. Localization of the binding site for cell attachment in the alpha1(I) chain of collagen. *J Biol Chem* 1978;253(16):5642-6.
15. Garcia AJ, Vega MD, Boettiger D. Modulation of cell proliferation and differentiation through substrate-dependent changes in fibronectin conformation. *Mol Biol Cell* 1999;10(3):785-98.
16. Prime KL, Whitesides GM. Self-assembled organic monolayers: model systems for studying adsorption of proteins at surfaces. *Science* 1991;252(5010):1164-7.
17. Mrksich M, Dike LE, Tien J, Ingber DE, Whitesides GM. Using microcontact printing to pattern the attachment of mammalian cells to self-assembled monolayers of alkanethiolates on transparent films of gold and silver. *Exp Cell Res* 1997;235(2):305-13.
18. Vallieres K, Chevallier P, Sarra-Bournet C, Turgeon S, Laroche G. AFM imaging of immobilized fibronectin: does the surface conjugation scheme affect the protein orientation/conformation? *Langmuir* 2007;23(19):9745-51.
19. Vallieres K, Petitclerc E, Laroche G. Covalent grafting of fibronectin onto plasma-treated PTFE: influence of the conjugation strategy on fibronectin biological activity. *Macromol Biosci* 2007;7(5):738-45.
20. Zhang Y, Chai C, Jiang S, Teoh S, Leong K. Fibronectin immobilized by covalent conjugation or physical adsorption shows different bioactivity on aminated-PET. *Materials Science and Engineering C* 2007;27:213-219.
21. Powell HM, Boyce ST. EDC cross-linking improves skin substitute strength and stability. *Biomaterials* 2006;27(34):5821-7.
22. Powell HM, Boyce ST. Wound closure with EDC cross-linked cultured skin substitutes grafted to athymic mice. *Biomaterials* 2007;28(6):1084-92.
23. Pieper JS, Hafmans T, Veerkamp JH, van Kuppevelt TH. Development of tailor-made collagen-glycosaminoglycan matrices: EDC/NHS crosslinking, and ultrastructural aspects. *Biomaterials* 2000;21(6):581-93.
24. Pieper JS, van Wachem PB, van Luyn MJA, Brouwer LA, Hafmans T, Veerkamp JH, van Kuppevelt TH. Attachment of glycosaminoglycans to collagenous matrices modulates the tissue response in rats. *Biomaterials* 2000;21(16):1689-99.
25. Pieper JS, Oosterhof A, Dijkstra PJ, Veerkamp JH, van Kuppevelt TH. Preparation and characterization of porous crosslinked collagenous matrices containing bioavailable chondroitin sulphate. *Biomaterials* 1999;20(9):847-58.
26. Poumay Y, Pittelkow MR. Cell density and culture factors regulate keratinocyte commitment to differentiation and expression of suprabasal K1/K10 keratins. *J Invest Dermatol* 1995;104(2):271-6.

27. Watt FM, Lo Celso C, Silva-Vargas V. Epidermal stem cells: an update. *Curr Opin Genet Dev* 2006;16(5):518-24.
28. Kolly C, Suter MM, Muller EJ. Proliferation, cell cycle exit, and onset of terminal differentiation in cultured keratinocytes: pre-programmed pathways in control of C-Myc and Notch1 prevail over extracellular calcium signals. *J Invest Dermatol* 2005;124(5):1014-25.
29. Jones PH, Harper S, Watt FM. Stem cell patterning and fate in human epidermis. *Cell* 1995;80(1):83-93.
30. Lavker RM, Sun TT. Epidermal stem cells. *J Invest Dermatol* 1983;81(1 Suppl):121s-7s.
31. Boyce ST. Design principles for composition and performance of cultured skin substitutes. *Burns* 2001;27(5):523-33.
32. Sheridan RL, Tompkins RG. Skin substitutes in burns. *Burns* 1999;25(2):97-103.
33. Boukamp P, Breitkreutz D, Stark HJ, Fusenig NE. Mesenchyme-mediated and endogenous regulation of growth and differentiation of human skin keratinocytes derived from different body sites. *Differentiation* 1990;44(2):150-61.
34. Fusenig N. Epithelial-mesenchymal interactions regulate keratinocyte growth and differentiation in vitro. In: Leigh I, Lane B, F W, editors. *The Keratinocyte Handbook*. Cambridge: University Press; 1994. p 71-97.
35. Mackenzie IC. Epithelial-mesenchymal interactions in the development and maintenance of epithelial tissues. In: Leigh I, Lane B, Watt FM, editors. *The Keratinocyte Handbook*. Cambridge: University Press; 1994.
36. Vracko R. Basal lamina scaffold-anatomy and significance for maintenance of orderly tissue structure. *Am J Pathol* 1974;77(2):314-46.
37. Fusenig NE. Epithelial-mesenchymal interactions regulate keratinocyte growth and differentiation in vitro. In: Leigh I, Lane B, Watt FM, editors. *The Keratinocyte Handbook*. Cambridge: University Press; 1994.
38. Schroder JM. Cytokine networks in the skin. *J Invest Dermatol* 1995;105(1 Suppl):20S-24S.
39. Kupper TS, Groves RW. The interleukin-1 axis and cutaneous inflammation. *J Invest Dermatol* 1995;105(1 Suppl):62S-66S.
40. Luger TA, Schwarz T. The role of cytokines and neuroendocrine hormones in cutaneous immunity and inflammation. *Allergy* 1995;50(4):292-302.
41. Segal N, Andriani F, Pfeiffer L, Kamath P, Lin N, Satyamurthy K, Egles C, Garlick JA. The basement membrane microenvironment directs the normalization and survival of bioengineered human skin equivalents. *Matrix Biol* 2008;27(3):163-70.
42. Andriani F, Margulis A, Lin N, Griffey S, Garlick JA. Analysis of microenvironmental factors contributing to basement membrane assembly and normalized epidermal phenotype. *J Invest Dermatol* 2003;120(6):923-31.
43. Coulomb B, Friteau L, Baruch J, Guilbaud J, Chretien-Marquet B, Glicenstein J, Lebreton-Decoster C, Bell E, Dubertret L. Advantage of the presence of living dermal fibroblasts within in vitro reconstructed skin for grafting in humans. *Plast Reconstr Surg* 1998;101(7):1891-903.
44. Coulomb B, Lebreton C, Dubertret L. Influence of human dermal fibroblasts on epidermalization. *J Invest Dermatol* 1989;92(1):122-5.
45. El Ghalbzouri A, Hensbergen P, Gibbs S, Kempenaar J, van der Schors R, Ponc M. Fibroblasts facilitate re-epithelialization in wounded human skin equivalents. *Lab Invest* 2004;84(1):102-12.
46. El-Ghalbzouri A, Gibbs S, Lamme E, Van Blitterswijk CA, Ponc M. Effect of fibroblasts on epidermal regeneration. *Br J Dermatol* 2002;147(2):230-43.
47. Smola H, Thiekotter G, Fusenig NE. Mutual induction of growth factor gene expression by epidermal-dermal cell interaction. *J Cell Biol* 1993;122(2):417-29.
48. El Ghalbzouri A, Lamme E, Ponc M. Crucial role of fibroblasts in regulating epidermal morphogenesis. *Cell Tissue Res* 2002;310(2):189-99.

49. Erdag G, Sheridan RL. Fibroblasts improve performance of cultured composite skin substitutes on athymic mice. *Burns* 2004;30(4):322-8.
50. Adams JC, Watt FM. Fibronectin inhibits the terminal differentiation of human keratinocytes. *Nature* 1989;340(6231):307-9.
51. Tjia JS, Aneskievich BJ, Moghe PV. Substrate-adsorbed collagen and cell secreted fibronectin concertedly induce cell migration on poly(lactide-glycolide) substrates. *Biomaterials* 1999;20(23-24):2223-33.
52. Bohnert A, Hornung J, Mackenzie IC, Fusenig NE. Epithelial-mesenchymal interactions control basement membrane production and differentiation in cultured and transplanted mouse keratinocytes. *Cell Tissue Res* 1986;244(2):413-29.
53. Marinkovich MP, Keene DR, Rimborg CS, Burgeson RE. Cellular origin of the dermal-epidermal basement membrane. *Dev Dyn* 1993;197(4):255-67.
54. Fleischmajer R, Utani A, MacDonald ED, Perlish JS, Pan TC, Chu ML, Nomizu M, Ninomiya Y, Yamada Y. Initiation of skin basement membrane formation at the epidermo-dermal interface involves assembly of laminins through binding to cell membrane receptors. *J Cell Sci* 1998;111 ( Pt 14):1929-40.
55. Clark RA, Lanigan JM, DellaPelle P, Manseau E, Dvorak HF, Colvin RB. Fibronectin and fibrin provide a provisional matrix for epidermal cell migration during wound reepithelialization. *J Invest Dermatol* 1982;79(5):264-9.
56. Clark RA, Winn HJ, Dvorak HF, Colvin RB. Fibronectin beneath reepithelializing epidermis in vivo: sources and significance. *J Invest Dermatol* 1983;80 Suppl:26s-30s.
57. Gipson IK, Spurr-Michaud SJ, Tisdale AS. Hemidesmosomes and anchoring fibril collagen appear synchronously during development and wound healing. *Dev Biol* 1988;126(2):253-62.
58. El Ghalbzouri A, Jonkman MF, Dijkman R, Ponc M. Basement membrane reconstruction in human skin equivalents is regulated by fibroblasts and/or exogenously activated keratinocytes. *J Invest Dermatol* 2005;124(1):79-86.
59. Smola H, Stark HJ, Thiekotter G, Mirancea N, Krieg T, Fusenig NE. Dynamics of basement membrane formation by keratinocyte-fibroblast interactions in organotypic skin culture. *Exp Cell Res* 1998;239(2):399-410.